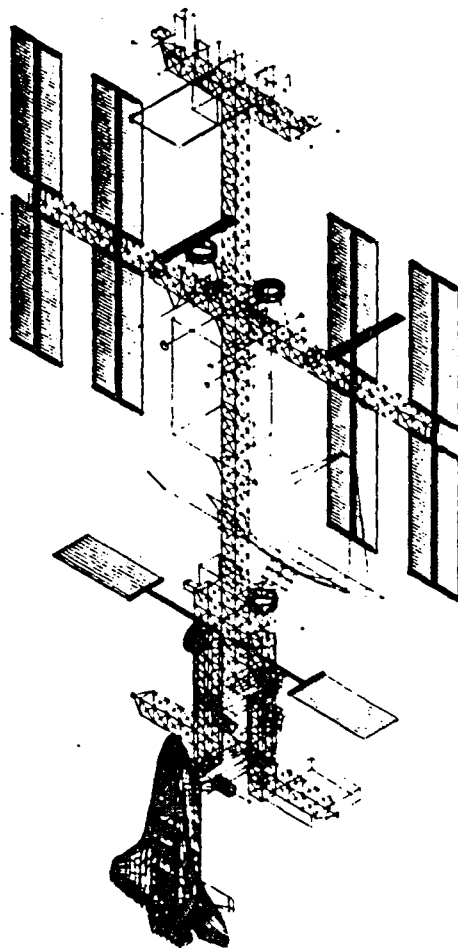


NASA Technical Memorandum 86386

STRUCTURAL DYNAMICS MODEL AND RESPONSE OF THE
DEPLOYABLE REFERENCE
CONFIGURATION SPACE STATION

NASA-TM-86386 19850025226



MAY 1985

JERROLD M. HOUSNER
NASA LANGLEY RESEARCH CENTER

LIBRARY COPY

LANGLEY RESEARCH CENTER
LIBRARY, NASA
HAMPTON, VIRGINIA

NASA

National Aeronautics and
Space Administration

Langley Research Center
Hampton, Virginia 23665



NF00582

TABLE OF CONTENTS

	Page
INTRODUCTION.....	1
ANALYTICAL MODEL OF THE INITIAL OPERATIONAL SINGLE-FOLD DEPLOYABLE REFERENCE CONFIGURATION.....	3
Truss Structure.....	4
Continuous beam representation of truss structure.....	4
Coordinate system and grid point locations.....	6
Modules.....	7
Module Attachment to Station.....	8
Radiators and Supporting Masts.....	8
Solar Array Blankets and Supporting Masts.....	9
Payloads and Orbiter.....	10
Alpha Joints, Fuel Cells and Resource Equipment.....	10
FREE VIBRATION FREQUENCIES AND MODE SHAPES.....	11
Solar Arrays Normal to Flight Path.....	11
Modes Dominated By Array Mast Cantilever Deformation....	12
Coupled Array Mast/Primary Structure Deformation Modes Below Array Mast Cantilever Mode.....	12
Primary Structure Dominated Modes Above Array Mast Cantilever Mode.....	13
Radiator Mast Modes.....	13
Solar Array Blanket Modes.....	14
Solar Arrays Tangent to the Flight Path.....	14
EVOLUTIONARY CONFIGURATION.....	15
TRANSIENT RESPONSE OF THE IOC STATION.....	16
Response Due to Orbiter Berthing.....	17
Solar Arrays Normal to the Flight Path.....	18
Solar Arrays Tangent to the Flight Path.....	19
Response Due to Crew-Push-Off Motions.....	20
Solar Arrays Normal to the Flight Path.....	20
Solar Arrays Tangent to the Flight Path.....	21
Isolation of Experimental Payloads.....	21
Response to Reaction Control System (RCS) Firing for Station Reboost.....	22
Response to Operations of the Mobile Remote Manipulator System.....	24
Effect of Bay Size on Peak Accelerations.....	25
CONCLUDING REMARKS.....	27
REFERENCES.....	29
ACKNOWLEDGEMENTS.....	29
TABLES.....	30
FIGURES.....	53

#

1105 22 520

INTRODUCTION

From April through August 1984 a NASA team assembled near the Lyndon B. Johnson Space Center in Houston Texas to define a reference configuration for the first U.S. Space Station. This reference configuration would serve as a guide, a point of departure and a standard for comparison for future NASA and contractor studies leading towards the design of the first U.S. manned space station.

Several technical studies of the reference configuration were made by that team. One item was the dynamic response and characteristics of the flexible space station reference configuration. The purpose of this report is to document the analytical models used in that study and the results derived from them. These results are of a preliminary nature and should be used only as a guideline and basis for further investigations. Better defined overall structure and the interfaces between structural components will lead to more precise investigations in the future.

Since the space station must accomodate evolutionary growth, both the Initial Operational Configuration (IOC) and a future larger space station, which the IOC could evolve into, (also known as the growth configuration), are addressed herein. Primary consideration is given to the IOC configuration with the results providing a reference point for considering the evolutionary configuration as well as construction stages of the IOC configuration and intermediate construction stages from IOC to evolutionary versions. Construction of the station may involve deployment, erection or a combination of both.

Three IOC reference configurations were considered by the NASA team; a deployable single-fold truss structure, a deployable double-fold truss structure and an erectable truss structure. (See ref. 1.) All three configurations orbit the earth in a gravity gradient stabilized orientation. Of the three versions of the reference configuration, the deployed single-fold version was the only one examined in depth and thus is the only configuration addressed in this report.

For both the IOC and evolutionary configurations, free-free vibration modes and frequencies are presented for the solar arrays normal and tangential to the flight path under the following conditions:

- (1) basic space station structure alone
- (2) with only space station payloads attached
- (3) with only shuttle orbiter attached
- (4) with both payloads and shuttle orbiter attached

In addition, transient responses of the IOC station are presented for these four conditions to loads due to the following:

- orbiter berthing
- crew motion
- reboost
- operation of a Mobile Remote Manipulator System (MRMS).

All results of this report were generated using the MSC version of NASTRAN.

ANALYTICAL MODEL OF THE IOC SINGLE-FOLD DEPLOYABLE REFERENCE CONFIGURATION

Figure 1 depicts the IOC single-fold deployable reference configuration. The analytical model of the IOC single-fold deployable reference configuration contains 678 degrees-of-freedom.

In the coordinate system shown in figure 1, the station flight path is parallel to the X axis, the Z axis is directed away from the earth and the Y axis forms a right handed system with the X and Z axes. Rotation about the Y axis is referred to as pitch, rotation about the X axis is referred to as roll and rotation about the Z axis is referred to as yaw.

During the portion of the orbit in which the station is in the sunlight, the solar arrays continuously rotate so as to remain normal to the incident sunlight. This rotation is referred to as "alpha-rotation". It is assumed herein that the rate of alpha, namely, a nominal rate of one revolution per orbit (about 94 minutes) has a negligible affect on the structural dynamics of the station. It is also assumed that gravity gradient and pre-stress loads in the station members due to orbital mechanics are negligible.

Truss Structure

All versions of the reference configuration contain considerable truss structure. The truss components of the station as identified in figure 1 are referred to as,

- upper boom
- upper keel
- transverse boom
- lower keel
- keel extension
- lower boom

Even the deployable single-fold configuration involves truss erection. Following the deployment of all truss sections, the station looks as shown in figure 2. At some time in the future, some erecting would be performed to bring the lower keel to the state shown in figure 1. Inasmuch as the modules are in place and the station manned and operational in the state of figure 2, and since this earlier state is more flexible than the completed one, it was considered more critical to perform the analytical studies on this earlier state. Thus all results for the IOC station are for the deployed reference configuration of figure 2.

In the deployed reference configuration, the truss components have four longerons and are composed of repeating nine foot cubic bays. In particular, the reference configuration uses an orthogonal tetrahedral truss as described in reference 1 and depicted in figure 2. All truss members (longitudinals and diagonals) have the same elastic moduli and cross-sectional area. The truss members are circular graphite-epoxy tubes with a 40 million psi modulus, two inch radius and 0.060 inch thick wall. To derive the dynamic characteristics and response of the reference configuration in a short time, it was elected to model these discrete truss components using a continuous beam representation.

Continuous beam representation of truss structure - The truss portions of the station are discretized into continuous beam finite elements. Equivalent values of EI, GJ and EA for the beam finite elements are calculated from appropriate formulas using the properties of the individual members and then appropriately used as input to the MSC NASTRAN structural analysis computer program.

Considerable literature presently exists which provide formulas for calculating continuous beam properties from discrete truss properties, (e.g., Refs. 2 and 3). For equivalent continuous beams representing trusses with cubic repeating bays these formulas take the form,

$$EI = C_{EI} b^2 (EA)_m$$

$$GJ = C_{GJ} b^2 (EA)_m$$

$$EA = C_{EA} (EA)_m$$

where b is the dimension of the cubic repeating truss bay, $(EA)_m$ is the axial stiffness of every truss member and C_{EI} , C_{GJ} and C_{EA} are dimensionless coefficients whose values depend only on the geometrical arrangement of the members comprising a repeating truss bay.

For the geometrical member arrangement of the orthogonal tetrahedral truss of the reference configuration, values of C_{EI} , C_{GJ} and C_{EA} are not given in the literature. Nevertheless, upper bounds on these coefficients for this member arrangement can be derived by assuming that the cross section battens of the truss behave as rigid members. This yields values of 1.18, 0.35 and 6.0 for C_{EI} , C_{GJ} and C_{EA} , respectively. In addition, through a recent correspondence with the authors of reference 2, values of the coefficients were derived for the truss in question. This led to values of 1.07, 0.26 and 5.41 for C_{EI} , C_{GJ} and C_{EA} , respectively. Unless otherwise stated, these latter values were used in calculating the equivalent beam EI , GJ and EA .

The reference configuration uses 2 inch diameter graphite epoxy members with 0.060 inch wall thickness. This leads to a cross-sectional area of about 0.38 square inches. The modulus of the members was taken to be 5.76×10^9 pounds per square foot (40 million psi). As summarized in Table 1, this leads to nominal equivalent values of 1.31×10^9 and 3.18×10^8 pound-feet² for EI and GJ , respectively, and 8.16×10^7 pounds for EA .

The equivalent mass density of the continuous beam is chosen so as to provide the mass per unit length of the deployable reference truss namely, 0.25 slugs per foot. Torsional mass inertia of the truss is not accounted for in the NASTRAN analysis. It is safe to neglect this inertial contribution since it is negligible in comparison to the torsional inertia contribution of the components and/or payloads

attached to truss sections. For example, the twist frequency of the entire keel with the transverse and upper booms unattached is about 366 Hertz. However, with these components attached, their torsional inertia dominates the keel twist response so that the twist frequency of the keel drops to 0.138 Hertz.

The continuous beam representation also reveals some torsional bending coupling in the orthogonal tetrahedral truss as well as some higher order beam effects. For the preliminary nature of the analysis performed, it was considered appropriate to ignore these effects. They may be included in future studies.

Coordinate system and grid point locations - The coordinate system for the model is shown in figure 1 with the Z axis along the centerline of the upper and lower keels and with the origin at the bottom of the station. The analytical model of the truss structure contains 69 grid points. A more refined finite element discretization was also examined, but had an insignificant effect on the results.

Grid point numbers were chosen so as to indicate to some extent the physical location of the grid point. Coordinate locations for the grid points of the truss structure are given in Table 2. Flexible beam elements connect these grid points and have material properties as given in Table 1. Generally, the grid point number indicates position along the Z axis. On the right hand side of the keel extension, on the lower keel and on the upper keel, a grid point number equals the Z coordinate of the grid point to the nearest foot. On the left hand side of the keel extension, the grid point number equals the Z coordinate plus one thousand. On the lower boom, the last two digits give the magnitude of the Y coordinate. On the transverse boom, the first three digits give the Z coordinate to the nearest foot while the last three digits indicate the magnitude of the Y coordinate to the nearest foot plus one hundred if on the right hand side of the transverse or plus 400 if on the left hand side of the transverse. Grid point numbers on the upper boom go from 401 to 408.

Modules

The modules of the reference configuration are ring and stringer stiffened cylinders with conical caps. There are two habitation modules, one laboratory module, one control module and one logistics module. The weights of each is provided in Table 3. They are placed in the keel extension of the station in a "race track" arrangement as shown in figure 3. In this analysis the modules were modeled as rigid bars with mass uniformly distributed along the length. This modeling accounted for both translational and rotational inertias of each module. Grid point locations for the ends of the rigid bars representing the modules are provided in Table 2 and the arrangement of these grid points is illustrated in figure 3.

It was assumed that the connections between modules are sufficiently rigid so that the centerline of the race track moves as a rigid plane, (i.e., no distortion of the race track arrangement either in its plane nor out of its plane is possible). In the analytical NASTRAN model this was accomplished by defining a fictitious grid point, 2700, which lies in the center of the race track pattern as shown in figure 3. Grid points 7, 8, 9, 10 and 13 which lie on the modules are constrained with the use of multi-point constraints, (MPC's) to translate and rotate with this grid point.

Module Attachment to Station

At the time this analysis was performed, the module attachment to the keel extension was not fully defined, though possible scenarios for performing the attachment were considered. It was therefore reasonable to assume for the purposes of this preliminary analysis that the attachment of modules to the truss of the keel extension was effectively rigid. To accomplish this within the MSC NASTRAN framework, a series of multi-point constraint (MPC) relationships were imposed.

The MPC relationships were composed between grid point 2700 and grid point 27 on the right hand side of the keel extension and grid point 1027 on the left hand side of the keel extension. (The coordinate locations of these grid points are given in Table 2.) These relationships constrain grid point 2700 to lie always on a straight line joining grid points 1027 to 27.

Radiators and Supporting Masts

The reference configuration has four radiators, two on the keel extension and two on the transverse boom. The radiator masts and the radiators on the keel extension were each modeled using beam elements connecting the grid points listed in Table 2. Properties of these elements are such as to represent a keel extension radiator mast. The radiator masts are each a two foot diameter aluminum tube with a 0.1 inch thick wall.

The keel extension radiators are assumed to have a backbone which consists of a deployable 30 inch diameter coilable longeron truss the properties of which were supplied by the Astro Corporation and are provided in Table 1. The radiator backbones are modeled with flexible beam elements and the mass of the radiators (which weigh 30 pounds per linear foot) is uniformly distributed along these beam elements. Grid point locations for the radiator backbones are provided in Table 2.

The radiators on the transverse boom are smaller than those on the keel extension and only their mass is accounted for in the analytical model.

Solar Array Blankets and Supporting Masts

The solar array blankets are assumed to be supported by a deployable 30 inch diameter coilable longeron mast. Each mast supports two fifteen by eighty square foot solar array blankets. Array mast properties were supplied by the Astro Corporation and are provided in Table 1. Models of the IOC station were assembled with the solar arrays either normal or tangential to the flight path. The grid point locations for a flexible beam element discretization of the array masts is given in Table 2 where the arrays are normal to the flight path.

Each array mast is 84.5 feet long and supports two solar array blankets over 80 feet of its length as shown in figure 2. Each blanket weighs one-half a pound per square foot for a total of 600 pounds per array blanket. A blanket is attached to a mast at the mast tip and near the mast root. In order to simplify the structural modeling it was elected not to model the array blankets except for their mass. In doing so it is important to account for both the translational and rotational inertias of the blankets accurately as these effect the bending and twisting frequencies of the transverse boom.

It was considered reasonable to assume that the blanket deformation shape follows that of the mast. Consequently, the blanket mass was uniformly distributed along the mast. This was done in order to account for both the translational and rotational inertias of the blanket. However, it has recently been recognized that the NASTRAN program does not calculate the appropriate rotational (i.e., twisting inertia) when this procedure is followed. Rather, the rotational inertia must be accounted for through the use of lumped masses either offset from the mast centerline or lying on the mast centerline, but with a specified rotational inertia. Rather than re-executing all the results of the NASTRAN models with this correction, it is reasonable to approximate the twisting frequencies of the masts assuming that the twist mode follows a half-sine wave from the mast root out to the mast tip.

An alternative representation of the blanket mass would have been to model the blanket as a rigid member joining the two mast/blanket attachment points. This would also accounts for both translational and rotational blanket inertias. Another representation of the blanket mass is to lump the some of the mass at the mast tip and the remainder at the mast root, (e.g., half at the tip and half at the mast root). However, this cannot accurately account for both blanket inertial properties.

Payloads and Orbiter

Table 4 provides the weight and center-of-gravity location of each payload in the coordinate system of figure 1. All payloads are modeled as lumped masses with appropriate offsets from their structural attachment to the station. The orbiter is also modeled as a lumped mass with offset and with both translational and rotational inertias. The orbiter, when included in the analysis, is assumed to be attached to the forward end of the lower habitation module at grid point 7 with (X, Y, Z) coordinates of (9, 18, 0) feet. Its mass properties and center-of-gravity location in the coordinate system of figure 1 are given in Table 5. Since the payloads are not symmetrically situated with respect to the X-Z plane, the station is in general only symmetrical in the absence of payloads.

Total inertial properties of the station as generated from the finite element model are provided in Table 6 for no attachments, all payloads attached, an orbiter attached, and all payloads and an orbiter attached.

Alpha Joints, Fuel Cells and Resource Equipment

In addition to the payloads and orbiter, which are modeled as non-structural attachments, other items exist on the station which are also modeled as non-structural attachments. The weights and locations of these items are tabulated in Table 3.

FREE VIBRATION FREQUENCIES AND MODE SHAPES

Solar Arrays Normal To Flight Path

Frequencies were calculated within the NASTRAN computer program using the Givens method. The problem size of 678 degrees was handled without resorting to a Guyan reduction

Tables 7-10 provide the free vibration frequencies and a brief verbal description of their corresponding mode shape when the arrays are normal to the flight path. In these tables, the mode shape descriptions are provided for the four cases of the IOC station without any attachments, with all payloads attached, with orbiter attached and with all payloads and orbiter attached. Each table contains the results of all four cases and a brief description of the mode shape associated with one of the four cases whose values are tabulated in the first column of each table. Thus the order of the columns for each table is changed so that mode shape descriptions are provided for all four cases and a glance across the columns of any of these tables indicates changes in frequency as attachments are added or subtracted.

Characterization of individual modes based on mode shape is in some cases obscure. In Tables 7-10 an attempt is made to characterize the mode shapes using the symbols defined in the Tables. Further, it is attempted to reflect the relative contribution of different station components to each mode shape by the order in which the symbols are given.

In addition to the tabular mode shape description, selected mode shape deformations are presented in figures 4-8 for the station without attachments; in figures 9-13 for the station with all payloads attached; in figures 14-17 for the station with an orbiter attached; and in figures 18-21 for the station with all payloads and an orbiter attached.

In general, mode shapes fall into the following four categories:

- (a) modes dominated by array mast cantilever deformation
- (b) coupled array-mast/primary-structure modes below array mast cantilever mode
- (c) primary structure (keel deformation) dominated modes above array mast cantilever mode
- (d) radiator mast modes

Each of these categories is discussed separately.

Modes Dominated By Array Mast Cantilever Deformation - Without payloads attached, the station is symmetrical about the X-Z plane. For this situation there exist two modes in which the array masts deform as fundamental cantilever beam modes in the Y-Z plane of the station and the remainder of the station does not move, (except for perhaps some stretching and compressing of the transverse boom). These modes occur at about a frequency of 0.1648 to 0.16486 Hertz. The small difference in these values is probably due to round-off errors in the analysis.

Independently of whether the station is geometrically symmetrical (payloads not attached) or asymmetrical (all payloads attached), there are other modes in which the array masts deform in or out of the Y-Z plane as cantilever beams relative to the rest of the station, but the station moves and/or deforms slightly so as to maintain dynamic equilibrium of the entire station. The movement of the station may be imperceivable as shown in figures 4 and 9 or perceivable as shown in figures 5 and 10. These modes occur at frequencies very close to the cantilever array mast frequency, from about 0.150 to 0.177 Hertz, depending upon station attachments. It appears that these modes are dominated by the array mast cantilever deformation.

As discussed under the section on modeling the array masts and blankets, the NASTRAN program fails to compute a torsional inertia property of beams when they are modeled with only distributed mass. However, an approximation to the twisting frequencies of the mast with the blankets attached is given by the formula,

$$\omega = (1/4)[GJ/(LI_r)]^{1/2}$$

where GJ represents the effective torsional stiffness of the mast and transverse boom in series, L is the length of the mast and I_r is the rotational inertia of the mast with the blankets attached. On this basis, the torsional frequencies of the mast are approximately 0.24 Hertz and thus lie above the lower primary structure modes and the cantilever bending frequencies of the mast; i.e. 0.16 Hertz.

Coupled Array Mast/Primary Structure Deformation Modes Below Array Mast Cantilever Mode - The modes of the station having the lowest natural frequencies, lie below the array mast dominated modes. These modes have frequencies ranging from 0.0965 to 0.138 Hertz depending upon station attachments. (See figures 6, 11, 15, 19.) In general, these modes involve array mast deformation coupled with deformation of the keels and transverse boom.

As depicted in figure 6, when there are no station attachments, the lowest mode occurs at 0.1385 Hertz. This is an asymmetrical mode involving keel twist, pitch bending of the array masts out of the Y-Z plane and rigid body yaw of the radiator masts and lower booms. The keel twist frequency is strongly affected by the torsional inertias

afforded by the transverse and upper booms for without their presence, the torsional mode would be about 366 Hertz.

When all payloads are attached, (see figure 11), or when only an orbiter is attached, (see figure 15), this is still the lowest mode, but its frequency decreases to 0.1233 and 0.120 Hertz, respectively. When all payloads and an orbiter are attached, (see figure 19), the lowest frequency decreases to 0.0965 Hertz and the station mode shape associated with this mode is a symmetrical mode involving bending of the array masts out of the Y-Z plane and pitch bending of the upper and lower keels. Also when all payloads and orbiter are attached, the lowest asymmetric mode decreases to 0.1139 Hertz as shown in figure 19. Stiffening the station keels or booms would raise the frequency of these modes, but not above the array mast cantilever frequency. Consequently, in a sense, the frequency of the lowest station modes are dominated from above by the behavior of the array masts.

Primary Structure Dominated Modes Above Array Mast Cantilever Modes -
Above the array mast cantilever modes are those modes which are dominated by deformation of the primary structure; see figures 7, 12, 16, 20. Of these modes the lowest frequency of about 0.18 Hertz occurs when all payloads and an orbiter are attached. These modes may involve keel bending in or out of the Y-Z plane or keel torsion. Considerable bending of the transverse boom occurs at a frequency of about 0.526 Hertz in the absence of attachments, at about 0.509 Hertz when only an orbiter is attached, at about 0.486 Hertz when all payloads are attached, and at about 0.475 Hertz when all payloads and an orbiter are attached. Thus the transverse bending mode frequency is not very sensitive to station attachments.

Radiator Mast Modes - The lowest radiator mast dominated mode occurs at about a frequency of 0.572 Hertz in the absence of attachments. The frequency changes little with attachments. If the radiator mast properties are changed as the configuration is refined, the radiator mast frequency will necessarily also change however, since its mass is relatively low, it will have little affect on the primary station modes.

Solar Array Blanket Modes - As mentioned earlier, the NASTRAN finite element model does not permit solar array blanket modes inasmuch as only the nonstructural mass of the array blankets is accounted for. In order to produce a first approximation to the array blanket modes, it is assumed that each blanket behaves as a membrane grounded at the mast attachment points. Consequently, the lowest blanket frequencies are given by the formula,

$$\text{frequency in Hertz} = (1/2) \frac{P}{LM}^{1/2}$$

Where P is the blanket tension, L is the blanket length and M is the blanket mass. For the IOC station, the blanket length is 80 feet and weight is 600 pounds. Since an array mast supports two blankets, tension in the blanket must be reacted by half the compressive load in the mast. It is assumed that the compressive mast load is 50 percent of the mast axial strength. For the 30 inch diameter collable longeron mast, the axial compressive strength is about 2000 pounds, so that the blanket tension is 500 pounds. Then a first approximation to the blanket frequency is 0.29 Hertz. In addition, the axial compression would reduce the array mast frequency from about 0.16 to 0.11 Hertz. Presence of the axial compression will also reduce the mast bending strength. This is an important consideration, since (as will be shown later) the array mast root has the smallest margin of safety on the station.

Solar Arrays Tangent to the Flight Path

Vibration modes for the case of the solar arrays tangential to the flight path are quite similar to those normal to the flight path. For this reason, the results for such are not presented herein. Nevertheless, transient response results for both solar array orientations are presented in a subsequent section.

EVOLUTIONARY CONFIGURATION

A possible candidate for the evolutionary configuration is depicted in figure 22. This evolutionary configuration differs from the IOC configuration in size, number of modules and the use of a solar dynamic system for power generation rather than a solar array based system. A significant structural difference between the IOC and evolutionary stations is the use of a three-bay-wide keel in the evolutionary station rather than the single-bay-wide keel of the IOC station. Approximate continuous beam properties of the three-bay-wide keel are provided in Table 1.

Evolutionary station modes are similar in character to the IOC modes and fall into the following general categories:

- a. support truss for solar collector
- b. keel twist
- c. keel pitch bending
- d. transverse boom bending

Selected mode shapes and frequencies for each of these categories are displayed in figures 23 - 25 for the evolutionary station without attachments and with the solar collectors normal to the flight path. The lowest modes involve deformation of the support truss for the solar collectors with possible rigid body motions of the remainder of the station. (See figure 23.) These modes occur over a frequency range from about 0.138 to 0.18 Hertz.

The lowest mode having deformation of primary structure involves keel twist and occurs at a frequency of about 0.21 Hertz. (See figure 24.) This is 52 percent higher than the lowest IOC keel twist mode in a similar condition and is probably attributable to the increased stiffness of the three-bay-wide keel section.

TRANSIENT RESPONSE OF IOC STATION

In this section transient responses of the IOC reference configuration are presented for four dynamic load cases:

- (1) orbiter berthing
- (2) crew motion
- (3) firing sequence of Reaction Control System (RCS) for station reboost
- (4) operations of the Mobile Remote Manipulator System (MRMS)

At the time when these cases were studied, accurate definition of the four load cases was not available and consequently the results herein must be viewed as preliminary. As better load definitions are derived, these load cases should be revisited. Nevertheless, the preliminary results herein yield reasonable insight into the station's dynamic response and highlight areas which require more careful scrutiny.

In general, the transient responses were generated using the lowest 80 modes in the method of modal superposition. This captures modes with frequencies up to about 2.5 to 10 Hertz depending on station attachments.

Response due to Orbiter Berthing

Berthing of the Orbiter to the station occurs at the forward end of the lower habitation module as shown in figure 1. In the analytical model, grid point 7 (see Table 2), serves as the attachment point for the orbiter. Berthing may occur using the orbiter's Remote Manipulator System (RMS) which would attach itself to the station and pull the station and Orbiter together. Assuming a berthing pulse of 1 second duration, a station weight with attached payloads of about 610,000 pounds, an orbiter weight of about 240,000 pounds and a closing rate between orbiter and station of 0.175 feet per second, a berthing pulse of about 500 pounds may be derived. The berthing load is shown in figure 26. In addition, to simulate misalignment of the station and orbiter berthing ports, the effect of an additional torque about the y axis due to a four foot misalignment was also examined. This torque was also assumed to have a duration of one second and a magnitude of 2000 foot-pounds.

Station responses of particular interest due to berthing are the peak acceleration levels at the

- (1) modules
- (2) center of the upper boom
- (3) tip of the transverse boom
- (4) tip of an array mast.

These locations are labeled in figure 2.

At each selected station location, peak acceleration levels were obtained for both zero and one-half of one percent critical damping in each station mode. Peak accelerations for the conservative case of no damping are tabulated in Table 11. Also tabulated are the amplification factors which are defined as the ratio of the peak acceleration of the flexible station to that of a completely rigid station. These ratios are of interest in assessing the effects of flexibility on station response. Response time histories for the case of one-half of one percent critical damping are plotted in figures 27 - 30.

The peak acceleration responses of a 5000 pound experimental payload on a soft spring support were also examined in order to assess the practicality of isolating payloads which have low acceleration level requirements.

Also of interest are the peak bending moments or torques at the

- (5) root of the lower keel
- (6) top of the upper keel
- (7) root of the transverse boom
- (8) alpha rotary joint
- (9) root of an array mast.

Peak values at these selected station locations are tabulated for the conservative case of no damping. Margins of safety using of a safety factor of 1.5 are also presented in Table 12 using the structural strengths in Table 1.

It is observed that the longest period of vibration of a mode whose shape involves motion of the berthing port is from 7.2 to 10.4 seconds, depending on station attachments. Thus, it takes from 3.6 to 5.2 seconds for location furthest from the berthing port to experience the affect of the berthing load and 7.2 to 10.4 seconds for the berthing port to experience the wave reflected from these remote locations. These times are considerably longer than the assumed berthing pulse duration of one second and thus the assumed berthing load acts like an applied impulse on the station.

Solar Arrays Normal To The Flight Path - For the case of the solar arrays normal to the flight path, peak acceleration, magnitudes in the absence of damping range from about 0.0012 to 0.016 g's. With the exception of the center of the upper boom peak acceleration magnitudes change little with the attachment of payloads. Further, the amplification factor at the tip of the transverse boom is very large when payloads are present. This occurs, not because the flexible body acceleration is very large, but rather because in an entirely rigid station with payloads attached, the instantaneous axis of rotation due to the orbiter berthing load lies nearly along the transverse boom. Hence the rigid body rotation at this location is near zero and the resulting amplification factor is quite large.

The effect of damping on station response can be appreciated by comparing the peak acceleration values of Table 11 with those of figures 27 - 30. For example, the peak response at the center of the upper boom is about 39 percent lower in the presence of only one-half of one percent critical damping. The large reduction due to damping is basically attributable to the highest peaks, in the absence of damping, occurring long after the berthing load is applied. Damping reduces these later peaks; thus the lower initial peaks become the maximum ones experienced by the station. In addition, recent flight experiments have indicated that a half-percent damping may be very conservative and higher damping values should be used. Nevertheless, it is believed that the conservatism in using results without damping will compensate for the uncertainties in load definition. In future studies, when better load definitions are available, it would be desirable to use peak values in the presence of damping.

Inasmuch as no acceleration requirements during orbiter berthing operations exist at the present time, little can be said about the acceleration levels themselves. However, the internal structural force resultants require consideration relative to allowable station strength.

Table 12 contains peak bending moments and torque magnitudes at the selected locations on the station. The attachment of payloads has little effect on the bending moment at the root of the lower keel but more than doubles the bending moment at the root of the transverse boom. In addition, since the attachment of payloads to the station causes the station to become unsymmetric about the X-Z plane, torques exist at certain locations of the station where they did not exist in the absence of payloads.

Margins of safety at the selected locations are all positive and thus indicate residual strength. The lowest value during a berthing operation occurs at the root of the array mast with a value of 4.7. This location should be given careful scrutiny in future studies when the berthing load is better defined. Deflection results indicate that the flexible deformation of the array mast from root to tip did not exceed one-third of a foot.

As mentioned previously in this section, the assumed berthing load is essentially impulsive for this low frequency station. As shown in reference 4, but for a different station configuration, internal force resultants can be considerably higher when load duration is longer. To more accurately account for load duration during berthing operations, future studies should consider simulation of the berthing operation. This could be accomplished using a simplified berthing mechanism model between the station and orbiter berthing ports and with an initial orbiter velocity. Presently, initial berthing velocities are believed to be about 0.1 to 0.3 feet per second.

Solar Arrays Tangent To The Flight Path - Response results when the solar arrays are tangent to the flight path are summarized in Table 13. Results are similar to those already discussed for arrays normal to the flight path. The primary difference between the results for the two array orientations occurs at the tip of an array mast. At this location, the peak acceleration for arrays normal to the flight path is up to five times larger than that for arrays tangent to the flight path. This in turn indicates that bending moments due to orbiter berthing at the array mast roots are smaller when the arrays are tangent to the flight path. Thus, orientation of the arrays normal to the flight path appears to be a worse condition. This is due to the fact that the berthing load is itself tangent to the flight path and can most easily excite array mast flexural modes when the arrays are normal to it.

Response Due To Crew-Push-Off Motions

Two different crew-push-off and stop motions were examined. One of these is based on a crew member pushing-off from one side of a habitation module, traveling across the module width and subsequently stopping at the other side of the module. This is referred to herein as a transverse crew motion. The other crew-push-off motion is based on a crew member pushing-off one end of a habitation module, traveling to the other end and subsequently stopping at that end and is referred to herein as axial crew motion. The assumed load histories for these motions is depicted in figure 26. The push-off maneuver is assumed to take the shape of a ramp of one second duration from 0 to 25 pounds magnitude. The stopping maneuver is assumed to also be a ramp of one second duration from 25 to 0 pounds magnitude. The time lapse between the ramps allows for the motion across or along the module as the case may be.

Solar Arrays Normal To The Flight Path - Figures 31 thru 34 illustrate the time history of the acceleration responses due to axial crew motion, when the solar arrays are normal to the flight path, at the same selected station locations as those used for orbiter berthing. For the results presented in the figures, one-half of one percent damping was assumed in each mode. Response of the habitation module itself, as shown in figure 31 clearly reveals the occurrence of the crew push-off and stop. Table 14 summarizes the peak acceleration magnitudes at the selected station locations in the absence of damping for both axial and transverse crew motions. Internal structural loads are not provided for crew motion since they are expected to be insignificant from a strength point of view.

Table 14 indicates that with all payloads attached to the station, accelerations at some locations increase while others decrease. In general, when the orbiter is attached acceleration levels decrease as would be expected in the presence of the large orbiter mass near the load application points. As in the case of orbiter berthing, amplification factors are high at the transverse boom since the boom appears to lie near the instantaneous axis for rigid body response. When both orbiter and all payloads are attached to the station the instantaneous axis of rigid body rotation lies along the upper end of the vertically oriented solar array masts, so that amplification factors are very large. Moreover, when payloads and/or orbiter are attached to the station, there is generally little difference between the peak acceleration responses for transverse and axial crew motions.

Solar Arrays Tangent To The Flight Path - Peak accelerations at selected station locations when the arrays are tangent to the flight path are summarized in Table 15. A comparison with the results of Table 14 indicates that, in general, the peak accelerations are lower when the arrays are tangent to the flight path. A conclusion similar to that observed in the case of orbiter berthing.

Isolation Of Experimental Payloads

Certain payloads require quiescent conditions during nominal operations of the station. In particular it is required that crew motions not cause the accelerations of certain experiments to exceed on the order of 10^{-5} g's. Tables 14 and 15 indicate that this requirement is only met if the orbiter is attached to the station when the crew motion occurs. Hence it would be necessary for certain experiments to have isolation systems which retain the quiescent environment in the presence of crew motion. To ascertain the possibility of accomplishing this, the design of a soft spring isolator and its analytical verification was performed for a single experiment.

The spring stiffness of a soft spring capable of isolating a material science payload from axial crew motion was calculated. The experiment weighs 5000 pounds and is assumed to be located in laboratory module 2. (See figure 2 for module arrangement.) Calculation of the spring stiffness was determined on the basis of a simple two-mass problem in which one mass represents the station and the other the experiment. This is a reasonable model since the modules and their interconnections are much stiffer than the soft isolation spring and any motion in the habitation module is almost immediately experienced in the laboratory module.

As shown in figure 30, the peak accelerations associated with crew motion occurs immediately following the crew push-off or stop. Thus the spring stiffness is chosen so as to isolate the experiment from an impulsive load.

Since the isolator spring is soft, the peak response of the experiment will occur sometime after the crew motion impulse is removed and as such, the peak experiment acceleration is given by

$$\ddot{q}_e = I\omega / (m_s + m_e)$$

where I is the pulse magnitude, m_s is the station mass, m_e is the experiment mass, q_e is the displacement of the experiment and ω is the frequency of the two mass system, namely,

$$\omega = [k/m_s + k/m_e]^{1/2}$$

in which k is the isolator spring stiffness. Setting \ddot{q}_e to 10^{-5} g's, noting that I is 12.5 foot-pounds and the station weight is 269,000 pounds, the frequency of the isolation system is found to be

$$\omega = 0.034 \text{ Hz.}$$

and the spring stiffness is found to be,

$$k = 7.33 \text{ pounds/foot}$$

Also, the peak-to-peak oscillatory response of the experiment is about 0.16 inches.

Incorporating the soft spring and experiment into the NASTRAN analytical model, this isolation procedure was verified with the result that the acceleration of the experiment was reduced from 1.5×10^{-4} g's, without isolation, to an acceptable level of 1.2×10^{-5} g's, with isolation. Furthermore, the motion of the experiment due to crew motion was, as predicted, was only a fraction of an inch and the soft isolation system had a very low frequency. Since this frequency is considerably lower than the fundamental station frequency of about 0.1 Hertz, it could interact with a control system which operates only one order of magnitude below the fundamental station frequency.

Response To Reaction Control System (RCS) Firing For Station Reboost

One of the functions of the Reaction Control System (RCS) is to provide orbital reboost for the station. Four RCS jets are used to accomplish this maneuver. As shown in figure 1, two of these are located on the lower keel and the other two are located on the lower boom. Each delivers 75 pounds of thrust. Since the location of the station center-of-gravity is variable, depending on station attachments, the center-of-action of the jets does not coincide with the center-of-gravity. Consequently, a control system is used to modulate the firing of the jets in pairs so that the station orientation does not deviate more than plus or minus one degree from its nominal orientation in the pitch plane. This jet modulation eventually leads to a limit cycle

representation of the RCS firing sequence. A possible firing sequence is shown in figure 26.

Acceleration response histories at selected station locations due to the RCS firing sequence of figure 26 are provided in figures 35 - 38. Peak accelerations in g's are summarized in Table 16. These results assume one-half of one percent critical damping in each mode. The RCS reboost firing can occur over one or more orbits. However, in this study only 500 seconds of response to this sequence were simulated. The results indicate that acceleration levels are not increasing in an unbounded fashion during the first 500 seconds of response history.

After about 500 seconds, the thruster forces are removed and the responses decay to zero as expected. Furthermore, at station locations far from the station center-of-gravity, acceleration levels are generally higher due to reboost than due to orbiter berthing. (Compare Tables 11 and 16.) The peak acceleration at the upper boom, which accommodates several payloads, is about 0.024 g's. However, any low-g requirements for experimental payloads on this boom are expected to be relaxed during reboost operations.

Table 17 displays peak bending moments and torques at selected locations on the station. This table also displays margins of safety assuming a factor of safety of 1.5 and strength values used to perform these calculations are given in Table 1. All margins of safety are positive. As in the case of orbiter berthing, the lowest margins occur at the roots of the array masts. They are somewhat lower for reboost than for orbiter berthing. (Compare Tables 12 and 17.) Since there is considerable freedom in designing the RCS firing sequence and in adjusting the magnitude of the RCS thrust, it is important in future studies to give special attention to margins of safety at the roots of the array masts during reboost as these may become dangerously low.

Response To Operations Of The Mobile Remote Manipulator System (MRMS)

Space station studies have identified the need for a Mobile Remote Manipulator System (MRMS). (See reference 1.) The MRMS provides a logistics device outfitted with a space crane capability perhaps very similar to the shuttle RMS. The MRMS is considered necessary for initial station construction activities, for maintenance, repair and satellite assembly and servicing on the IOC station and for construction to achieve station growth. It can propel itself to nearly all parts of the station.

The MRMS can produce loads during its operations when accelerating or decelerating payloads. In order to assess the station dynamic response to MRMS operations, it was assumed that a worst case occurs when the MRMS is located at one end of the upper boom and its arm is decelerating a payload weighing 10,000 pounds. Deceleration loads for the shuttle RMS arm as given in reference 5 were scaled accordingly in order to simulate the MRMS loads for a 10,000 pound payload. This resulted in applied loads on the station of 17.2 pounds in the flight path direction and 877 foot-pounds of twist about the Z axis. These loads were assumed to occur as step loads with a 1 second duration.

Peak acceleration magnitudes in g's and amplification factors due to the foregoing operation are summarized in Table 18. Acceleration responses at selected locations are seen to be quite high. Of particular interest is the response at the end of the upper boom where the MRMS is assumed to be located. The response at this location, in the absence of attached payloads, is 0.0248 g's with an amplification factor of 33.9. The implication of this on station performance is a potential control interaction problem between the station controls and the MRMS controls when performing MRMS activities on flexible portions of the station.

The operations of the MRMS are presently the only defined source of disturbances at distances remote from the relatively rigid core of the station; i.e., the modules. Results obtained for this source indicate that any other such excitation sources identified in the future should receive careful scrutiny.

Effect Of Bay Size On Peak Accelerations

It is of interest to examine the sensitivity of the station responses to the choice of various bay dimensions. In figure 39 this is accomplished by considering peak acceleration responses at four station locations due to orbiter berthing. Peak acceleration responses are presented for cubic bay dimensions from 1 to 15 feet as amplification factors. These results were compiled using values of C_{EI} and C_{GJ} which are now known to be somewhat too high. Nevertheless, these results provide trends and insight into the effect of variations of truss stiffness about the nominal 9 foot bay IOC reference configuration on station response levels.

As the bay dimension is varied the station truss structural stiffnesses change in proportion to the square of the bay dimension. Only the array mast and radiator mast stiffnesses remain unchanged.

In the limit as the bay dimension goes to zero, all parts of the station become completely isolated from the rigid modules and are thus unaffected by any loads applied at the modules such as berthing and crew motion. Indeed the curves of figure 39 confirm this trend down to the bay dimension of one foot. The dashed continuation of the curves to the origin represents the consequence of this postulate. The curve for the berthing port, which is on one of the habitation modules, limits to a finite value as the bay dimension vanishes. This value is the response of the rigid modules due to orbiter berthing ratioed to the response of an entirely rigid station due to the orbiter berthing.

As the bay dimension is increased from zero, the response of the berthing port decreases because more of the mass of the station is allowed to participate in the response. The decrease in this response is not dramatic, going from a ratio of about 1.55 at a one-foot bay dimension to about 1.2 at a 15 foot bay dimension. Thus acceleration levels at the modules are not very sensitive to truss stiffness. On the other hand, the response of all other locations removed from the modules increases rapidly as the bay dimension is increased.

In addition, as the bay dimension is increased, the modal frequencies of the station undergo continuous change, while the frequency content of the applied pulse remains unchanged. For certain bay dimensions the station modal frequencies will better line up with the frequency content of the applied loads and hence larger responses will result. This helps to explain the rapid variations in response peaks as the bay dimension is varied.

For very large bay dimensions, the truss stiffness goes to infinity, and the curves should approach limiting values. These limiting values will not be unity, as though the station were entirely rigid, since the array and radiator masts remain flexible. Interestingly, a 15 foot bay dimension does not in this sense closely

approximate the rigid limiting case. In order to ascertain the limiting rigid structure values, results are shown for a 1000 foot bay dimension. Figure 39 indicates that amplification ratios limit to values between 1 and 1.2 depending on station location. The use of a 1000 foot bay dimension is purely an academic situation, but it does demonstrate that only for very high bay dimensions, can the station be considered to be rigid.

The fact that very small bay dimensions leads to essential isolation of parts of the station has benefits and drawbacks. It is beneficial that, for berthing and crew motion excitations, the acceleration levels and hence also internal loads are kept low in certain parts of the station far removed from the modules. On the other hand, too small a bay dimension can have the drawback to render the same parts of the station difficult to control. At present, precise control of portions of the station far removed from the modules has not been identified as a requirement to be met by the station control system. If needed, payloads must supply their own control. However, if payloads cannot provide their own control sufficient to their needs due to excessive responses of the station, control requirements on the station may become necessary. Furthermore, only one load condition, that arising from MRMS operations, has been identified which acts at locations remote from the modules. Possible future identified loads acting at locations remote to the modules could result in dangerously high internal loads at remote station locations, (e.g., an array mast root), and control of response at such locations may become necessary. If for these, or other reasons, the future control of locations remote from the modules becomes a requirement for the station control system, it would be extremely difficult to meet such a requirement using actuators at the modules when the bay dimension is excessively small and, consequently, a distributed control system would probably be required.

CONCLUDING REMARKS

Preliminary analytical results for the dynamic response of the reference space station configuration have been presented and discussed. Free-free vibration modes for both the IOC and evolutionary configurations were presented. For the IOC configuration with solar arrays both normal and tangent to the flight path, the following four cases were examined: station without attachments, station with payloads attached, station with orbiter attached, and station with both payloads and orbiter attached.

For the IOC configuration, modes were characterized into the following four basic types: modes dominated by array mast cantilever deformation, coupled array mast/primary structure modes below array mast cantilever mode, primary structure (keel deformation) dominated modes above array mast cantilever mode, and radiator mast modes.

Cantilever array mast modes occur at about 0.16 Hertz. Modes of the solar array blankets were not included in the finite element analysis but the lowest frequency of these modes was approximated as being 0.29 Hertz under certain blanket tension assumptions. Modes below the array mast cantilever modes involve deformation of the primary structure and can be as low as 0.098 Hertz when the orbiter and all payloads are attached to the station. Modes just above the array mast cantilever modes also involve primary structure deformation and can have a frequency as low as 0.172 when the orbiter is attached to the station.

Evolutionary configuration frequencies for a solar dynamic station without attached payloads were also provided, but detailed characterization was not given. The lowest frequencies for the evolutionary configuration involve deformation of the truss structure which supports the solar collectors. These have frequencies of about 0.14 Hertz. The lowest mode involving deformation of primary structure is a keel twist mode at a frequency of 0.21 Hertz. This is 52 percent higher than the comparable lowest IOC mode. The increase is attributable to the stiffened lower keel of the evolutionary station.

Transient disturbances due to orbiter berthing, certain crew motions, RCS reboost firing sequence and MRMS operation were also examined. The station with and without payloads and/or orbiter was considered and arrays were either normal or tangent to the station flight path. Time histories and summary tables of peak acceleration, amplification factors, peak bending moments and torques, margins of safety using a safety factor of 1.5 were presented and discussed. Results were obtained for the cases of zero and one-half of one percent critical damping in each retained mode. Generally 80 modes were retained in the analyses.

Considering all four load cases, maximum peak accelerations occur at the tip of the array mast due to RCS reboost firing with a magnitude

of 0.028 g's. This led to relatively high internal bending moments at the root of an array mast with a corresponding margin of safety of 4.1. Peak accelerations at an array mast root due to berthing were not much lower and the corresponding margin of safety was 4.71. Since neither the RCS firing sequence for reboost nor the berthing loads were very well defined when these studies were performed, future studies with better defined loads should give special attention to margins of safety at the root of the array masts. Furthermore, array mast flexible deformations from root to tip did not exceed about 4 inches in the worst case.

It was observed that crew motion led to acceleration levels which exceeded the 10^{-6} g order of magnitude requirement for the laboratory module. In order to determine the feasibility of using a soft spring isolator to reduce the acceleration level of an experimental payload to an acceptable level, such an isolator was designed for a 5000 pound experimental payload. The performance of the isolation was verified in the full finite element analysis and led to an acceptable level of 1.2×10^{-6} g's for the experimental payload.

Operations of the MRMS at one end of the upper boom produced large accelerations at the MRMS location itself relative to other station locations. This needs future attention as it could lead to potential problems in controlling the MRMS operations when such operations occur on very flexible portions of the station.

An examination of the effect of bay dimension on station response to orbiter berthing indicated that the bay dimension would have to be extremely large to provide dynamic responses approximating the limiting case of rigid keels and booms. Even the use of an erectable 15 foot bay truss would fall far short of achieving this. The reference configuration with 9 foot bays is therefore a very flexible structure. It appears to be able to meet dynamic performance requirements as they were defined at the time of this study.

References

1. Mikulas, M., Jr.; Croomes, S.; Schneider, W.; Bush, H.; Nagy, K.; Pellischek, T.; Lake, M.; and Wesselski, C.: Space Station Truss Structures and Construction Considerations. NASA TM-86338, January 1985.
2. Noor, A.K.; Anderson, M.S.; and Greene, W.H.: Continuous Models for Beam and Plate-like Lattice Structures. AIAA Journal, Vol. 16, No. 12, December 1978.
3. Noor, A.K.; Anderson, C.M.: Analysis of Beam-like Lattice Trusses. Computer Methods in Applied Mechanics and Engineering, Vol. 20, 1979.
4. Dorsey, J.T.; and Bush, H.G.: Dynamics Characteristics of a Space Station Solar Wing Array. NASA TM-85780, 1984.
5. Loads Specification - SRMS Manipulator Arm. SPAR-SG. 409 SPAR Aerospace, Toronto, Ontario, Canada. September 1978.

ACKNOWLEDGEMENTS

The author wishes to acknowledge H. Edighoffer of Edighoffer Inc., P. McGowan of the NASA Langley Research Center, and J. Dagen and W. Renegar of the NASA Johnson Space Center for their assistance in generating the data compiled in this report. Also, the author wishes to thank C. K. Chiang of Old Dominion University, and B. Holder and D. McCutchen of the NASA Johnson Space Center for their help in compiling and editing this report.

TABLE 1 - PROPERTIES OF ANALYTICAL REFERENCE
CONFIGURATION SPACE STATION MODEL

COMPONENT	BENDING STIFFNESS (LBS-FT ²)	TORSIONAL STIFFNESS (LBS-FT ²)	MASS/ LENGTH (SLUGS/FT)	BENDING STRENGTH (FT-LBS)	TORSIONAL STRENGTH (FT-LBS)
BOOMS & IOC KEELS	1.31x10 ⁹	3.18x10 ⁸	0.25	35,000	15,000
30-INCH ASTRO MAST	3.13x10 ⁶	2.08x10 ⁵	0.071	3,480	208
RADIATOR MAST	3.93x10 ⁷	3.02x10 ⁷	0.28	-	-
GROWTH 3-BAY WIDE KEEL					
(WEAK DIR.)	3.01x10 ⁹	2.10x10 ⁹	0.51	80,500	15,000
(STRONG DIR.)	1.53x10 ¹⁰	2.10x10 ⁹	0.51	136,000	15,000

TABLE 2 - GRID POINT COORDINATE TABLE

COMPONENT	GRID	COORDINATES (FEET)		
	POINT NO.	X	Y	Z
Keel Extension right-hand side				
	1	0.0	18.0	0.0
	14	0.0	18.0	13.5
	22	0.0	18.0	22.5
	27	0.0	18.0	27.0
	30	0.0	18.0	30.0
	40	0.0	18.0	40.0
	54	0.0	18.0	54.0
	60	0.0	18.0	60.0
	82	0.0	18.0	82.0
	90	0.0	18.0	90.0
	99	0.0	18.0	99.0
Keel Extension left-hand side				
	1001	0.0	-18.0	0.0
	1004	0.0	-18.0	13.5
	1022	0.0	-18.0	22.5
	1027	0.0	-18.0	27.0
	1030	0.0	-18.0	30.0
	1040	0.0	-18.0	40.0
	1054	0.0	-18.0	54.0
	1060	0.0	-18.0	60.0
	1082	0.0	-18.0	82.0
	1090	0.0	-18.0	90.0
	1099	0.0	-18.0	99.0
Lower Boom right-hand side				
	1427	0.0	27.0	13.5
	1436	0.0	36.0	13.5
	1445	0.0	45.0	13.5
	1460	0.0	60.0	13.5
	1472	0.0	72.0	13.5

GRID POINT COORDINATE TABLE (CONTINUED)				
COMPONENT	GRID POINT NO.	COORDINATES (FEET)		
		X	Y	Z
Lower Boom left hand side				
	14327	0.0	-27.0	13.5
	14336	0.0	-36.0	13.5
	14345	0.0	-45.0	13.5
	14360	0.0	-60.0	13.5
	14372	0.0	-72.0	13.5
Radiator Mast right hand side				
	8230	0.0	30.0	82.5
	8244	0.0	44.0	82.5
	8260	0.0	60.0	82.5
	8270	0.0	70.0	82.5
	8280	0.0	80.0	82.5
	8294	0.0	94.0	82.5
Radiator Mast left hand side				
	1130	0.0	-30.0	82.5
	1144	0.0	-44.5	82.5
	1160	0.0	-60.0	82.5
	1170	0.0	-70.0	82.5
	1180	0.0	-80.0	82.5
	1194	0.0	-94.0	82.5
Lower Keel				
	100	0.0	0.0	99.0
	140	0.0	0.0	140.0
	180	0.0	0.0	180.0
	220	0.0	0.0	220.0
	265	0.0	0.0	265.5

GRID POINT COORDINATE TABLE (CONTINUED)

COMPONENT	GRID	COORDINATES (FEET)		
	POINT NO.	X	Y	Z
Upper Keel				
	280	0.0	0.0	280.0
	300	0.0	0.0	300.0
	340	0.0	0.0	340.0
	360	0.0	0.0	360.0
	380	0.0	0.0	380.0
	396	0.0	0.0	396.0
Upper Boom				
	401	0.0	-40.5	396.0
	402	0.0	-30.0	396.0
	403	0.0	-20.0	396.0
	404	0.0	-10.0	396.0
	396	0.0	0.0	396.0
	405	0.0	10.0	396.0
	406	0.0	20.0	396.0
	407	0.0	30.0	396.0
	408	0.0	40.5	396.0

GRID POINT COORDINATE TABLE (CONTINUED)

COMPONENT	GRID POINT NO.	X	Y	Z
-----------	-------------------	---	---	---

Transverse Boom
right-hand side

	265	0.0	0.0	265.5
	265115	0.0	15.0	265.5
	265130	0.0	30.0	265.5
	265145	0.0	45.0	265.5
	265160	0.0	60.0	265.5
	265178	0.0	78.0	265.5
	265191	0.0	91.0	265.5
	265205	0.0	105.0	265.5
	265220	0.0	120.0	265.5
	265232	0.0	132.0	265.5

Transverse Boom
left-hand side

	265	0.0	0.0	265.5
	265415	0.0	-15.0	265.5
	265430	0.0	-30.0	265.5
	265460	0.0	-60.0	265.5
	265478	0.0	-78.0	265.5
	265491	0.0	-91.0	265.5
	265505	0.0	-105.0	265.5
	265520	0.0	-120.0	265.5
	265532	0.0	-132.0	265.5

GRID POINT COORDINATE TABLE (CONTINUED)

COMPONENT	GRID POINT NO.	COORDINATES (FEET)		
		X	Y	Z
Array Masts normal to flight path	265178	0.0	78.0	265.5
	265180	0.0	78.0	295.0
	265182	0.0	78.0	324.5
	265184	0.0	78.0	350.0
	265178	0.0	78.0	265.5
	265186	0.0	78.0	236.0
	265188	0.0	78.0	206.5
	265190	0.0	78.0	181.0
	265232	0.0	132.0	265.5
	265234	0.0	132.0	295.0
	265236	0.0	132.0	324.5
	265238	0.0	132.0	350.0
	265232	0.0	132.0	265.5
	265240	0.0	132.0	236.0
	265242	0.0	132.0	206.5
	265244	0.0	132.0	181.0
	265478	0.0	-78.0	265.5
	265480	0.0	-78.0	295.0
	265482	0.0	-78.0	324.5
	265484	0.0	-78.0	350.0
	265478	0.0	-78.0	265.5
	265486	0.0	-78.0	236.0
	265488	0.0	-78.0	206.5
	265490	0.0	-78.0	181.0
	265532	0.0	-132.0	265.5
	265534	0.0	-132.0	295.0
	265536	0.0	-132.0	324.5
	265538	0.0	-132.0	350.0
	265532	0.0	-132.0	265.5
	265540	0.0	-132.0	236.0
	265542	0.0	-132.0	206.5
	265544	0.0	-132.0	181.0

GRID POINT COORDINATE TABLE (CONTINUED)

COMPONENT	GRID POINT NO.	COORDINATES (FEET)		
		X	Y	Z
modules	7	18.0	0.0	9.0
	8	18.0	0.0	45.0
	9	-18.0	0.0	45.0
	10	-18.0	0.0	9.0
	13	18.0	0.0	81.0
	2700	0.0	0.0	27.0

TABLE 3 - WEIGHTS AND COORDINATE LOCATIONS OF MODULES
AND OTHER OPERATIONAL ITEMS

ITEM	WEIGHT (LBS)	COORDINATES (FEET)			
			X	Y	Z
HABITATION MODULE 1	37,942	from	18.0	0.0	9.0
		to	18.0	0.0	45.0
HABITATION MODULE 2	34,163	from	-18.0	0.0	9.0
		to	18.0	0.0	9.0
LOGISTICS MODULE	33,884	from	18.0	0.0	45.0
		to	18.0	0.0	81.0
LABORATORY MODULE 1	39,495	from	-18.0	0.0	45.0
		to	-18.0	0.0	9.0
LABORATORY MODULE 2	55,305	from	18.0	0.0	45.0
		to	-18.0	0.0	45.0
RESOURCE EQUIPMENT	16,170		0.0	60.0	265.5
	16,170		0.0	-60.0	265.5
ALPHA JOINTS	1,000		0.0	45.0	265.5
	1,000		0.0	-45.0	265.5
FUEL CELLS	4,620		0.0	18.0	99.0
	4,620		0.0	-18.0	99.0
	9,240		0.0	0.0	99.0

TABLE 4 - PAYLOAD WEIGHTS AND LOCATIONS

CODE	PAYLOAD	WEIGHT	COORDINATES
		(LBS.)	X,Y,Z (FEET)
SAA0005	TRANSITION RADIATION & ION CALORIMETER	12,675	0,0,396
SAA0006	STARLAB	7,055	0,-32,396
SAA0009	PINHOLE OCCULTER FACILITY	7,940	0,32,396
SAA0201	LIDAR FACILITY	4,190	-18,0,0
SAA0207	SPACE PLASMA PAYLOAD (UPPER BOOM) (HAB 2)	3,528	0,15,400
		3,528	-25,0,9
COM1202	EOS PRODUCTION UNIT	9,920	-22,0,68
COM1203	ECG PRODUCTION UNIT	11,025	0,-23,18
TDM2010	MATERIALS PERFORMANCE	1,545	9,-63,266
TDM2060/ 2070	DEPLOYMENT/ASSEMBLY /CONSTRUCTION TECH.	8,820	-50,0,96
TDM2260	EARTH OBSERVATION INSTRUMENT	132	0,27,7
		132	0,36,7
		132	0,45,7
		132	0,60,7
		132	0,72,7
TDM2310	FLUID MANAGEMENT	5,510	0,-10,105
TDM2410	ATTITUDE CONTROL	1,100	-9,-12,390
TDM2420	FIGURE CONTROL	1,100	-9,12,390
TDM2510	ENVIRONMENTAL EFFECTS	6,175	25,0,396
TDM2560	SATELLITE SERVICING	7,055	0,30,296
TDM2570	ORBITER TRANSFER VEHICLE SERVICING	17,640	-15,-15,211

TABLE 5 - ORBITER PROPERTIES

WEIGHT:

239,800 POUNDS

LOCATION OF ORBITER CENTER-OF-GRAVITY:

X=29.0, Y=0.0, Z=-26.8

MOMENTS OF INERTIA ABOUT ORBITER CENTER-OF-GRAVITY (SLUGS-FEET²):

IXX = 7,839,000; IYY = 7,490,000; IZZ = 1,001,000

TABLE 6 - INERTIAL PROPERTIES OF ANALYTICAL IOC MODEL

CASE	WEIGHT	C.G. COORDINATES	MOMENTS OF INERTIA
	(LBS)	X, Y, Z (FEET)	I_{XX} , I_{YY} , I_{ZZ} (SLUGS- FEET^2)
WITHOUT PAYLOADS AND ORBITER	269,000	1.1, 0, 84.2	8.63×10^7 , 7.81×10^7 , 1.20×10^7
WITH PAYLOADS ONLY	373,200	1.1, 0, 128.2	2.06×10^8 , 1.9×10^8 , 1.45×10^7
WITH ORBITER ONLY	508,800	5.7, 0, 34.4	1.45×10^8 , 2.37×10^8 , 1.35×10^7
WITH PAYLOADS AND ORBITER	608,600	3.59, 0, 68.3	3.21×10^8 , 3.14×10^8 , 1.62×10^7

TABLE 7 - IOC REFERENCE CONFIGURATION FREQUENCIES IN Hz WITH MODE SHAPE DESCRIPTIONS FOR THE CASE WITHOUT PAYLOADS AND ORBITER ATTACHED

MODE SHAPE DESCRIPTION*	WITHOUT PAYLOADS AND ORBITER	WITH PAYLOADS ONLY	WITH ORBITER ONLY	WITH PAYLOADS AND ORBITER
KT/AMB	0.138	0.123	0.120	0.0963
TBB/KPB/AMB	0.148	0.130	0.135	0.102
KPB/AMB	0.1502	0.132	0.138	0.1139
	0.1525	0.1540	0.153	0.1515
	0.161	0.1544	0.158	0.153
	0.1630	0.161	0.1613	0.1613
	0.1636	0.162	0.1632	0.1626
	0.1642	0.16310	0.16325	0.1628
AMB	0.16426	0.16315	0.1643	0.1631
	0.1643	0.1633	0.16435	0.16315
	0.1644	0.1642	0.1644	0.1638
	0.1646	0.16439	0.1646	0.1642
	0.1648	0.16445	0.1647	0.1645
	0.16486	0.1648	0.16475	0.1647
AMB/KRP	0.1752	0.16485	0.1648	0.16475
AMB/KRR	0.1770	0.16486	0.172	0.1648
KT/KRB/AMB	0.2094	0.173	0.1840	0.16485
KT/KRB/AMB	0.2126	0.178	0.188	0.1695
KPB/AMB/RMB	0.2640	0.198	0.209	0.1970
KRB/AMB	0.5218	0.299	0.403	0.2627
TBB/AMB/RMB	0.526	0.319	0.501	0.2983
RMB/KPB	0.572	0.320	0.565	0.3168
RMB	0.587	0.430	0.568	0.3713
RMB/TBB	0.592	0.475	0.588	0.4280
KPB/RMB/TBB/AMB	0.675	0.486	0.589	0.4745
KPB/AMB	0.720	0.570	0.709	0.5572
KPB/AMB	0.879	0.579	0.873	0.5671
AMB	0.901	0.590	0.901	0.5874
KPB	0.921	0.624	0.918	0.5885
AMB/KRB	0.948	0.707	0.948	0.6889

KEY:

AMB - ARRAY MAST BENDING
LBB - LOWER BOOM BENDING
KT - KEEL TWIST
KRB - KEEL ROLL BENDING
KRR - KEEL RIGID BODY ROLL

RMB - RADIATOR MAST BENDING
TBB - TRANSVERSE BOOM BENDING
KPB - KEEL PITCH BENDING
KRP - KEEL RIGID BODY PITCH

* MODE SHAPE DESCRIPTIONS CORRESPOND TO FIRST COLUMN OF VALUES ONLY

TABLE 8 - IOC REFERENCE CONFIGURATION FREQUENCIES IN Hz WITH MODE SHAPE DESCRIPTIONS FOR THE CASE OF PAYLOADS ATTACHED

MODE SHAPE DESCRIPTION*	WITH PAYLOADS ONLY	WITHOUT PAYLOADS AND ORBITER	WITH ORBITER ONLY	WITH PAYLOADS AND ORBITER
KT/AMB	0.123	0.138	0.120	0.0965
KT/AMB	0.130	0.148	0.135	0.1020
KPB/AMB	0.132	0.1502	0.138	0.1139
KPB/AMB	0.1542	0.1525	0.153	0.1515
	0.1544	0.161	0.158	0.1530
	0.1613	0.1630	0.1613	0.1613
	0.1623	0.1636	0.1632	0.1626
	0.1631	0.1642	0.16325	0.16285
	0.16315	0.16426	0.1643	0.1631
	0.1633	0.1643	0.16435	0.16315
AMB	0.1642	0.1644	0.1644	0.1638
	0.1644	0.1646	0.1646	0.1642
	0.16445	0.1648	0.1647	0.1645
	0.1648	0.16486	0.16475	0.1647
	0.16485	0.1752	0.1648	0.16475
	0.16486	0.1770	0.172	0.1648
KPB/AMB	0.173	0.2094	0.1840	0.16485
KRB/AMB	0.178	0.2126	0.188	0.1695
KT/AMB	0.198	0.2640	0.209	0.1970
KT/AMB	0.299	0.5218	0.403	0.2627
KT/RKB/AMB	0.319	0.526	0.501	0.2983
KPB/AMB/RMB/MRP	0.320	0.572	0.565	0.3168
AMB	0.430	0.587	0.568	0.3713
KT/KRB	0.475	0.592	0.588	0.4280
TBB/KPB/RMB	0.486	0.675	0.589	0.4745
RMB	0.570	0.720	0.709	0.5572
RMB	0.579	0.879	0.873	0.5671
RMB	0.590	0.901	0.901	0.5874
RMB/KRB/KT	0.624	0.921	0.918	0.5885
KPB/AMB/RMB	0.707	0.948	0.948	0.6889

KEY:

AMB - ARRAY MAST BENDING
LBB - LOWER BOOM BENDING
KT - KEEL TWIST
KRB - KEEL ROLL BENDING

RMB - RADIATOR MAST BENDING
TBB - TRANSVERSE BOOM BENDING
KPB - KEEL PITCH BENDING
MRP - MODULE RIGID BODY PITCH

* MODE SHAPE DESCRIPTIONS CORRESPOND TO FIRST COLUMN OF VALUES ONLY

TABLE 9 - IOC REFERENCE CONFIGURATION FREQUENCIES IN Hz WITH MODE SHAPE DESCRIPTIONS FOR THE CASE OF ORBITER ATTACHED

MODE SHAPE DESCRIPTION*	WITH ORBITER ONLY	WITH PAYLOADS ONLY	WITHOUT PAYLOADS AND ORBITER	WITH PAYLOADS AND ORBITER
KT/AMB	0.120	0.123	0.138	0.0963
KPB/AMB	0.135	0.130	0.148	0.1020
KRB/AMB	0.138	0.132	0.1502	0.1139
AMB	0.153	0.1542	0.1525	0.1515
KPB/AMB	0.158	0.1544	0.161	0.1530
	0.1613	0.1613	0.1630	0.1613
	0.1632	0.1623	0.1636	0.1626
	0.16325	0.1631	0.1642	0.16285
	0.1643	0.16315	0.16426	0.1631
AMB	0.16435	0.1633	0.1643	0.16315
	0.1644	0.1642	0.1644	0.1638
	0.1646	0.1644	0.1646	0.1642
	0.1647	0.16445	0.1648	0.1645
	0.16475	0.1648	0.16486	0.1647
	0.1648	0.16485	0.1752	0.16475
KRB/AMB	0.172	0.16486	0.1770	0.1648
KRB/AMB	0.1840	0.173	0.2094	0.16485
KPB/AMB	0.188	0.178	0.2126	0.1695
KT/AMB	0.209	0.198	0.2640	0.1970
KRB/AMB	0.403	0.299	0.5218	0.2627
TBB/AMB/RMB	0.501	0.319	0.526	0.2983
RMB	0.565	0.320	0.572	0.3168
RMB	0.568	0.430	0.587	0.3713
RMB	0.588	0.475	0.592	0.4280
RMB	0.589	0.486	0.675	0.4745
KPB/TBB/AMB	0.709	0.570	0.720	0.5572
KPB/TBB/AMB	0.873	0.579	0.879	0.5671
AMB	0.901	0.590	0.901	0.5874
KPB/AMB	0.918	0.624	0.921	0.5885
AMB	0.948	0.707	0.948	0.6889

KEY:

AMB - ARRAY MAST BENDING
LBB - LOWER BOOM BENDING
KT - KEEL TWIST
KRB - KEEL ROLL BENDING

RMB - RADIATOR MAST BENDING
TBB - TRANSVERSE BOOM BENDING
KPB - KEEL PITCH BENDING

* MODE SHAPE DESCRIPTIONS CORRESPOND TO FIRST COLUMN OF VALUES ONLY

TABLE 10 - IOC REFERENCE CONFIGURATION FREQUENCIES IN Hz WITH MODE
SHAPE DESCRIPTIONS FOR THE CASE OF ORBITER ATTACHED

MODE SHAPE DESCRIPTION*	WITH PAYLOADS AND ORBITER	WITH ORBITER ONLY	WITH PAYLOADS ONLY	WITHOUT PAYLOADS AND ORBITER
KPB/AMB	0.0963	0.120	0.123	0.138
KRB/AMB	0.1020	0.135	0.130	0.148
KRB/KT/AMB	0.1139	0.138	0.132	0.1502
	0.1515	0.153	0.1542	0.1525
	0.1530	0.158	0.1544	0.161
	0.1613	0.1613	0.1613	0.1630
	0.1626	0.1632	0.1623	0.1636
	0.1628	0.16325	0.1631	0.1642
	0.1631	0.1643	0.16315	0.16426
AMB	0.16315	0.16435	0.1633	0.1643
	0.1638	0.1644	0.1642	0.1644
	0.1642	0.1646	0.1644	0.1646
	0.1645	0.1647	0.16445	0.1648
	0.1647	0.16475	0.1648	0.16486
	0.16475	0.1648	0.16485	0.1752
	0.1648	0.172	0.16486	0.1770
KRB/AMB	0.16485	0.1840	0.173	0.2094
KRB/AMB	0.1695	0.188	0.178	0.2126
KT/AMB	0.1970	0.209	0.198	0.2640
KPB/AMB	0.2627	0.403	0.299	0.5218
KT/AMB	0.2983	0.501	0.319	0.526
KRB/AMB	0.3169	0.565	0.320	0.572
KRB/AMB	0.3713	0.568	0.430	0.587
AMB/TBB	0.4280	0.588	0.475	0.592
TBB	0.4745	0.589	0.486	0.675
RMB	0.5572	0.709	0.570	0.720
RMB	0.5671	0.873	0.579	0.879
RMB	0.5874	0.901	0.590	0.901
RMB	0.5885	0.918	0.624	0.921
TBB/TPB/AMB/RMB	0.6889	0.948	0.707	0.948

KEY:

AMB - ARRAY MAST BENDING
LBB - LOWER BOOM BENDING
KT - KEEL TWIST
KRB - KEEL ROLL BENDING

RMB - RADIATOR MAST BENDING
TBB - TRANSVERSE BOOM BENDING
KPB - KEEL PITCH BENDING

* MODE SHAPE DESCRIPTIONS CORRESPOND TO FIRST COLUMN OF VALUES ONLY

TABLE 11 - PEAK ACCELERATION RESPONSE IN G'S AT SELECTED STATION
LOCATIONS DUE TO ORBITER BERTHING FOR SOLAR ARRAYS
NORMAL TO THE FLIGHT PATH

CASE	LOCATION	BERTHING PORT	CENTER OF UPPER BOOM	TIP OF TRANSVERSE BOOM	TIP OF ARRAY MAST
WITHOUT		0.00478	0.0162	0.00460	0.00123
PAYLOADS		a=1.70	a=5.21	a=4.48	a=5.05
WITH		0.00432	0.00280	0.00596	0.00126
PAYLOADS		a=1.77	a=2.44	a=92.3	a=17.5

KEY: a = amplification factor = (accel. of flexible station)/(accel. of rigid station)

TABLE 12 - PEAK BENDING MOMENTS AND TORQUES IN FOOT-POUNDS AT
SELECTED STATION LOCATIONS DUE TO ORBITER BERTHING
FOR SOLAR ARRAYS NORMAL TO THE FLIGHT PATH

LOCATION	KEEL EXT. ROOT	TOP OF UPPER KEEL	TRANSVERSE BOOM ROOT	ALPHA JOINT	ARRAY MAST ROOT
CASE					
WITHOUT	Moment: 6390. M.S.=7.15	Moment: 0.004 M.S.=*	Moment: 2890. M.S.=18.5	Moment: 1172. M.S.=#	Moment: 406. M.S.=4.71
PAYLOADS	Torque: 350. M.S.=67.6	Torque: 0.0 M.S.=*	Torque: 1009. M.S.=22.8	Torque: 1008. M.S.=#	Torque: 0.16 M.S.=865
WITH	Moment: 6990. M.S.=7.08	Moment: 248. M.S.=227.	Moment: 7120. M.S.=6.93	Moment: 3170. M.S.=#	Moment: 381. M.S.=5.09
PAYLOADS	Torque: 510. M.S.=46.1	Torque: 728. M.S.=32.	Torque: 2500. M.S.=8.6	Torque: 2400. M.S.=#	Torque: 0.0 M.S.=*

KEY: M.S. = Margin of Safety = (strength)/(1.5 x moment or torque) - 1

*: Margin of Safety exceeds one million

#: Allowable strength for alpha joint presently unavailable

TABLE 13 - PEAK ACCELERATION RESPONSE IN G'S AT SELECTED STATION
LOCATIONS DUE TO ORBITER BERTHING FOR SOLAR ARRAYS
TANGENT TO THE FLIGHT PATH

CASE	LOCATION	BERTHING PORT	CENTER OF UPPER BOOM	TIP OF TRANSVERSE BOOM	TIP OF ARRAY MAST
WITHOUT		0.0044	0.0125	0.00275	0.00275
PAYLOADS		a=1.52	a=4.46	a=3.09	a=3.09
WITH		0.0041	0.0027	0.0056	0.0056
PAYLOADS		a=1.71	a=1.14	a=18.1	a=18.1

KEY: a = amplification factor = (flexible response)/(rigid station response)

TABLE 14 - PEAK ACCELERATION RESPONSE IN G'S AT SELECTED STATION
LOCATIONS DUE TO AXIAL AND TRANSVERSE CREW MOTION FOR
SOLAR ARRAYS NORMAL TO THE FLIGHT PATH

	LOCATION	HABITATION MODULE	CENTER OF UPPER BOOM	TIP OF TRANSVERSE BOOM	TIP OF ARRAY MAST
WITHOUT PAYLOADS AND ORBITER	AXIAL KICK	1.49×10^{-4} a=1.23	5.37×10^{-4} a=1.0	1.5×10^{-4} a=2.91	5.47×10^{-4} a=4.46
	TRANS. KICK	2.35×10^{-4} a=1.54	8.07×10^{-4} a=5.2	1.51×10^{-4} a=2.94	5.16×10^{-4} a=4.23
WITH PAYLOADS	AXIAL KICK	1.70×10^{-4} a=1.39	1.25×10^{-4} a=2.18	2.68×10^{-4} a=82.7	6.18×10^{-4} a=17.2 ONLY
	TRANS. KICK	1.86×10^{-4} a=1.52	1.42×10^{-4} a=2.47	3.10×10^{-4} a=95.4	6.89×10^{-4} a=19.1
WITH ORBITER	AXIAL KICK	5.68×10^{-5} a=1.08	1.88×10^{-4} a=63.1	6.77×10^{-5} a=4.27	2.03×10^{-4} a=55.9 ONLY
	TRANS. KICK	5.34×10^{-5} a=1.01	1.92×10^{-4} a=64.3	7.42×10^{-5} a=4.69	2.54×10^{-4} a=69.8
WITH PAYLOADS AND ORBITER	AXIAL KICK	4.91×10^{-5} a=1.01	2.27×10^{-5} a=3.26	9.78×10^{-5} a=8.08	2.01×10^{-4} a=94.6
	TRANS. KICK	4.66×10^{-5} a=0.94	1.16×10^{-5} a=1.67	5.50×10^{-5} a=4.5	1.62×10^{-5} a=76.2

KEY: a = amplification factor = (accel. of flexible station)/(accel. of rigid station)

TABLE 15 - PEAK ACCELERATION RESPONSE IN G'S AT SELECTED STATION
LOCATIONS DUE TO AXIAL AND CREW MOTION FOR SOLAR ARRAYS
TANGENT TO THE FLIGHT PATH

	LOCATION	HABITATION MODULE	CENTER OF UPPER BOOM	TIP OF TRANSVERSE BOOM	TIP OF ARRAY MAST
WITHOUT PAYLOADS AND	AXIAL KICK	1.45×10^{-4} a=1.58	2.6×10^{-4} a=2.89	4.0×10^{-4} a=4.44	3.5×10^{-4} a=3.4
WITH PAYLOADS	AXIAL KICK	1.35×10^{-4} a=1.96	1.17×10^{-4} a=1.77	2.1×10^{-4} a=3.09	2.5×10^{-4} a=3.42 ONLY
WITH ORBITER	AXIAL KICK	5.3×10^{-5} a=1.06	1.25×10^{-4} a=2.91	2.1×10^{-5} a=4.17	1.6×10^{-4} a=2.60 ONLY
WITH PAYLOADS AND	AXIAL KICK	5.4×10^{-5} a=1.32	8.8×10^{-5} a=4.1	1.3×10^{-4} a=4.1	1.4×10^{-4} a=3.18

KEY: a = amplification factor = (accel. of flexible station)/(accel. of rigid station)

TABLE 16 - PEAK ACCELERATION RESPONSE IN G'S AT SELECTED STATION LOCATIONS DUE TO STATION REBOOST

CASE	LOCATION	HABITATION MODULE	CENTER OF UPPER BOOM	TIP OF TRANSVERSE BOOM	TIP OF ARRAY MAST
WITHOUT PAYLOADS		0.0034	0.024	0.012	0.028
WITH PAYLOADS		0.0024	0.0062	0.0030	0.0037

TABLE 17 - PEAK BENDING MOMENTS AND TORQUES IN FOOT-POUNDS AT
SELECTED STATION LOCATIONS DUE TO REBOOST

LOCATION	LOWER KEEL ROOT	ROOT OF LOWER BOOM	TRANSVERSE BOOM ROOT	ALPHA JOINT	ARRAY MAST ROOT
CASE					
	Moment:	Moment:	Moment:	Moment:	Moment:
	9,134	12.6	3,460	2,800	452.3
WITHOUT	M.S.=8.62	M.S.=*	M.S.=15.3	M.S.=#	M.S.=4.10
PAYLOADS	Torque:	Torque:	Torque:	Torque:	Torque:
	0	0	942.0	856.0	0
	M.S.=*	M.S.=*	M.S.=24.7	M.S.=#	M.S.=*
WITH	Moment:	Moment:	Moment:	Moment:	Moment:
	15,820	20.8	5,260	2,750	357.0
	M.S.=8.36	M.S.=2700.	M.S.=9.70	M.S.=#	M.S.=8.65
PAYLOADS	Torque:	Torque:	Torque:	Torque:	Torque:
	1,925	0	1,660	1,660	0
	M.S.=9.26	M.S.=0	M.S.=13.6	M.S.=#	M.S.=*

KEY: M.S. = Margin of Safety = (strength)/(1.5 x moment or torque) - 1

*: Margin of Safety exceeds one million

#: Allowable strength for alpha joint presently unavailable

TABLE 18 - PEAK ACCELERATION RESPONSE IN G'S AT SELECTED STATION LOCATIONS DUE TO OPERATIONS OF THE MOBILE REMOTE MANIPULATOR SYSTEM ON THE UPPER BOOM

LOCATION	HABITATION MODULE	AT MRMS	TIP OF TRANSVERSE BOOM	TIP OF ARRAY MAST
<u>CASE</u>				
WITHOUT	0.000550	0.0248	0.0102	0.00870
PAYLOADS	a=5.7	a=33.9	a=22.0	a=13.8
WITH	0.00015	0.00030	0.0026	0.0050
PAYLOADS	a=1.15	a=1.25	a=17.6	a=24.2

KEY: a = AMPLIFICATION FACTOR = (ACCEL. RESPONSE OF FLEXIBLE STATION)/
(ACCEL. RESPONSE OF RIGID STATION)

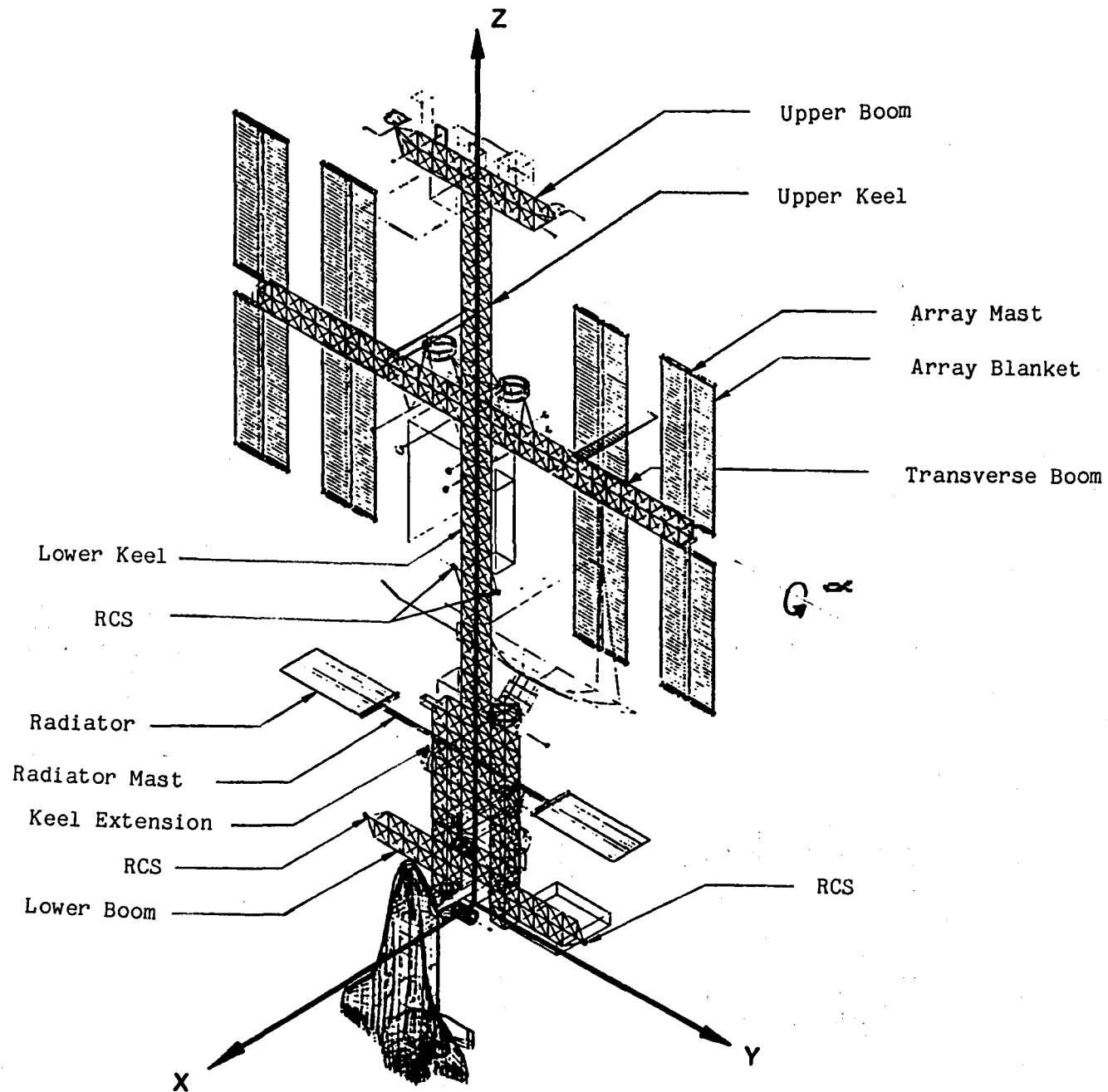


Figure 1. IOC Reference Space Station

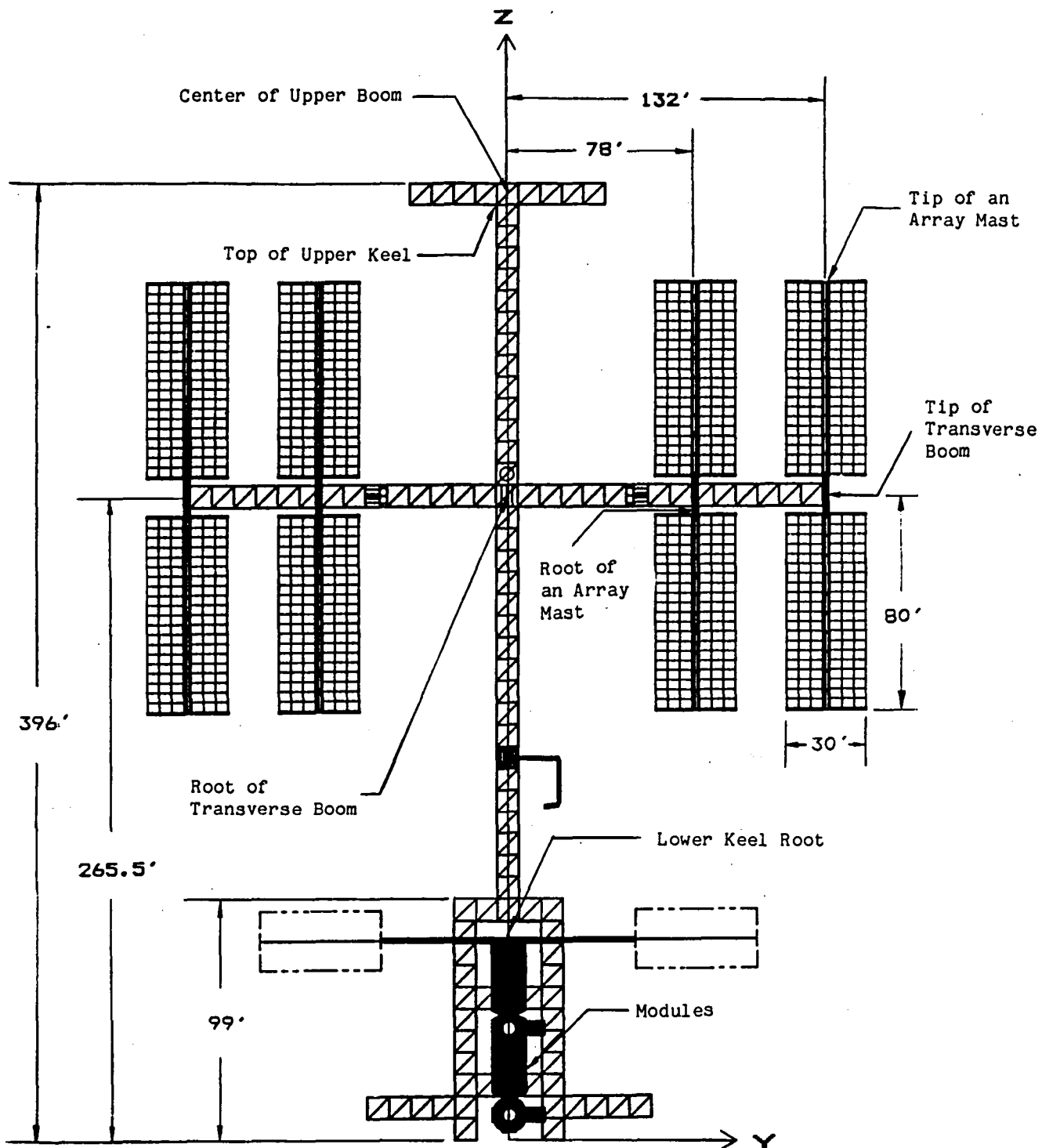


Figure 2. Ready-To-Be-Manned IOC Reference Configuration
Before Completion of Keel Extension

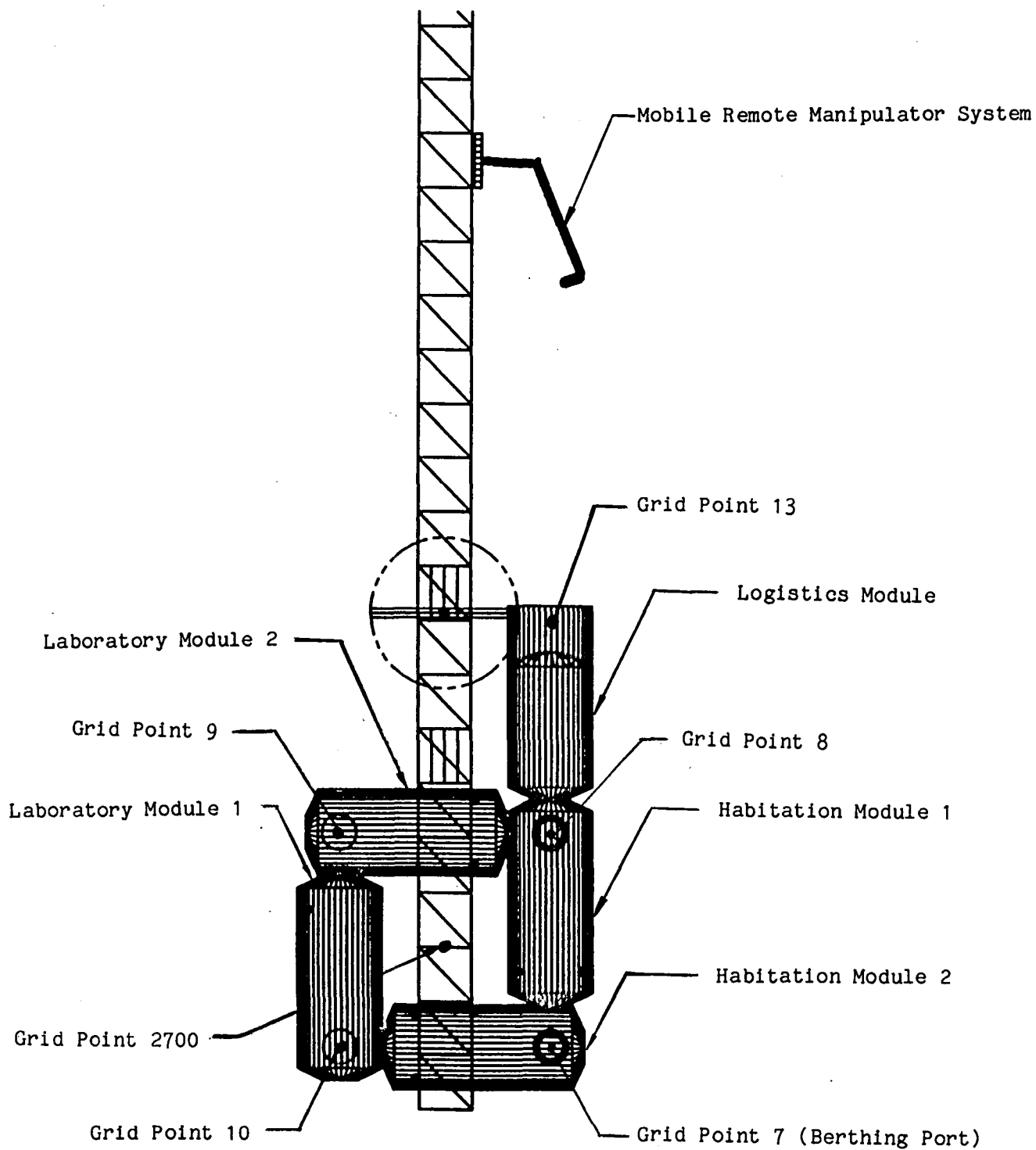
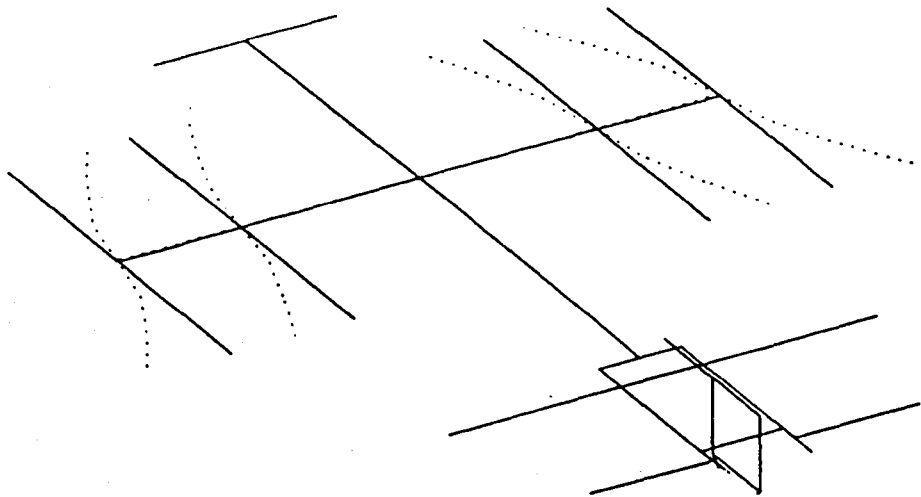
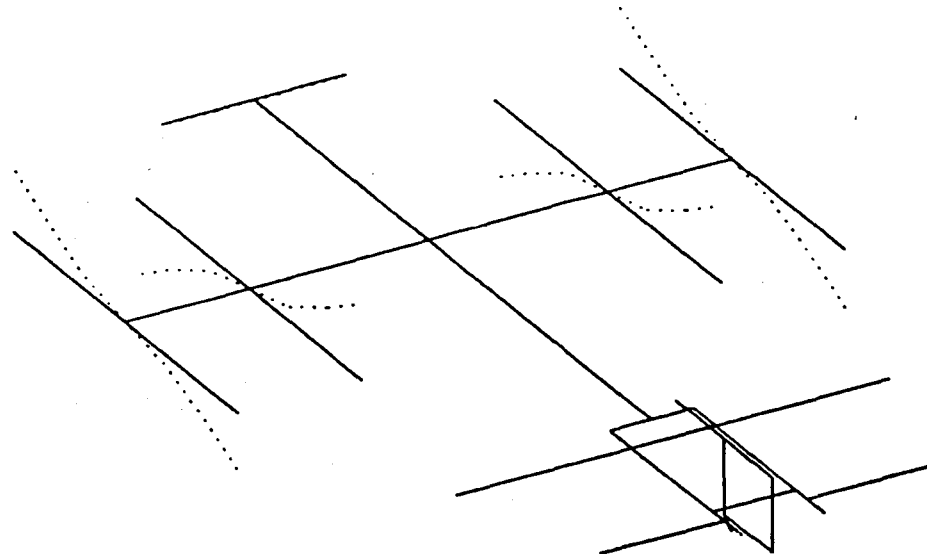


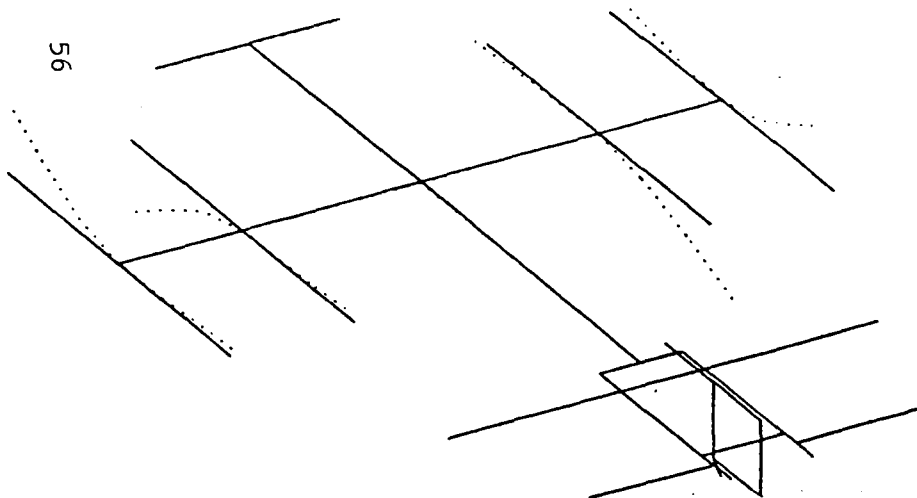
Figure 3. Racetrack Arrangement of Modules



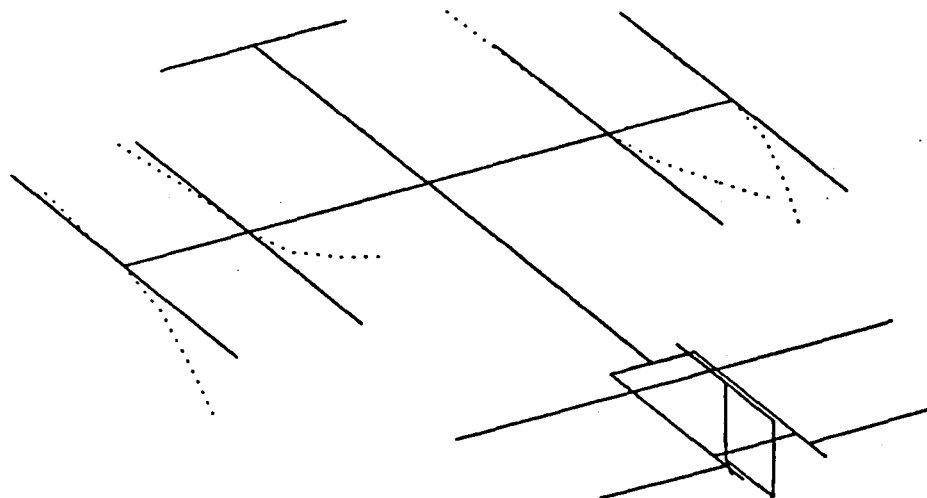
Freq. = 0.1613 Hz.



Freq. = 0.1630 Hz.



Freq. = 0.1636 Hz.



Freq. = 0.1642 Hz.

Figure 4. Selected Array Mast Dominated Modes in the Absence of Payloads and Orbiter

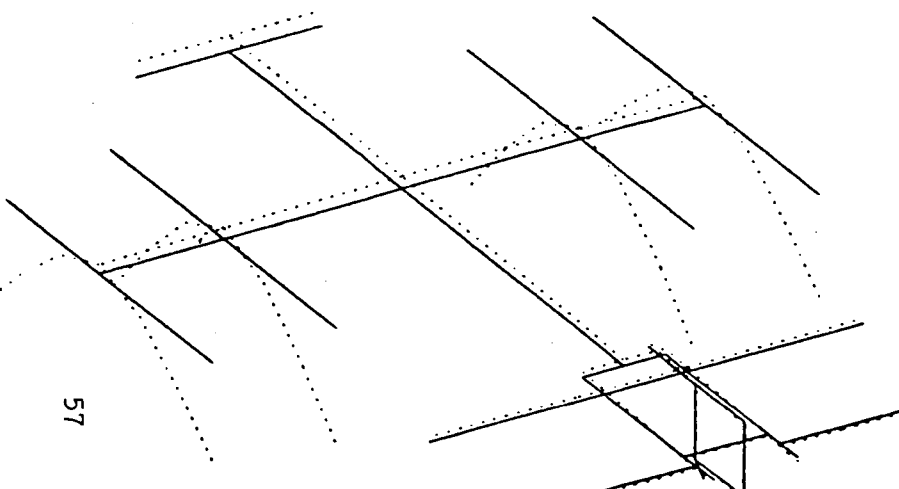


Diagram showing a structure with solid and dotted lines representing motion. The structure consists of a central rectangular frame with several diagonal and horizontal lines extending from it. The dotted lines show the displacement of various points on the structure.

Freq. = 0.1752 Hz.

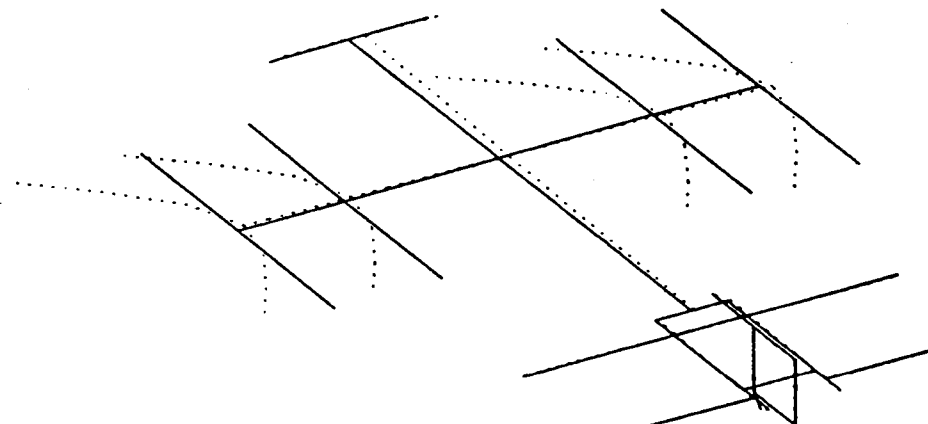
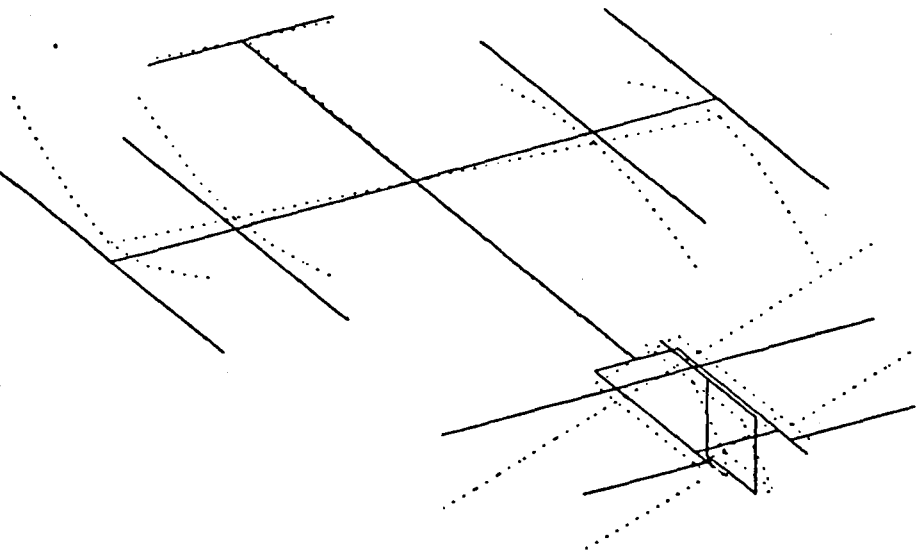


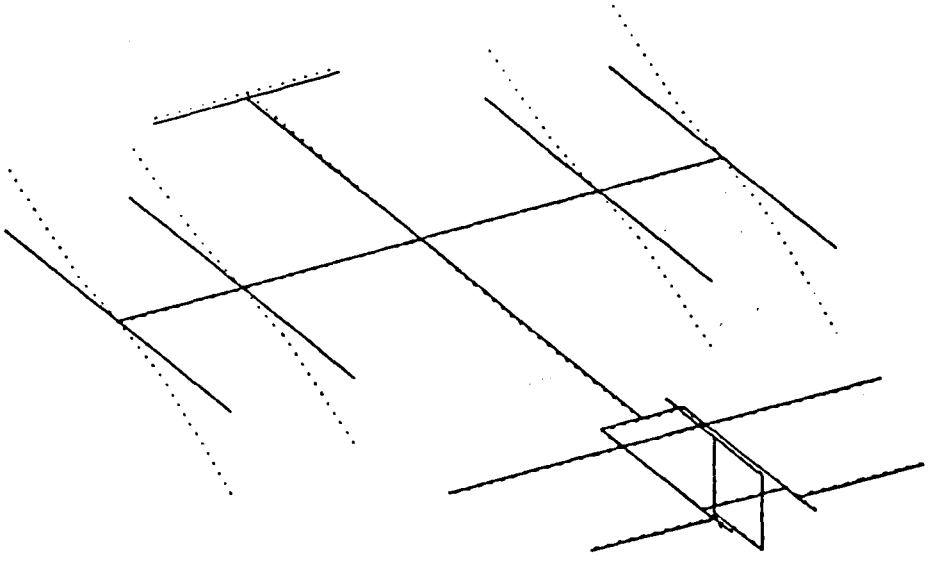
Diagram showing a structure with solid and dotted lines representing motion. The structure is similar to the one in the left diagram, with a central rectangular frame and various extending lines. The dotted lines indicate the motion of the structure at a slightly higher frequency.

Freq. = 0.1770 Hz.

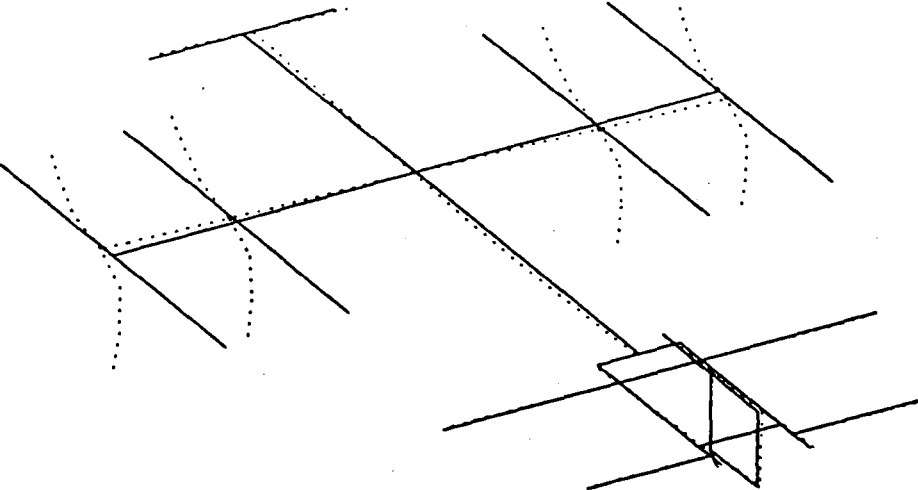
Figure 5. Selected Array Mast Dominated Modes With Some Primary Structure Motion in the Absence of Payloads and Orbiter



Freq. = 0.1385 Hz.

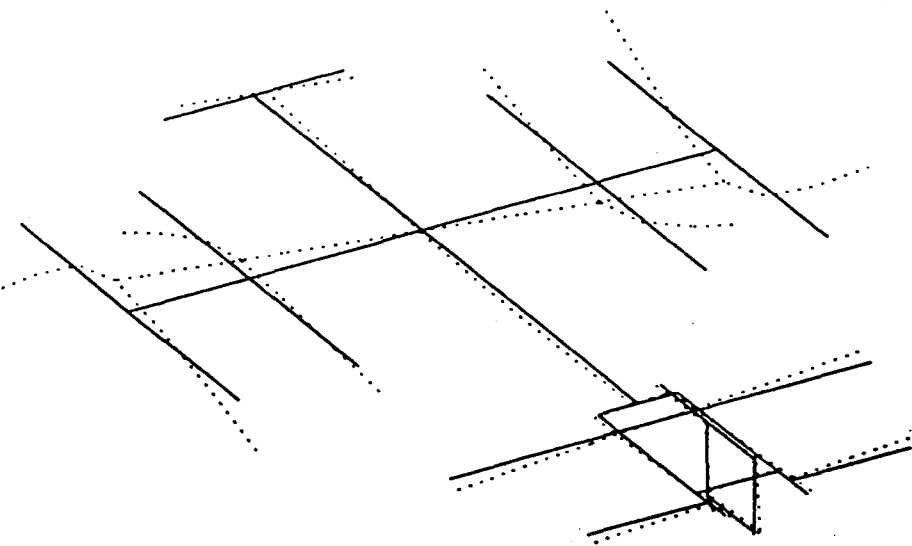


Freq. = 0.1479 Hz.

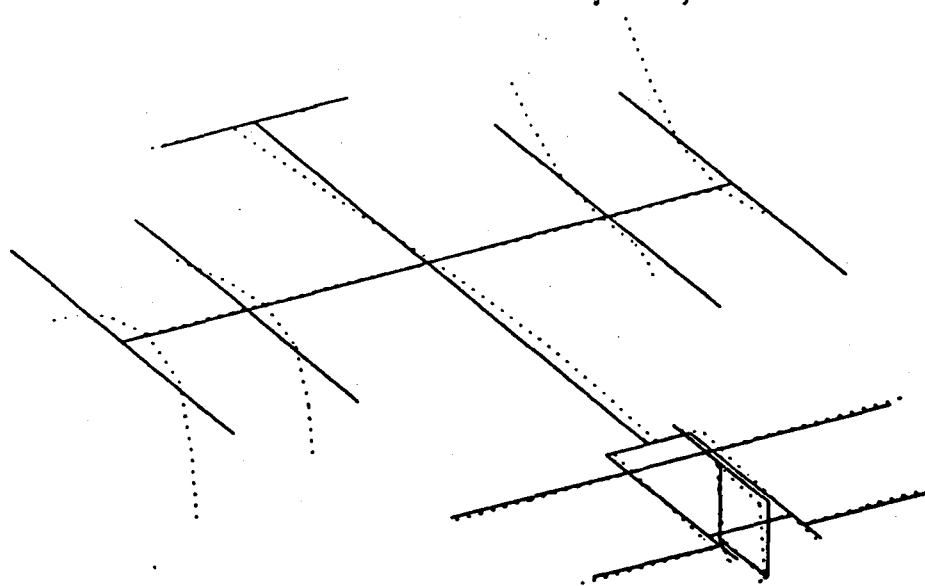


Freq. = 0.1502 Hz.

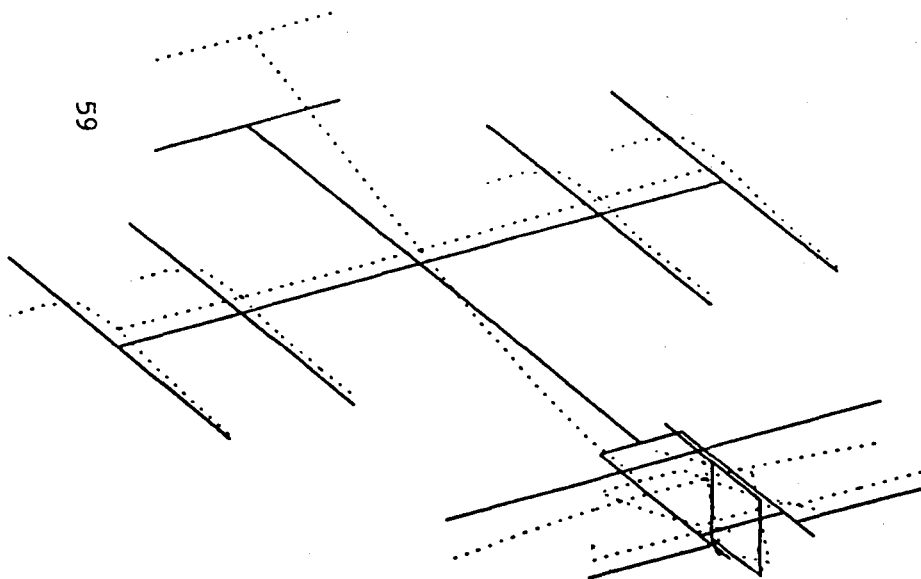
Figure 6. Primary Structure Deformation Modes Below Array Mast Cantilever
Modes in the Absence of Payloads and Oribter



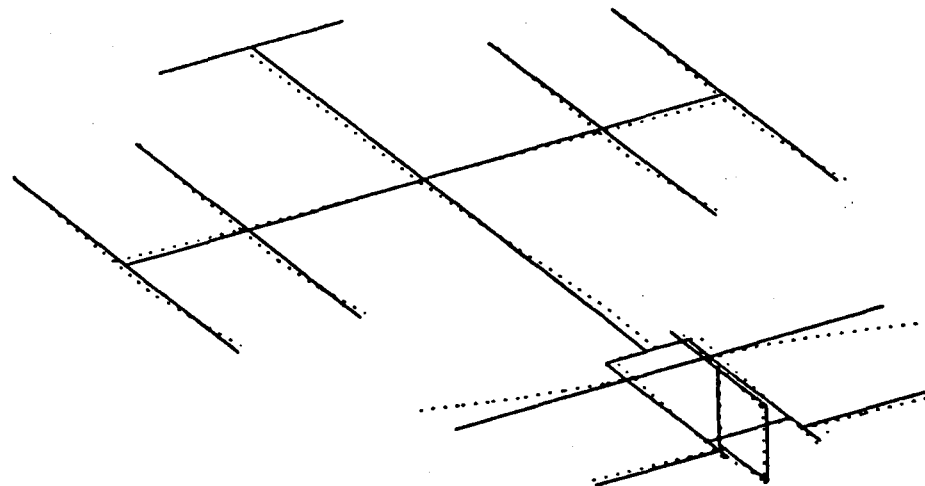
Freq. = 0.2094 Hz.



Freq. = 0.2126 Hz.

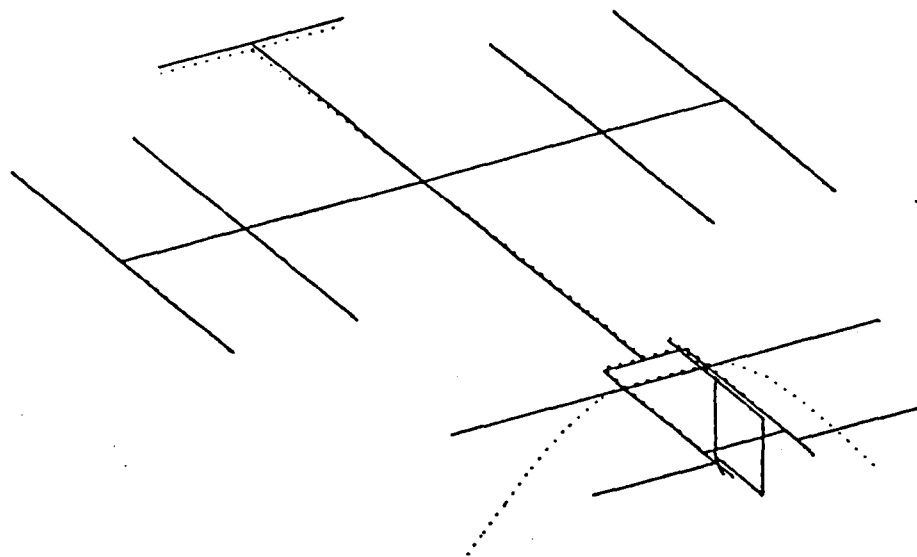


Freq. = 0.2640 Hz.

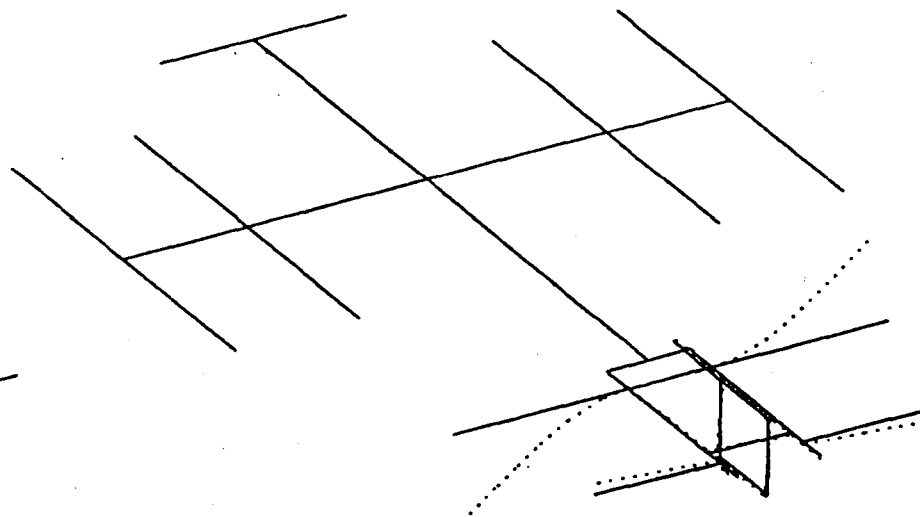


Freq. = 0.5218 Hz.

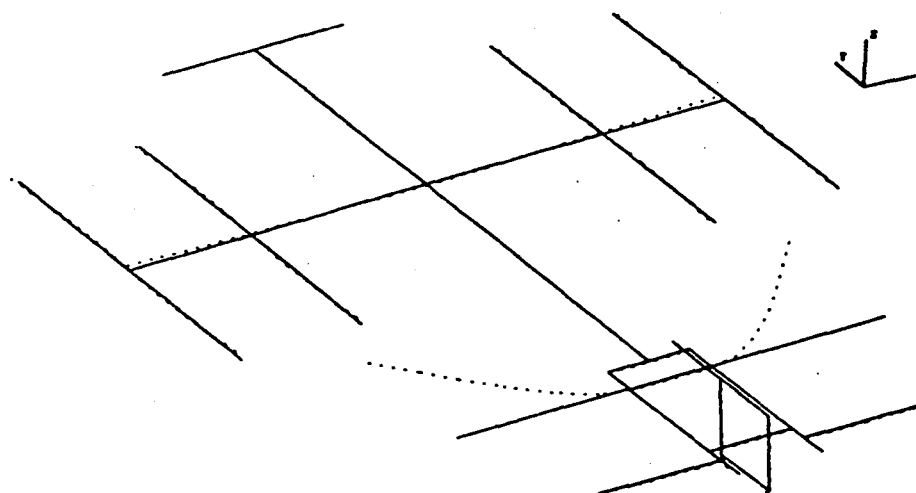
Figure 7. Selected Primary Structure Modes Above Array Mast Cantilever Modes
in the Absence of Payloads and Orbiter



Freq. = 0.5721 Hz.

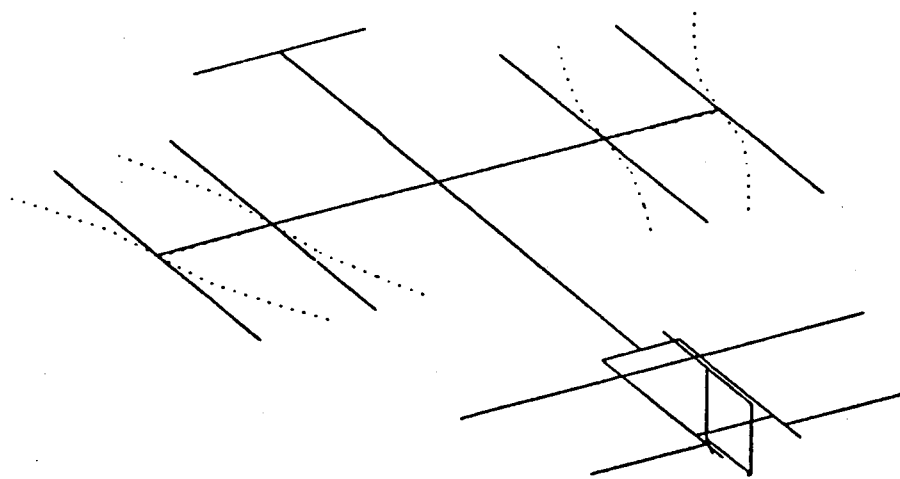


Freq. = 0.5866 Hz.

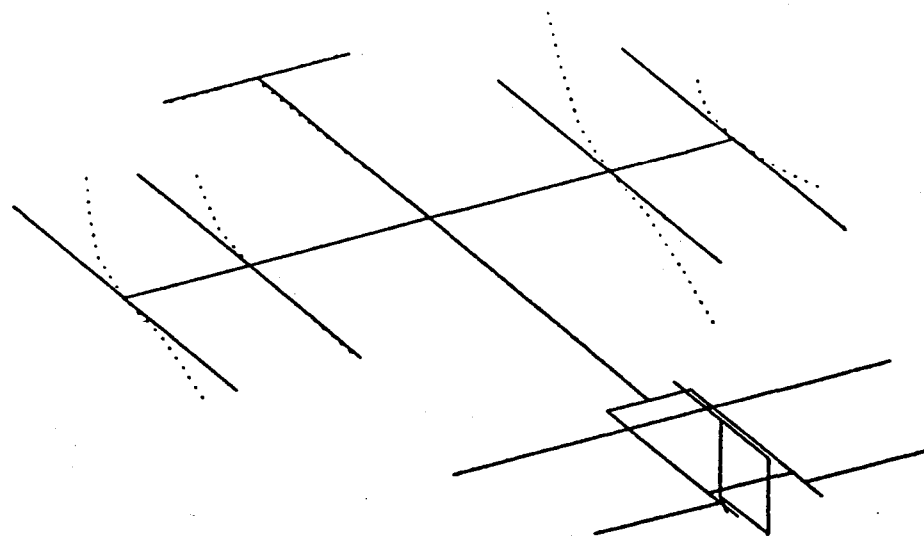


Freq. = 0.5920 Hz.

Figure 8. Selected Radiator Mast Modes in the Absence of Payloads and Orbiter

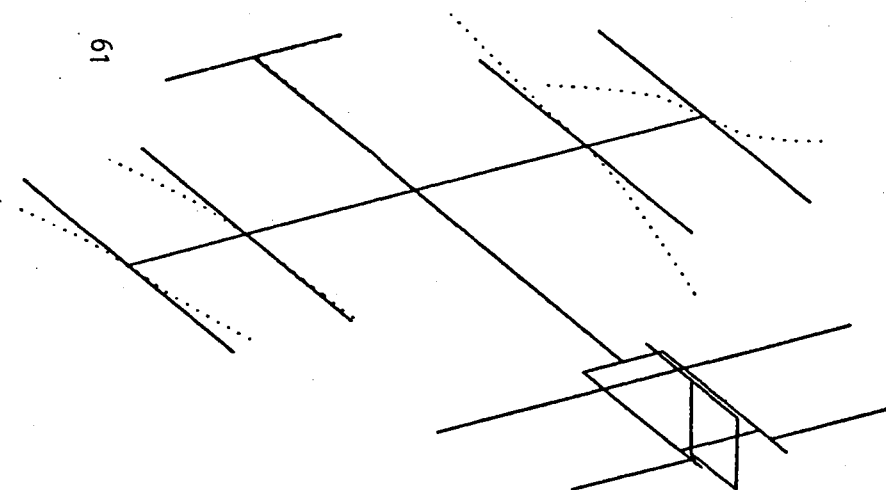


Freq. = 0.1613 Hz.

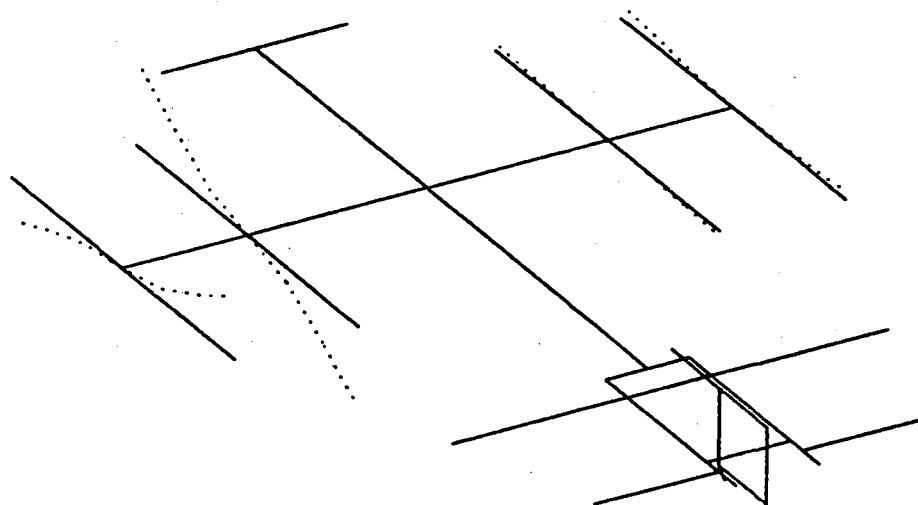


Freq. = 0.1623 Hz.

19

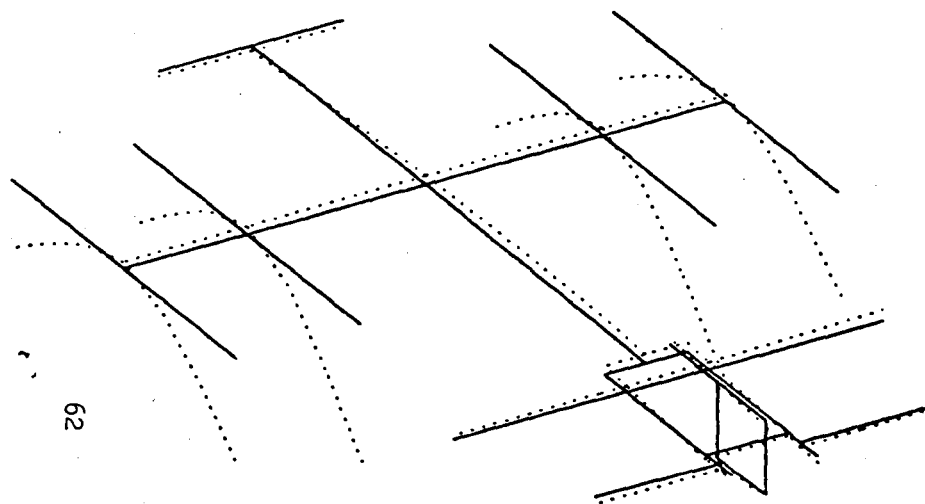


Freq. = 0.1631 Hz.

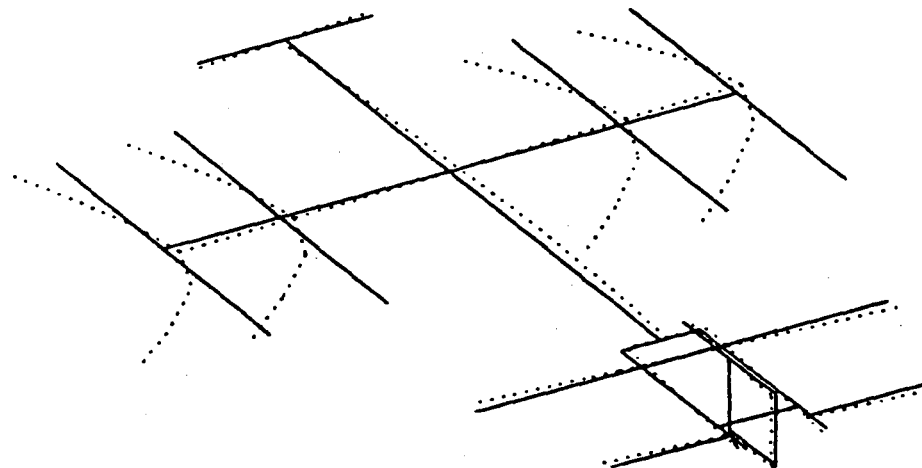


Freq. = 0.1631 Hz.

Figure 9. Selected Array Mast Dominated Modes With Payloads Attached

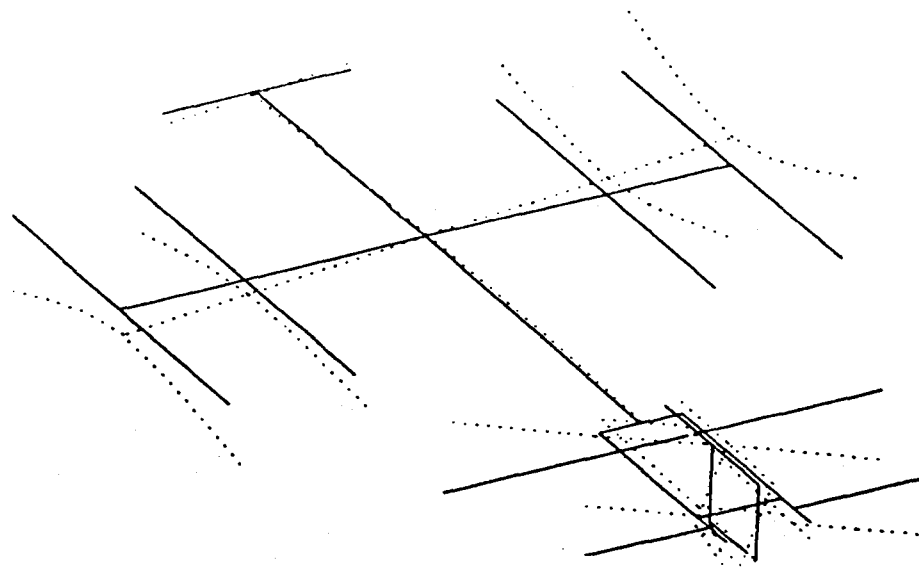


Freq. = 0.1733 Hz.

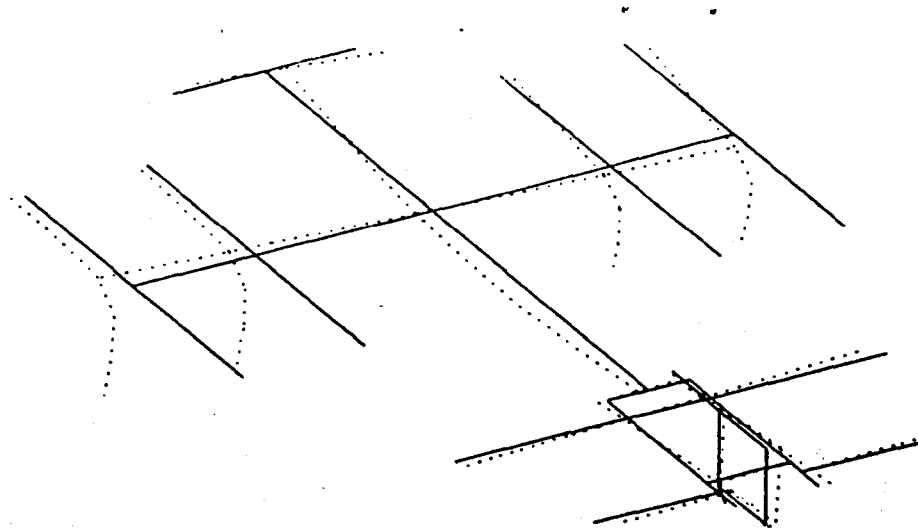


Freq. = 0.1778 Hz.

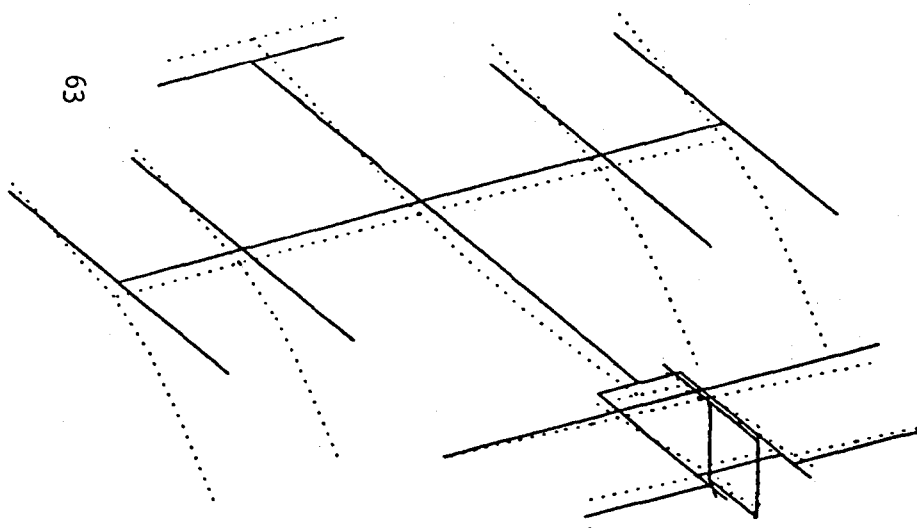
Figure 10. Selected Array Mast Dominated Modes With Some Primary Structure Motion and With Payloads Attached



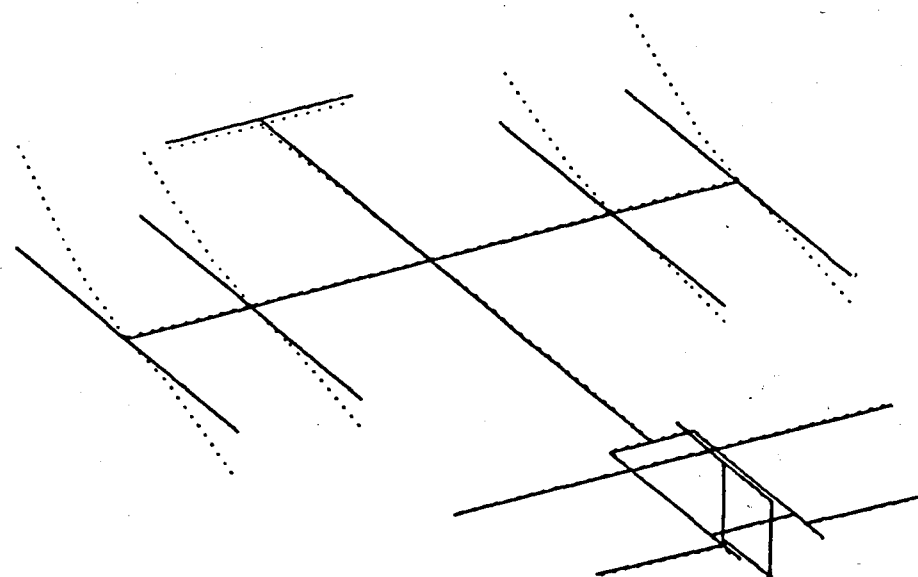
Freq. = 0.1233 Hz.



Freq. = 0.1304 Hz.

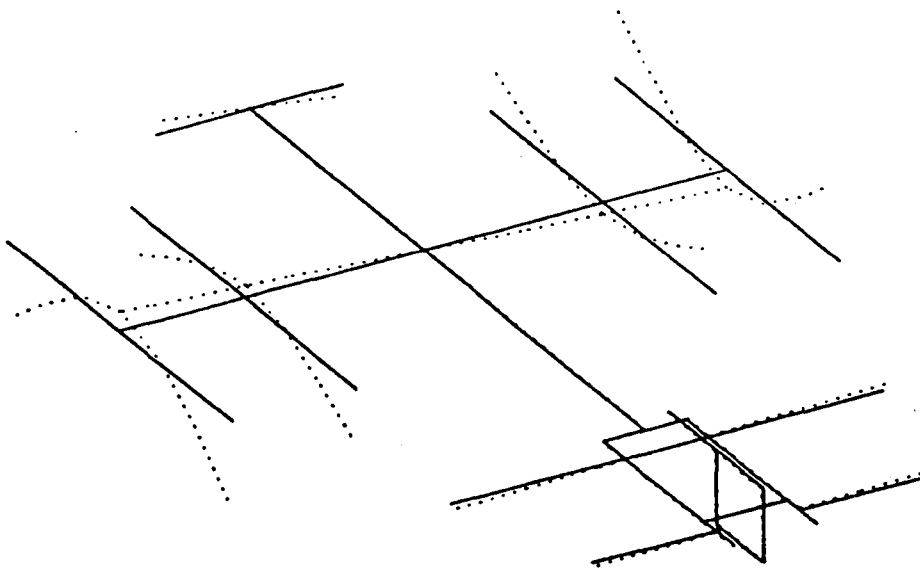


Freq. = 0.1317 Hz.

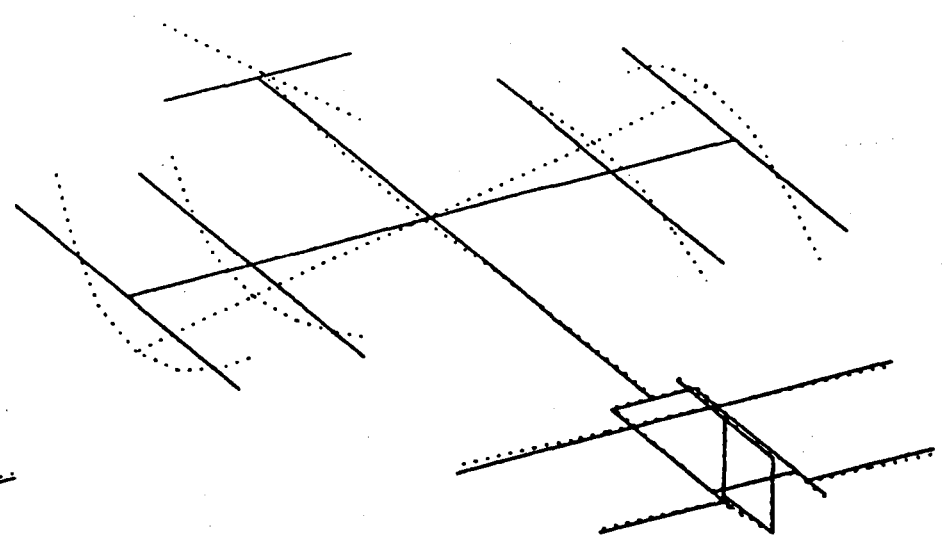


Freq. = 0.1542 Hz.

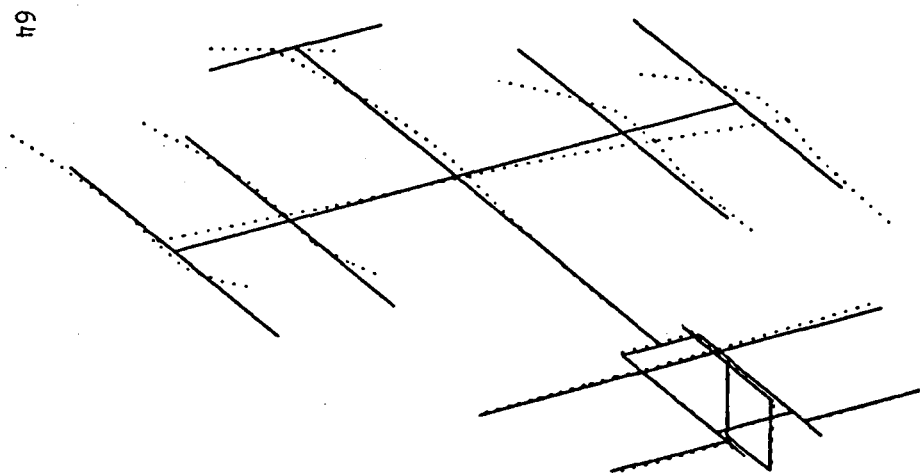
Figure 11. Primary Structure Modes Below Array Mast Cantilever Modes With Payloads Attached



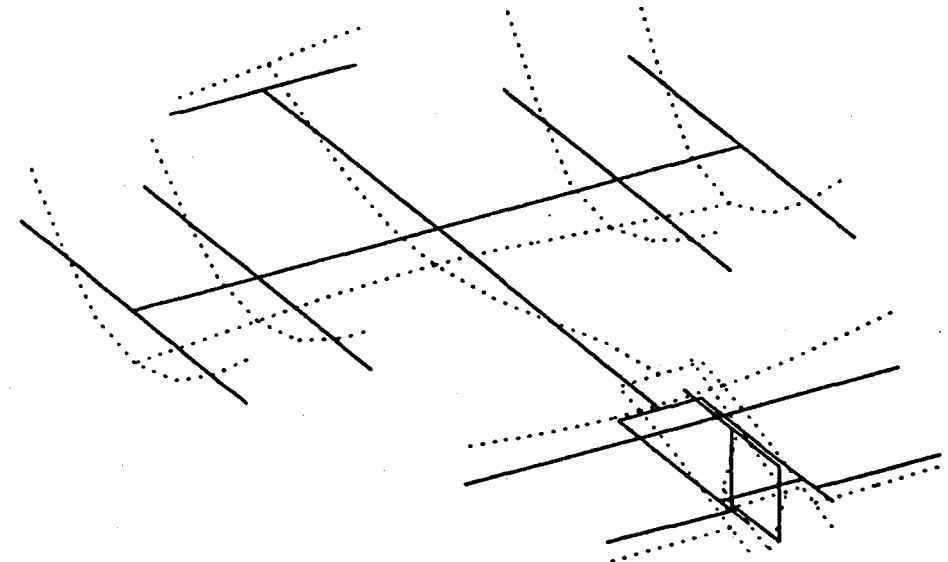
Freq. = 0.1983 Hz.



Freq. = 0.2988 Hz.

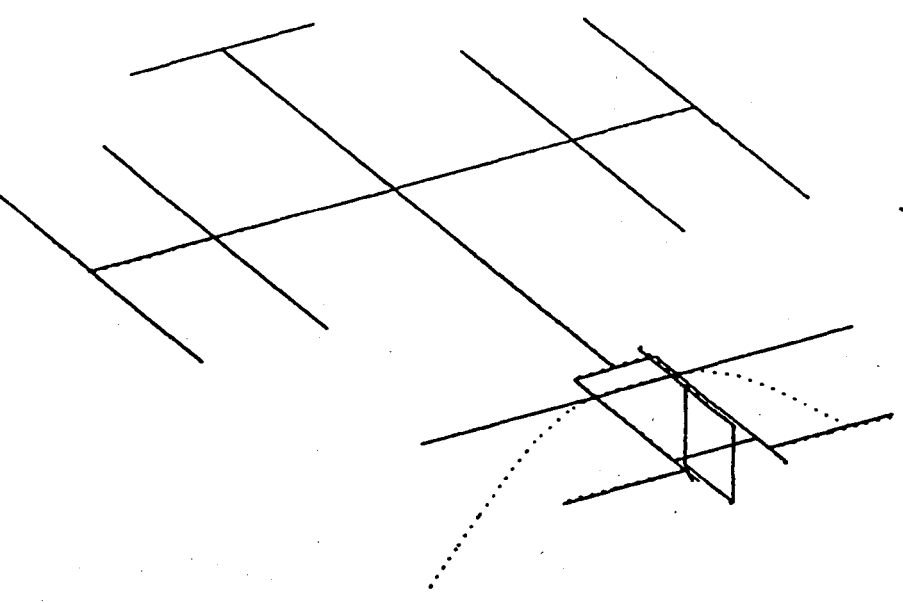


Freq. = 0.3190 Hz.

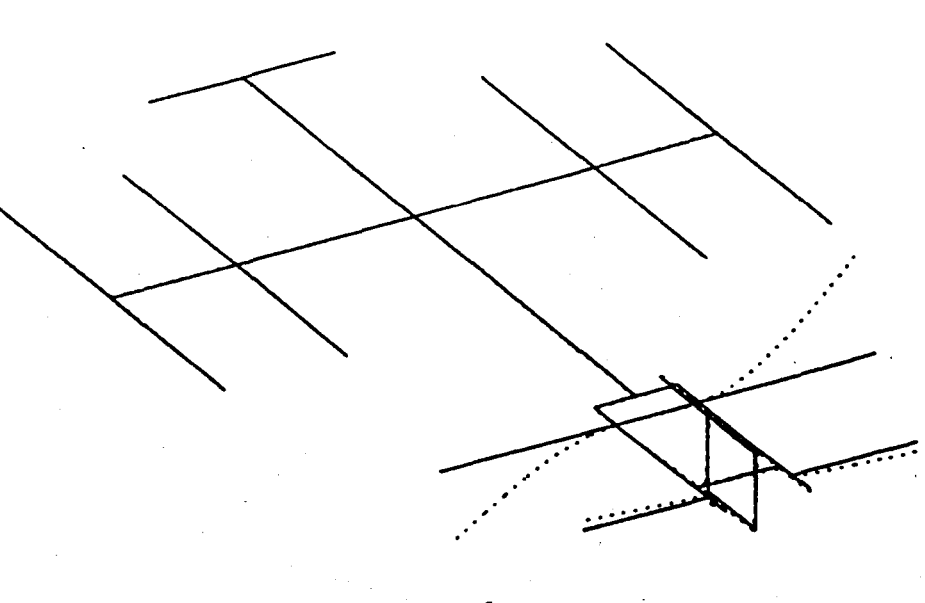


Freq. = 0.3195 Hz.

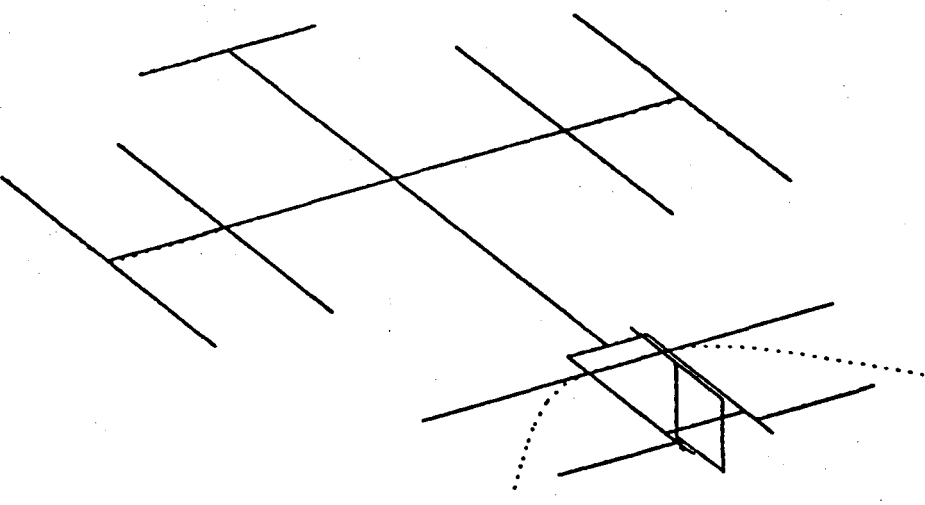
Figure 12. Selected Primary Structure Dominated Modes Above Array Mast
Cantilever Mode With Payloads Attached



Freq. = 0.5702 Hz.

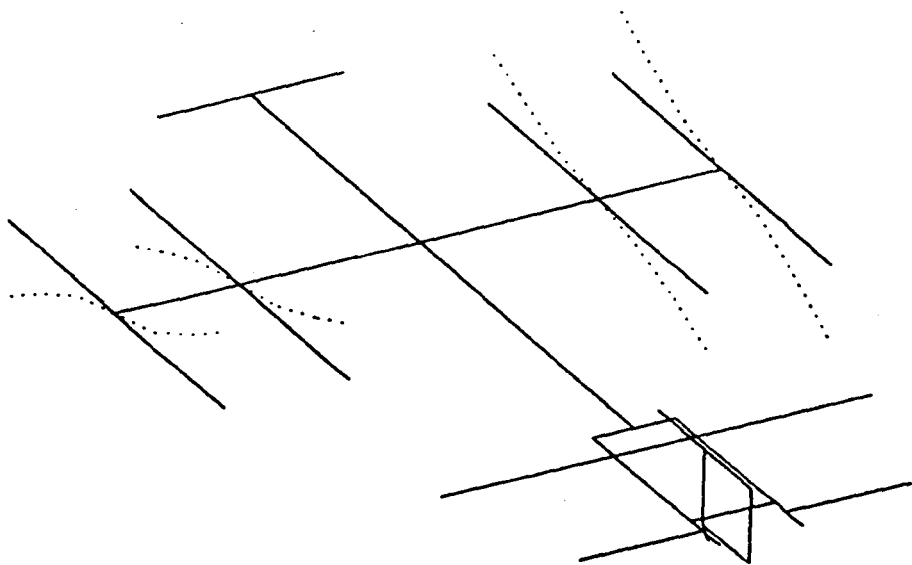


Freq. = 0.5785 Hz.

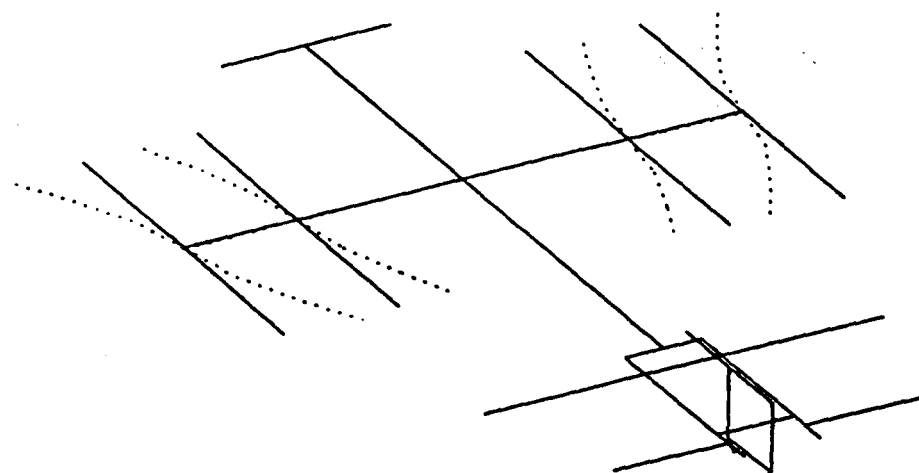


Freq. = 0.5897 Hz.

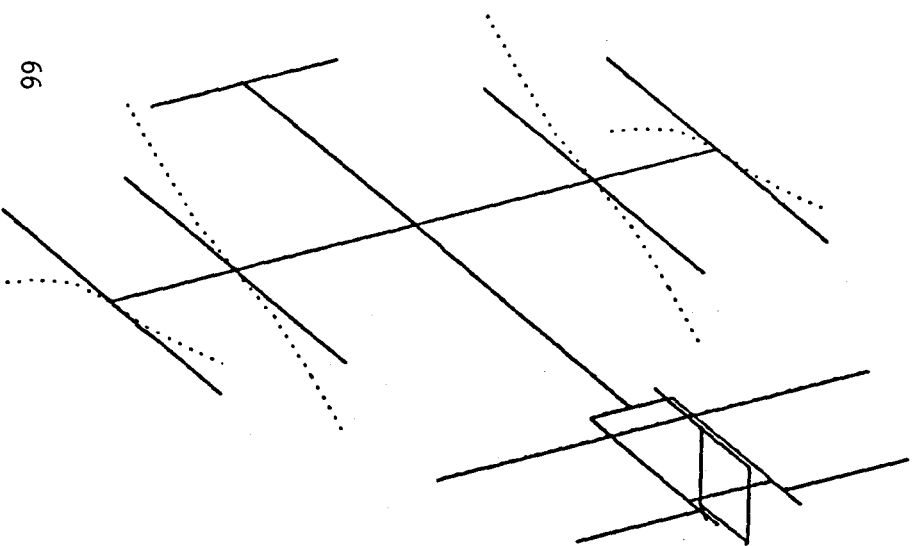
Figure 13. Selected Radiator Mast Modes With Payloads Attached



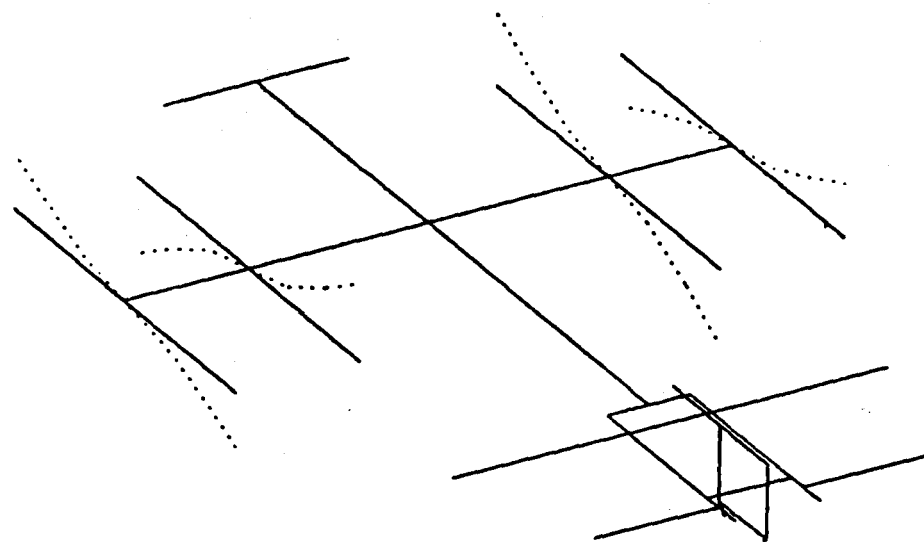
Freq. = 0.1525 Hz.



Freq. = 0.1613 Hz.

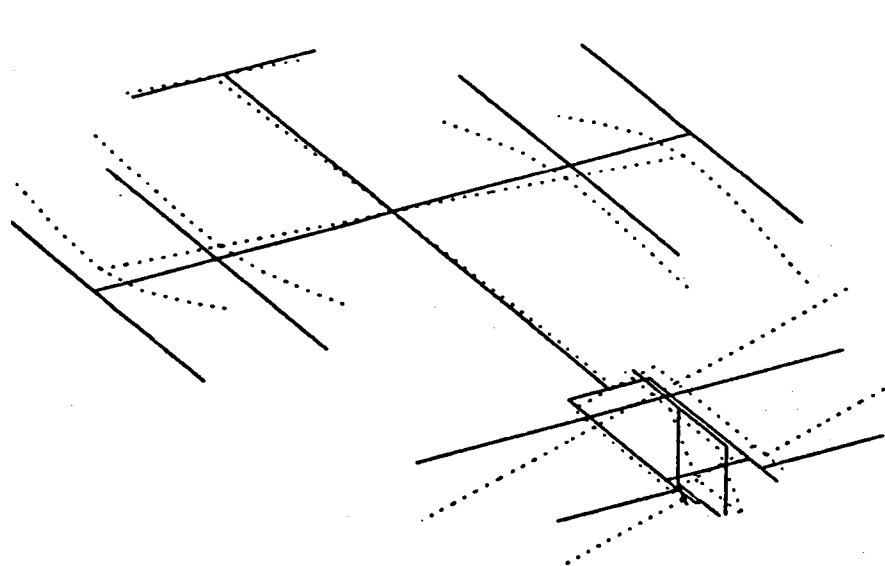


Freq. = 0.1632 Hz.

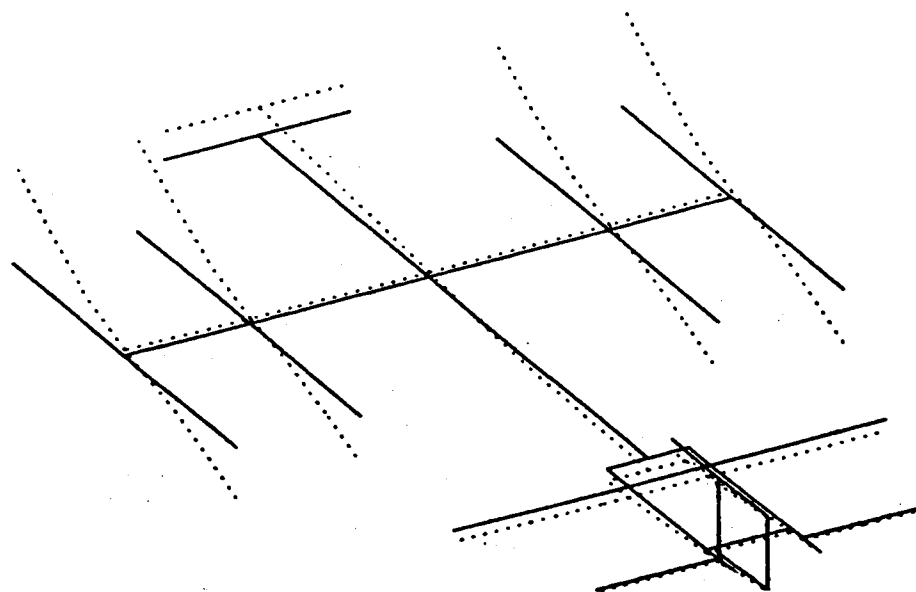


Freq. = 0.1632 Hz.

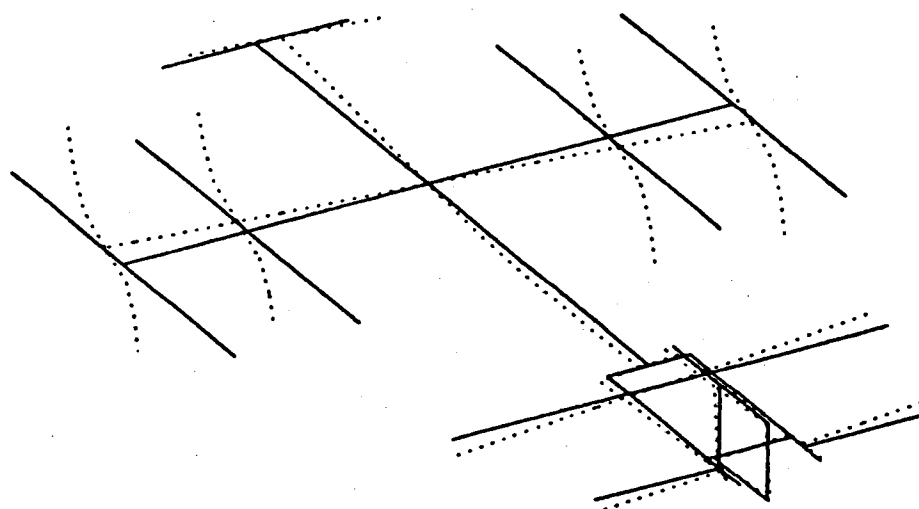
Figure 14. Selected Array Mast Modes With Orbiter Attached



Freq. = 0.1200 Hz.

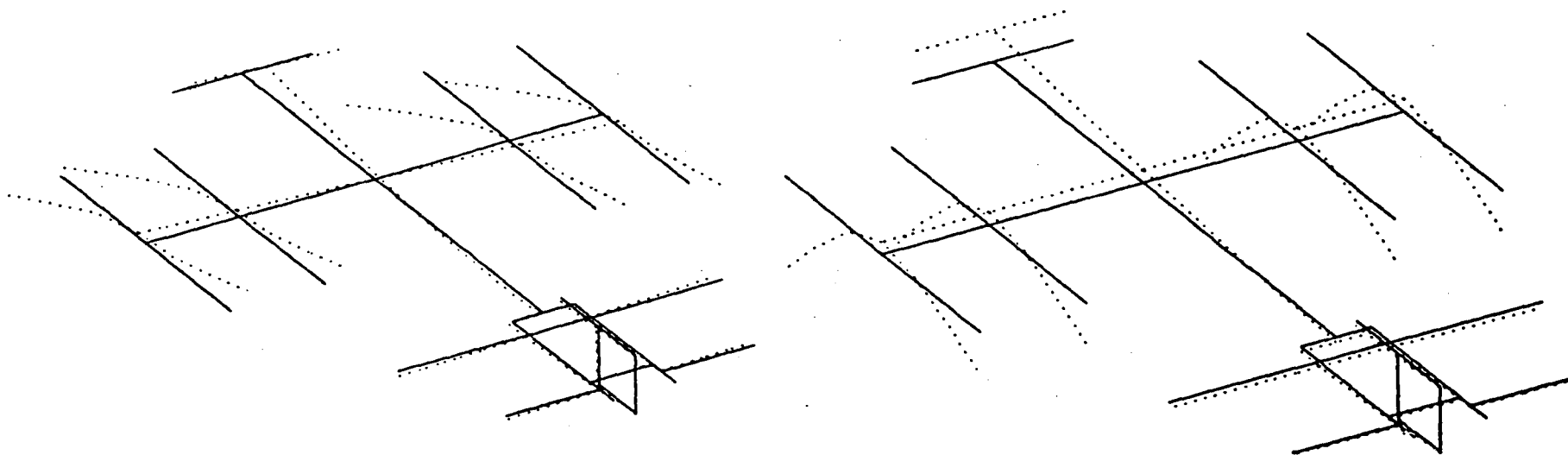


Freq. = 0.1345 Hz.



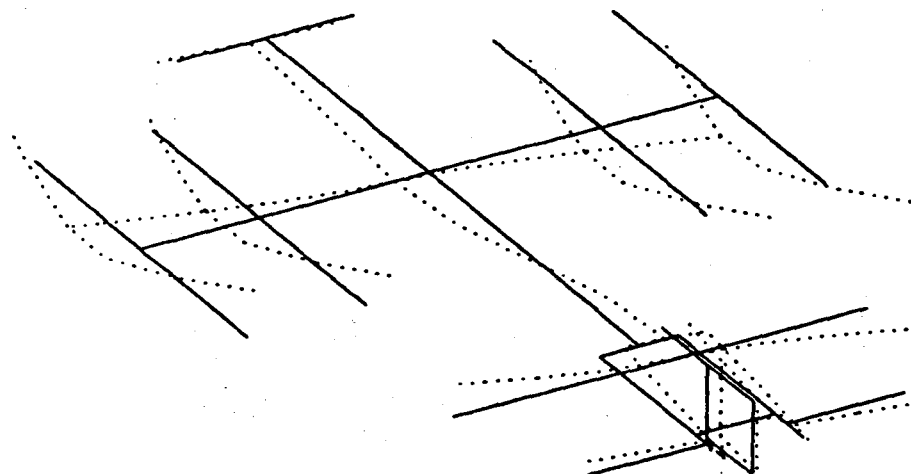
Freq. = 0.1376 Hz.

Figure 15. Primary Structure Modes Below Array Mast Modes With Orbiter Attached



Freq. = 0.1840 Hz.

Freq. = 0.1877 Hz.



Freq. = 0.4030 Hz.

Figure 16. Selected Primary Structure Modes Above Array Mast Cantilever Mode With Orbiter Attached

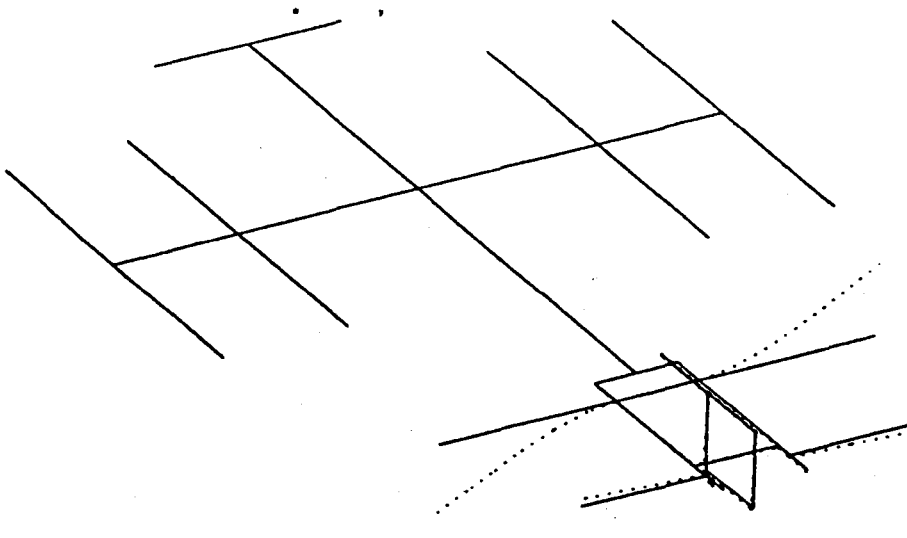


Diagram showing the radiator mast mode at 0.5650 Hz. The structure consists of a central rectangular frame with multiple diagonal bracing members. Dotted lines indicate the deflected shape of the mast, showing a significant lateral displacement at the top.

Freq. = 0.5650 Hz.

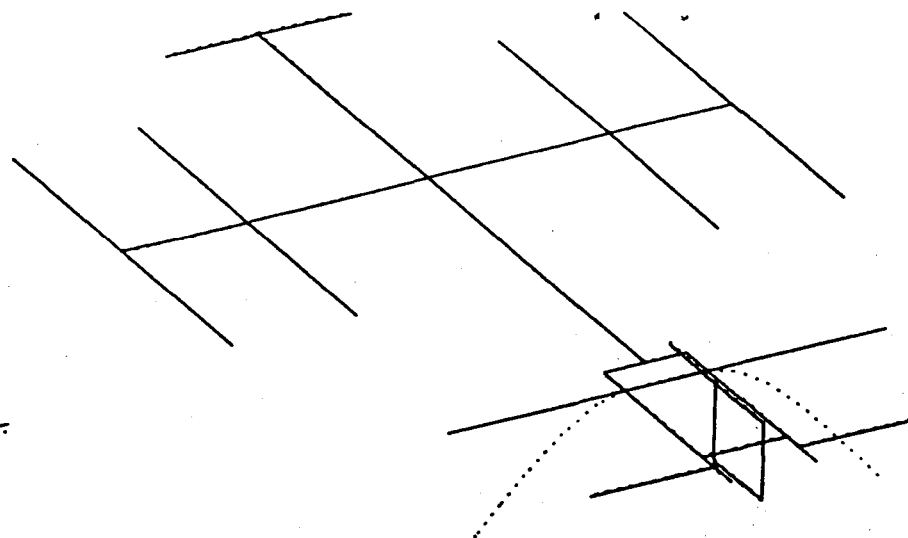


Diagram showing the radiator mast mode at 0.5676 Hz. The structure is similar to the previous one, but the deflection pattern (indicated by dotted lines) shows a different lateral displacement profile.

Freq. = 0.5676 Hz.

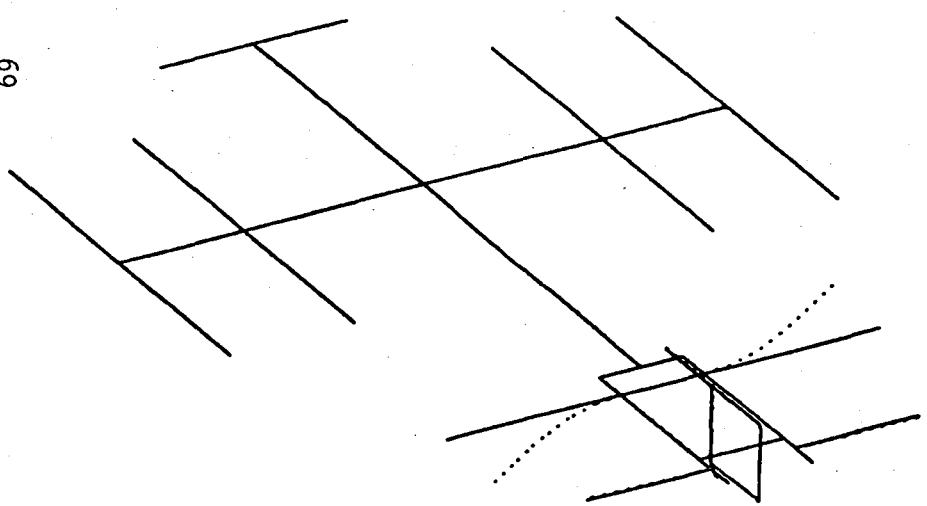


Diagram showing the radiator mast mode at 0.5881 Hz. The deflection pattern (dotted lines) shows a more pronounced lateral displacement compared to the lower frequency modes.

Freq. = 0.5881 Hz.

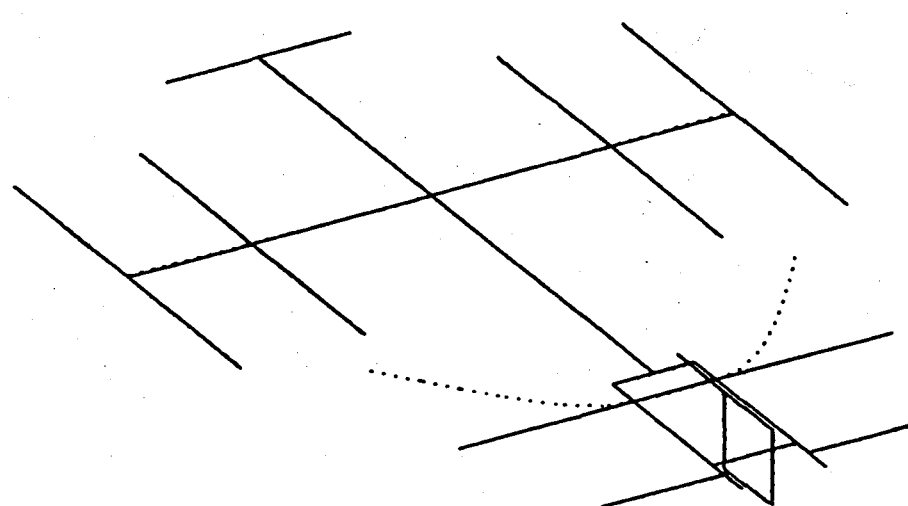
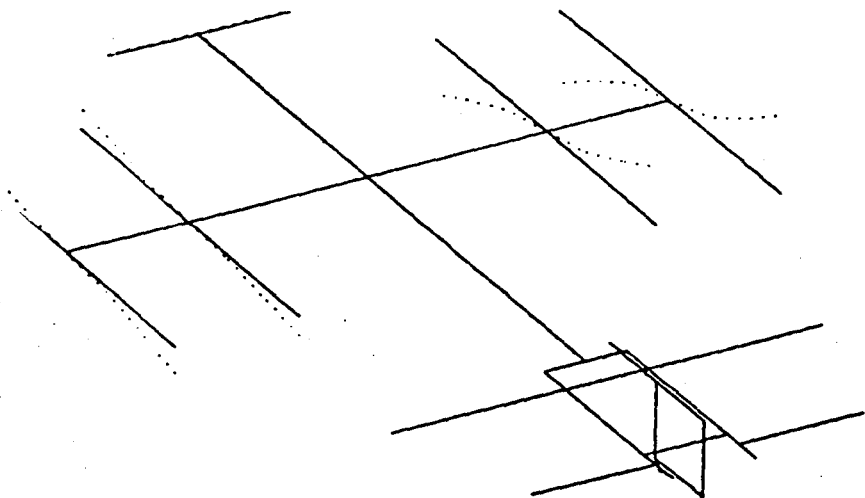


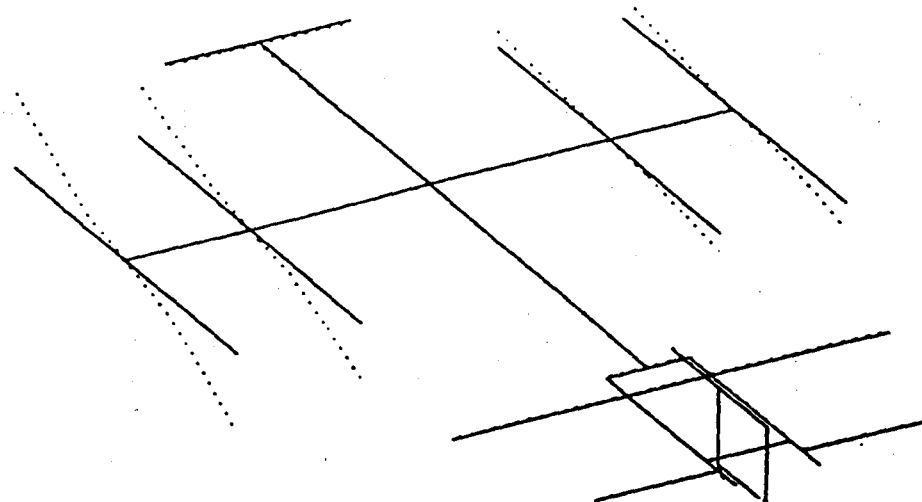
Diagram showing the radiator mast mode at 0.5890 Hz. The deflection pattern (dotted lines) shows a lateral displacement similar to the 0.5881 Hz mode.

Freq. = 0.5890 Hz.

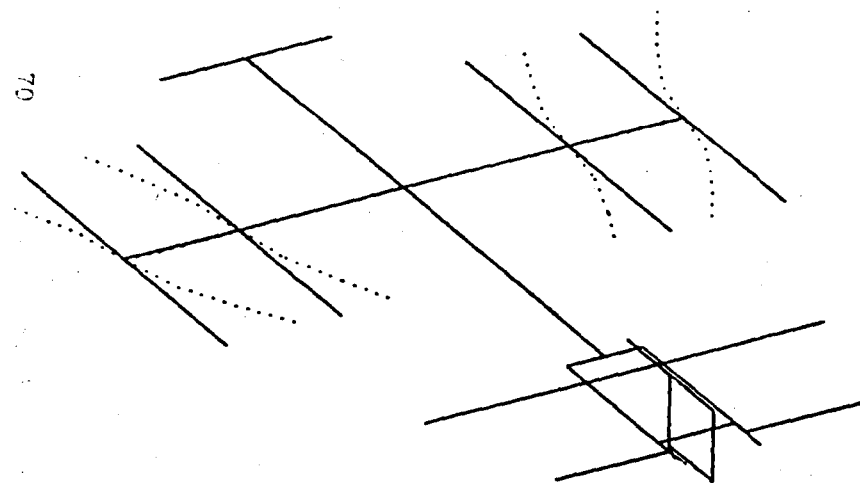
Figure 17. Selected Radiator Mast Modes With Orbiter Attached



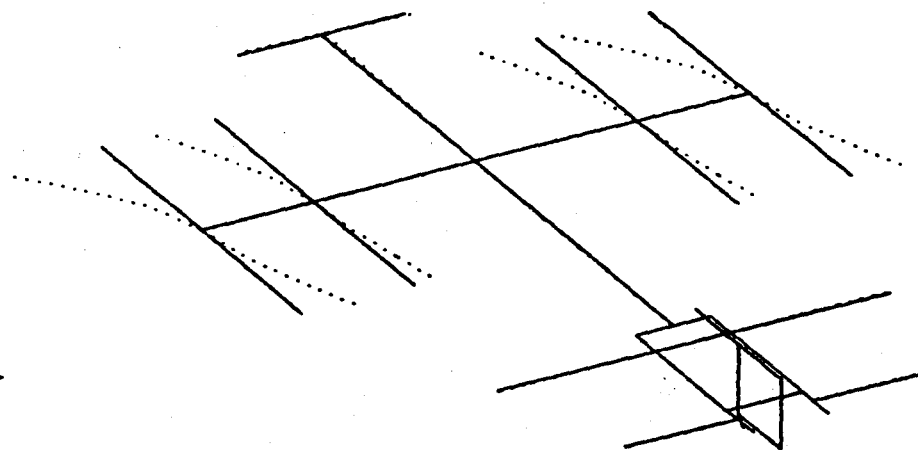
Freq. = 0.1515 Hz.



Freq. 0.1530 Hz.

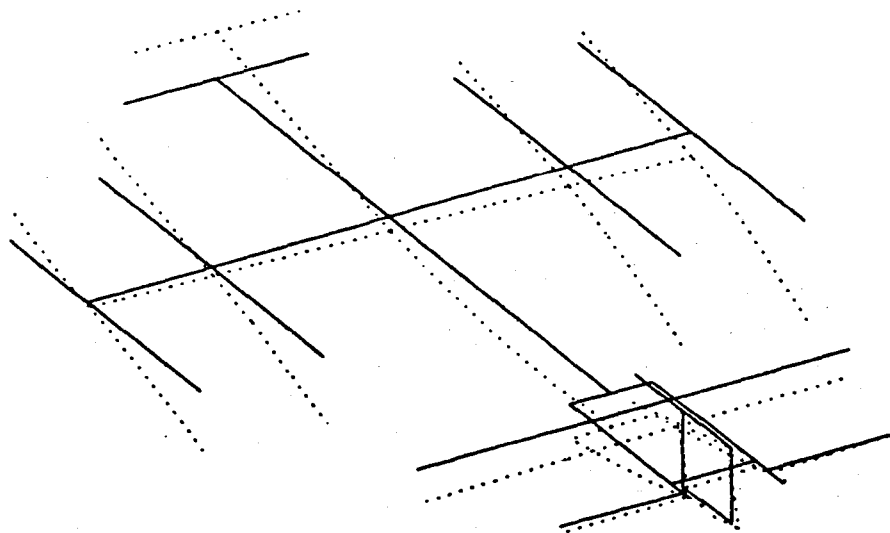


Freq. = 0.1613 Hz.

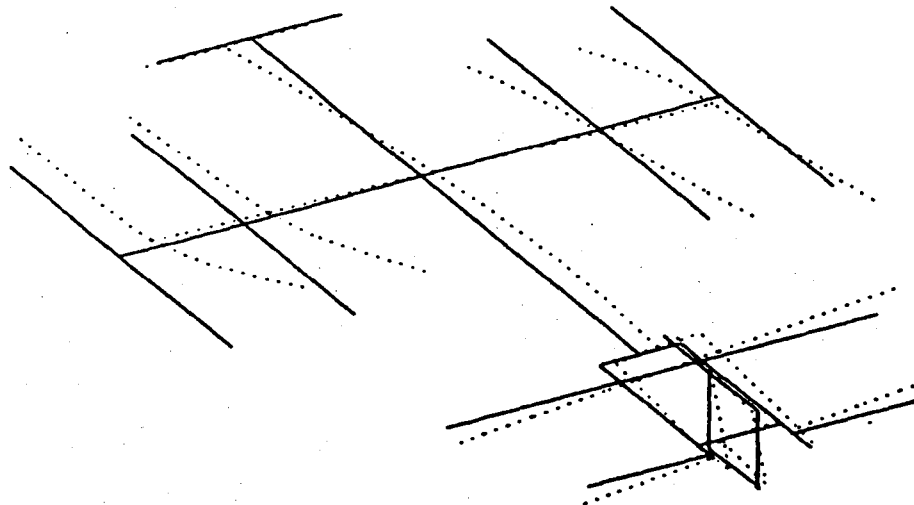


Freq. = 0.1626 Hz.

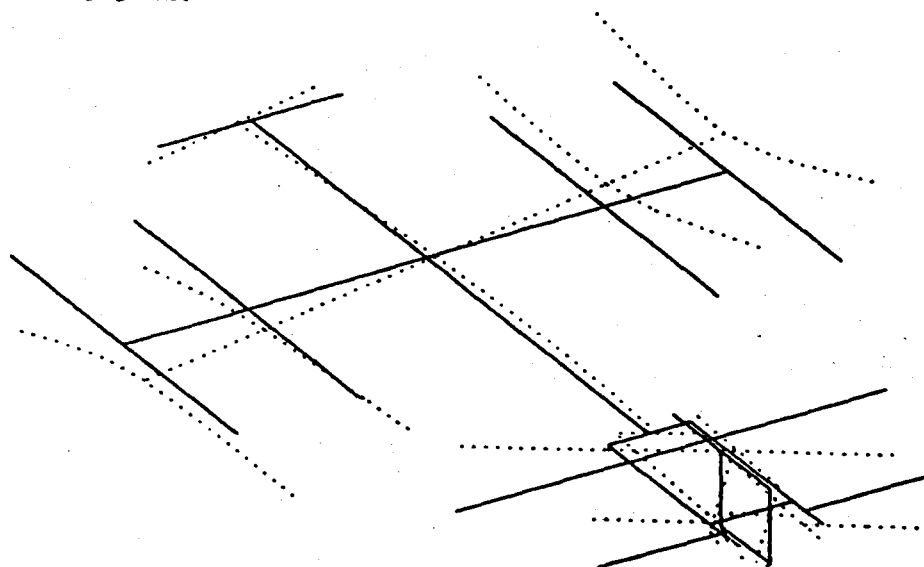
Figure 18. Selected Array Mast Dominated Modes With Both Payloads and Orbiter Attached



Freq. = 0.0965 Hz.

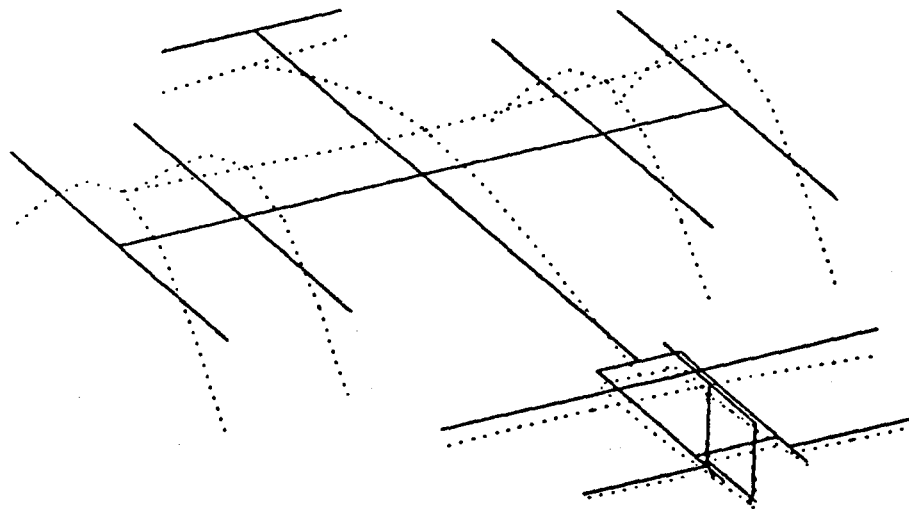


Freq. = 0.1020 Hz.

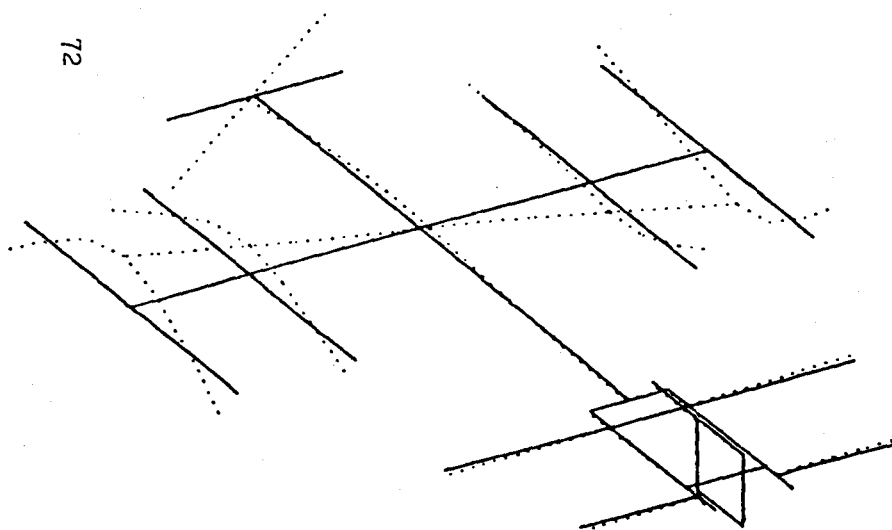


Freq. = 0.1139 Hz.

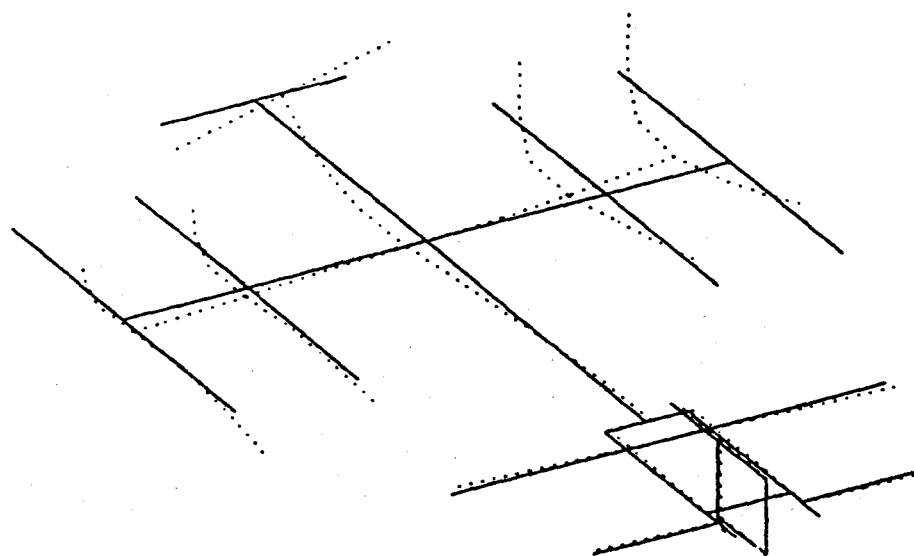
Figure 19. Primary Structure Modes Below Array Mast Canitlever Mode With Both Payloads and Orbiter Attached



Freq. = 0.2627 Hz.

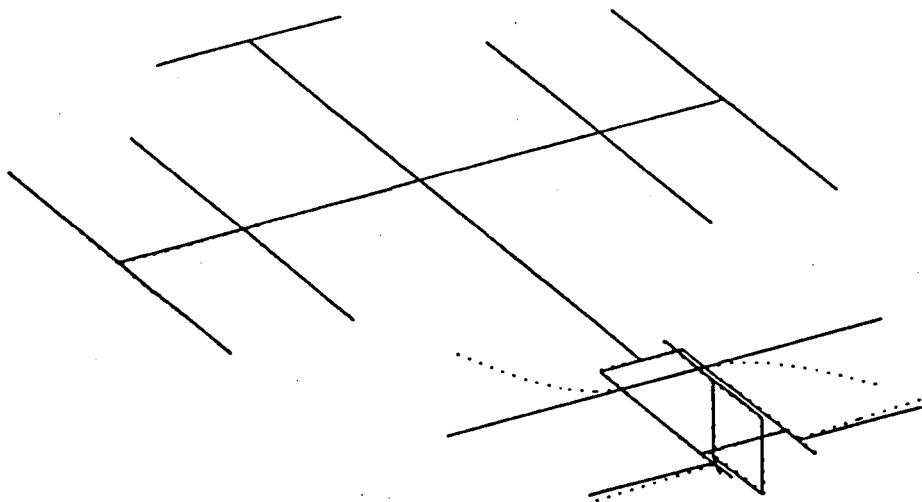


Freq. = 0.2983 Hz.

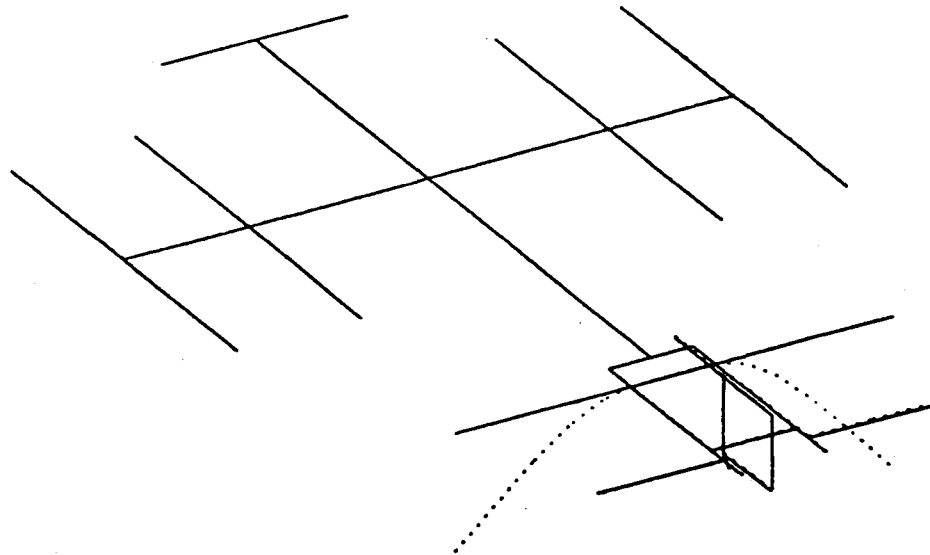


Freq. 0.3168 Hz.

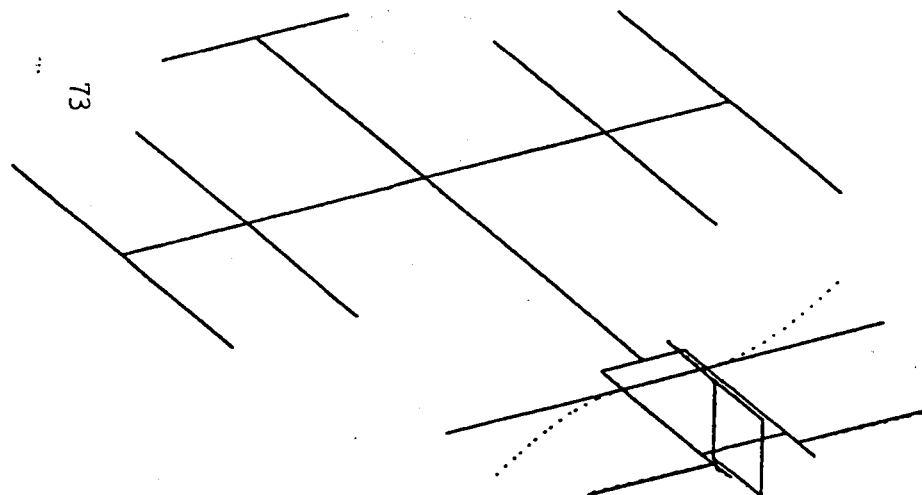
Figure 20. Selected Primary Structure Modes Above Array Mast Cantilever Mode
With Both Payloads and Orbiter Attached



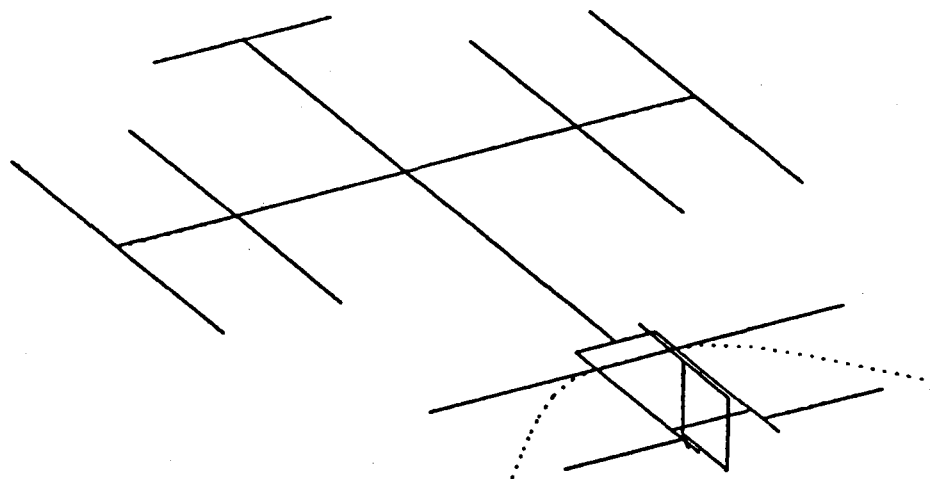
Freq. = 0.5572 Hz.



Freq. = 0.5671 Hz.



Freq. = 0.5874 Hz.



Freq. = 0.5885 Hz.

Figure 21. Selected Radiator Mast Modes With Both Payloads and Orbiter Attached

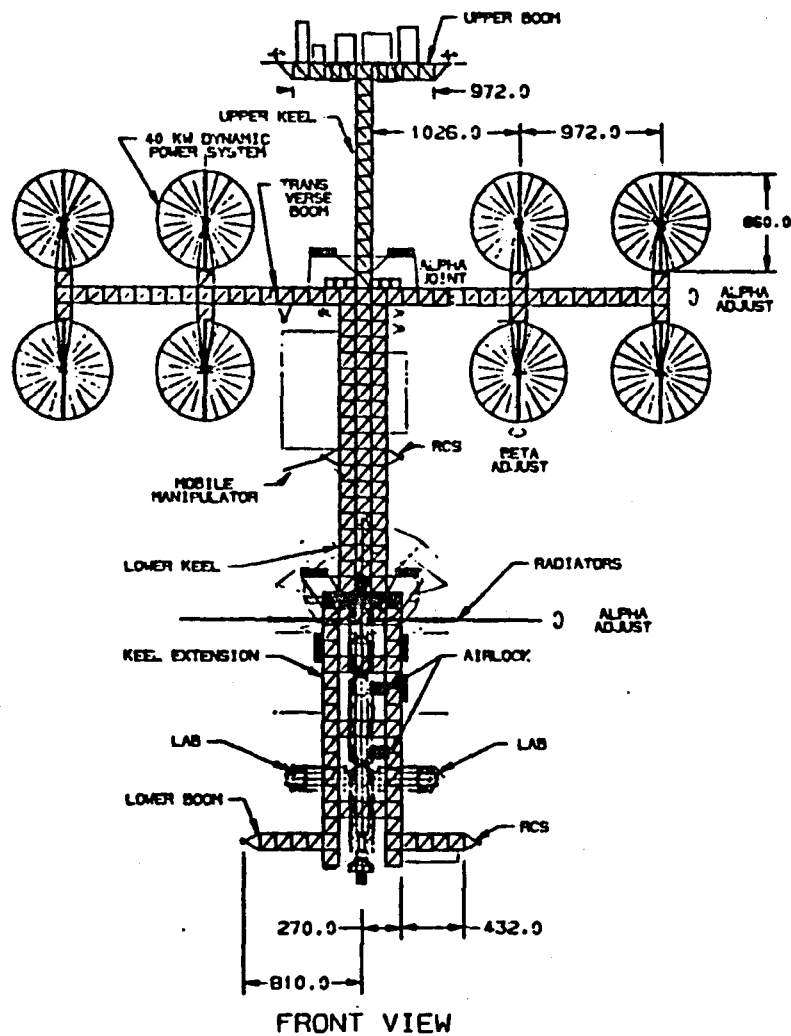
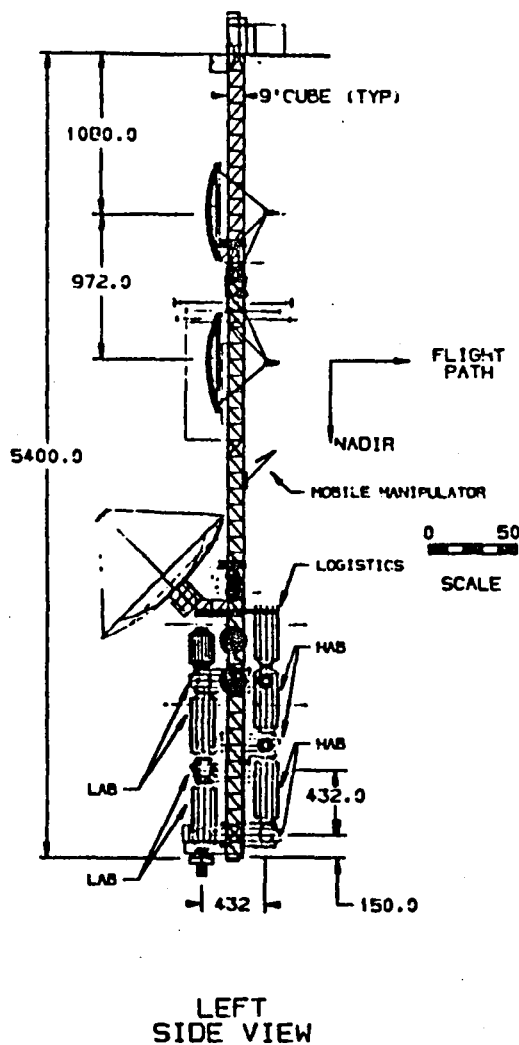
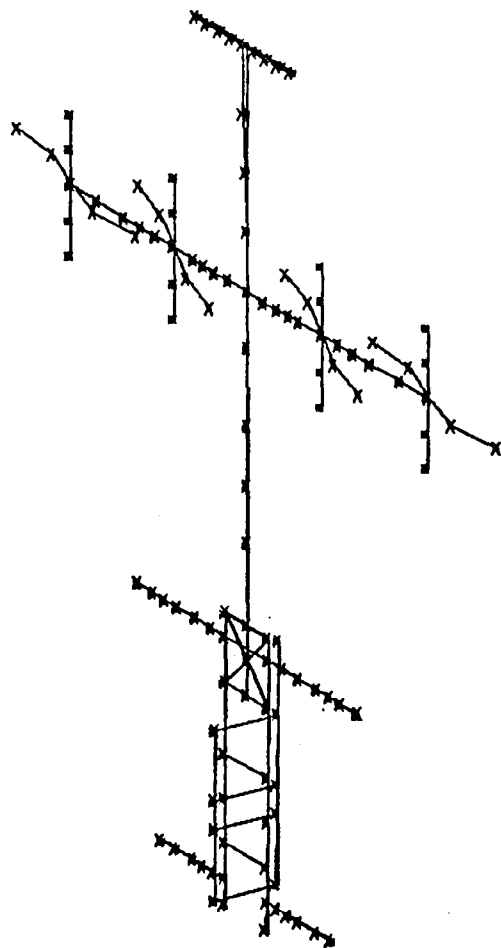
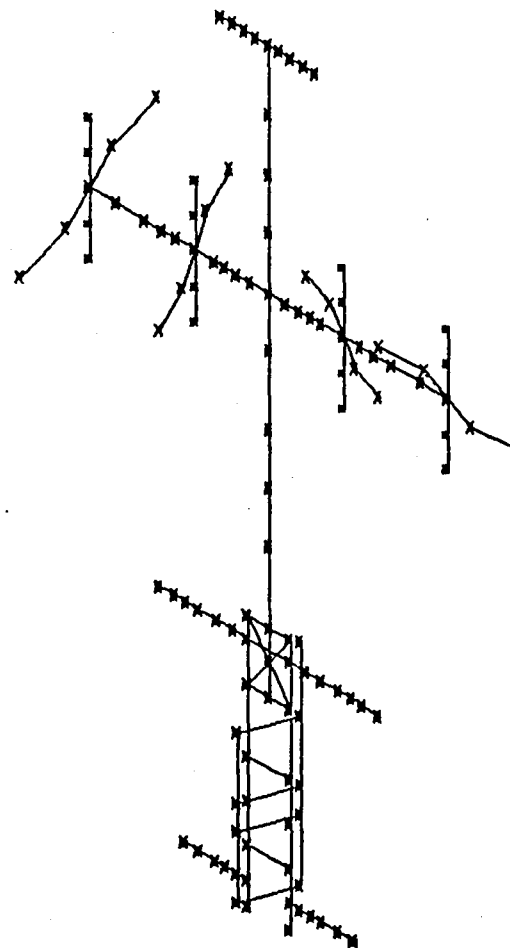


Figure 22. Growth Configuration Used in Dynamic Study

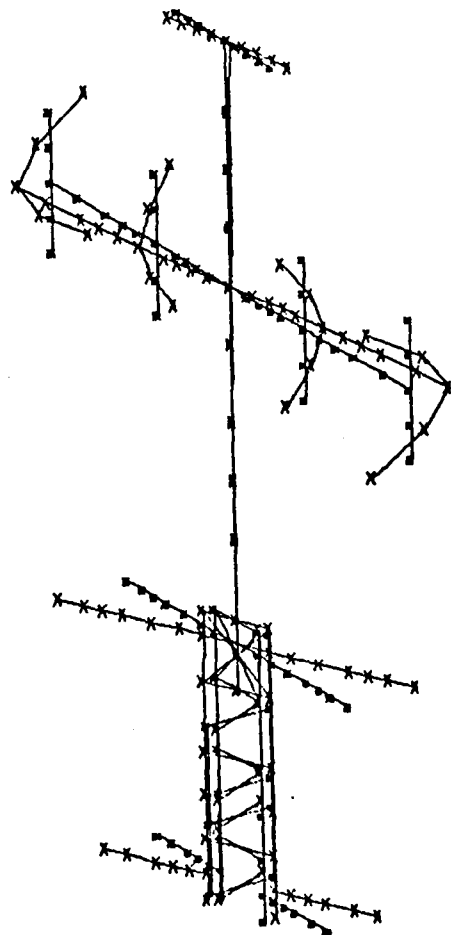


Freq. = 0.1374 Hz.

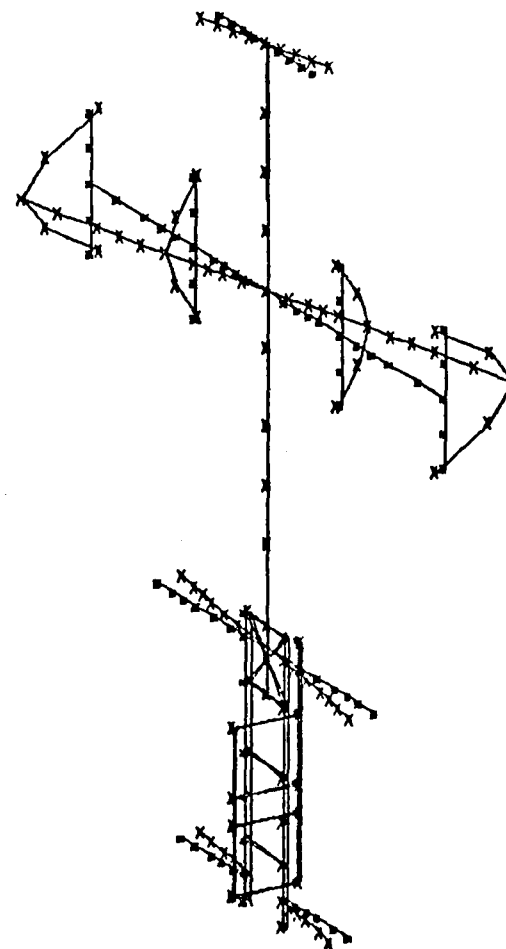


Freq. = 0.1392 Hz.

Figure 23. Selected Solar Collector Support Truss Modes for Growth Configuration

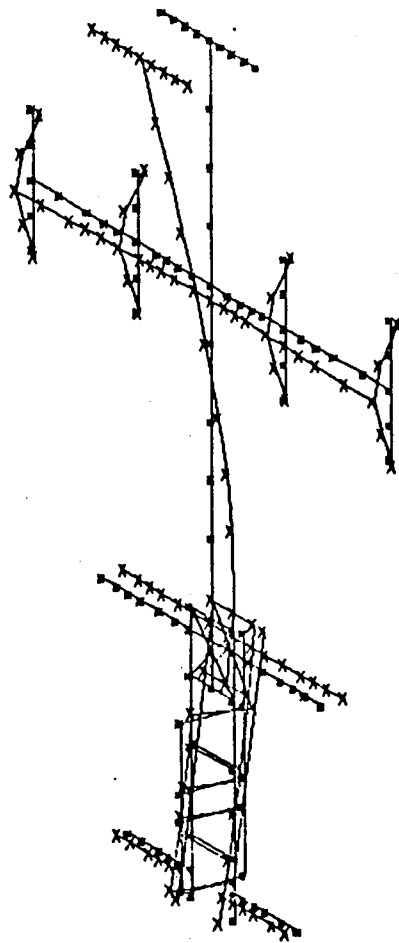


Freq. = 0.2116 Hz.

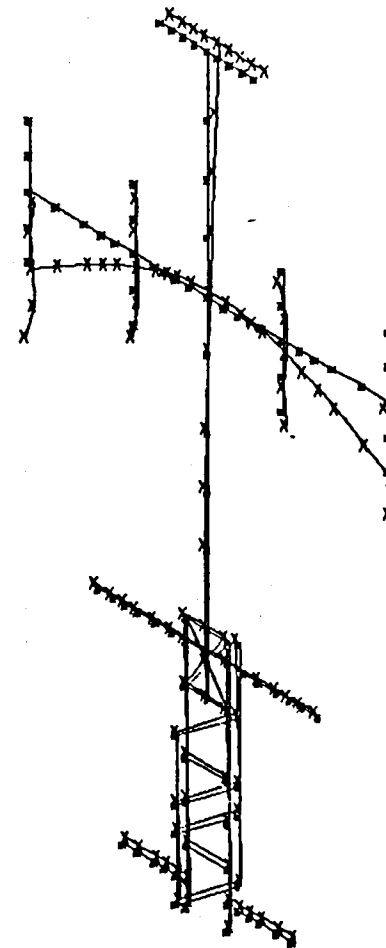


Freq. = 0.4569 Hz.

Figure 24. Selected Twist Modes of Growth Configuration

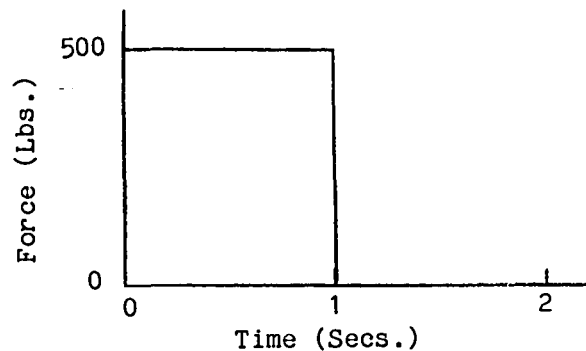


Freq. = 0.3305 Hz.

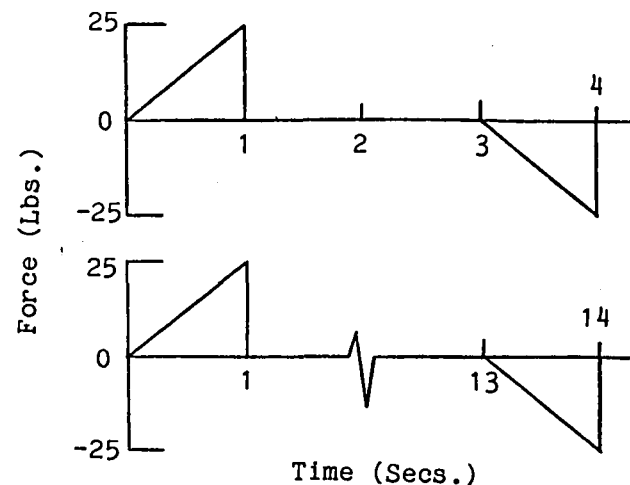


Freq. = 0.3419 Hz.

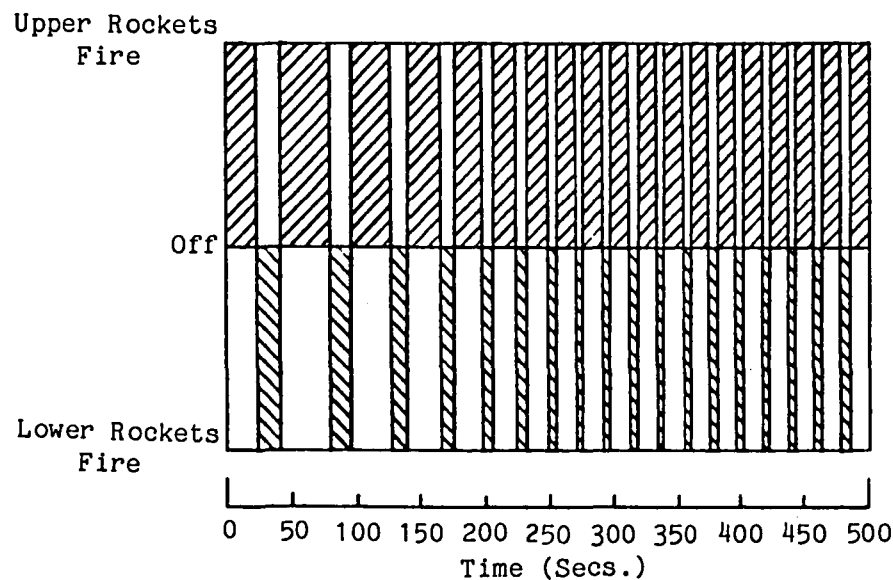
Figure 25. Selected Primary Structure Modes of Growth Configuration



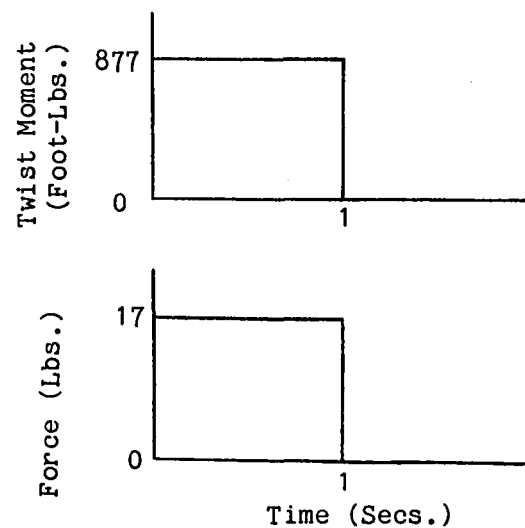
(a) Orbiter Berthing



(b) Transverse and Axial Crew Motions



(c) Reboost Firing Sequence For Upper and Lower-Rocket Pairs



(d) Mobile Remote Manipulator Operations

Figure 26. Time Histories of Four Load Cases

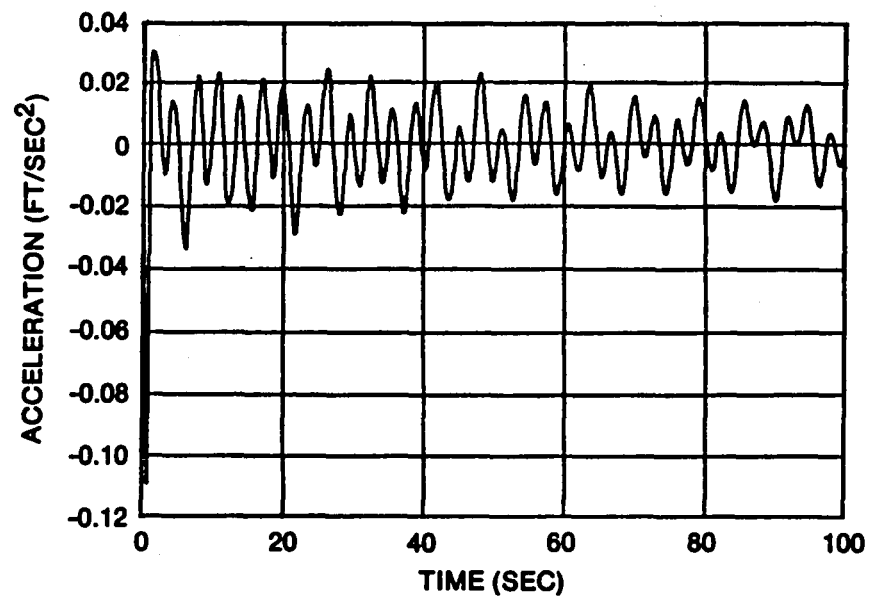
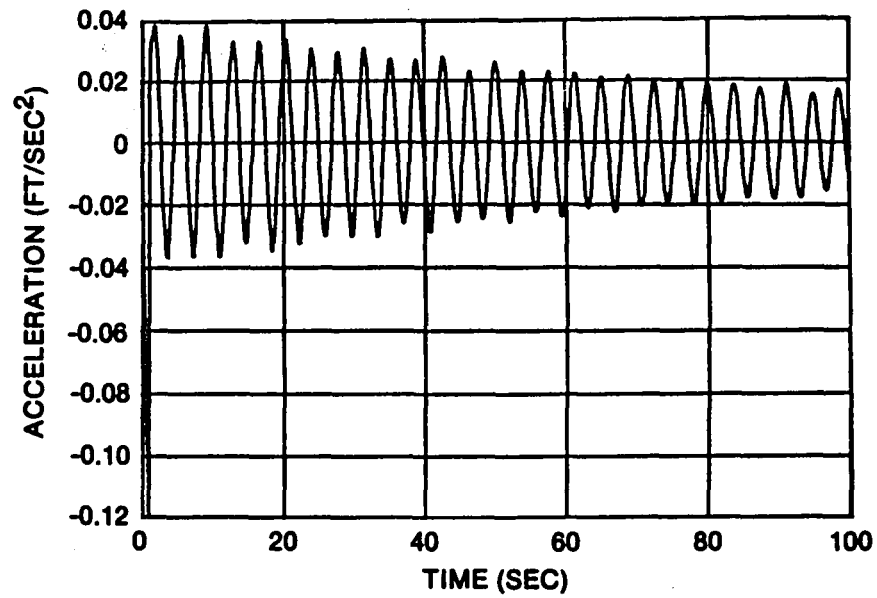


Figure 27. Transient Response at Berthing Port in X Direction
Due To Orbiter Berthing

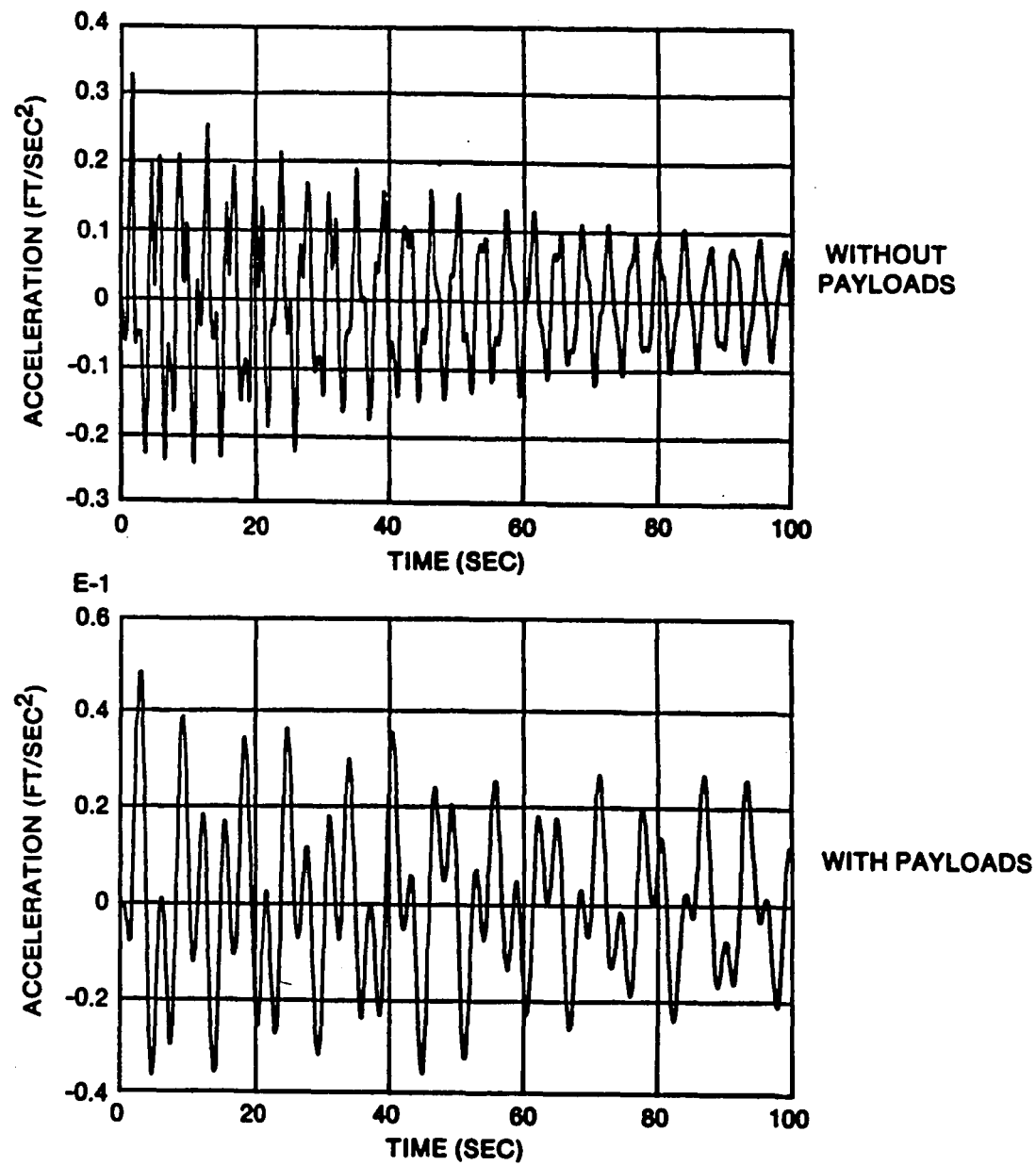


Figure 28. Transient Response at Center of Upper Boom in X Direction Due to Orbiter Berthing

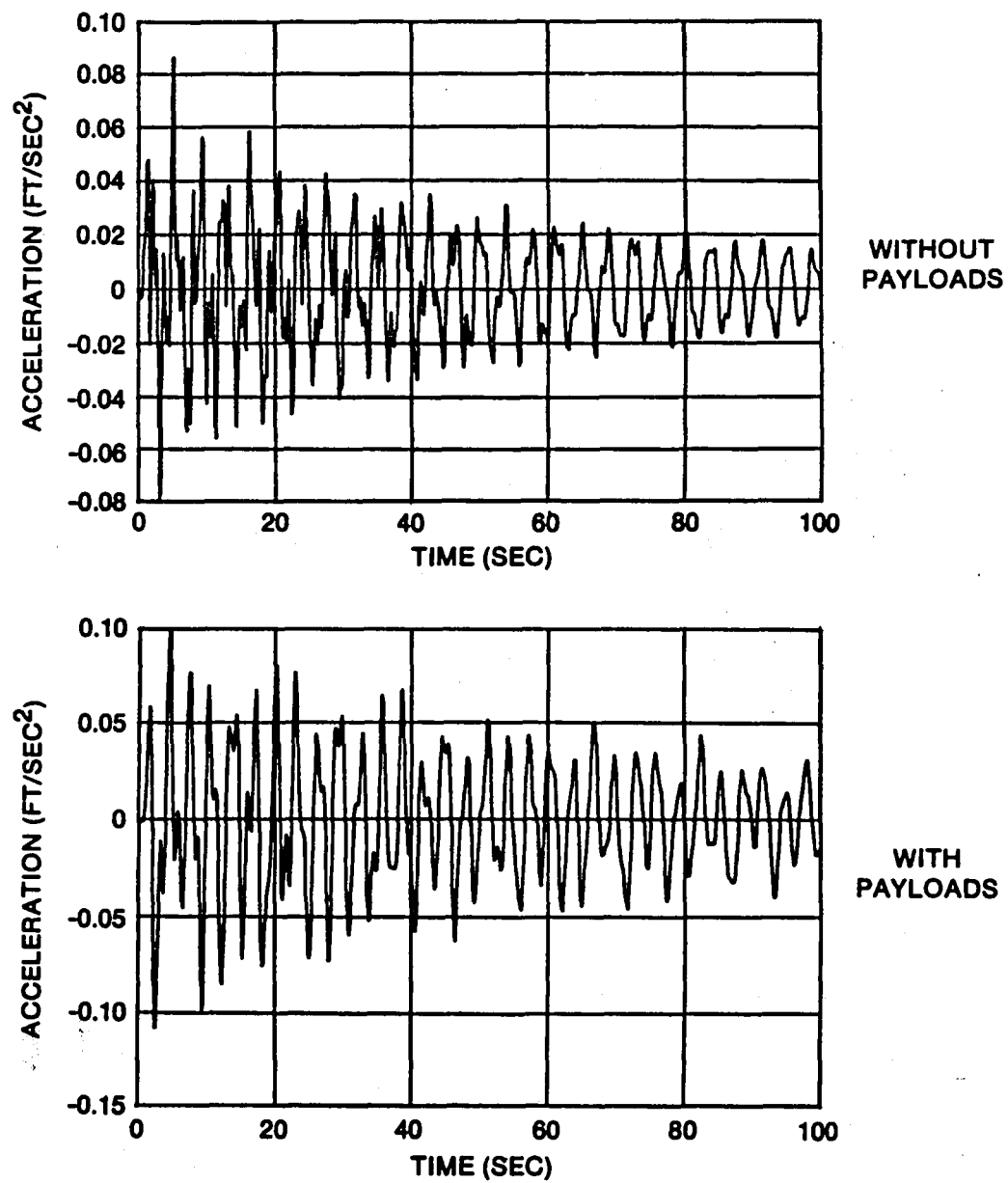


Figure 29. Transient Response at Tip of Transverse Boom in X Direction Due to Orbiter Berthing

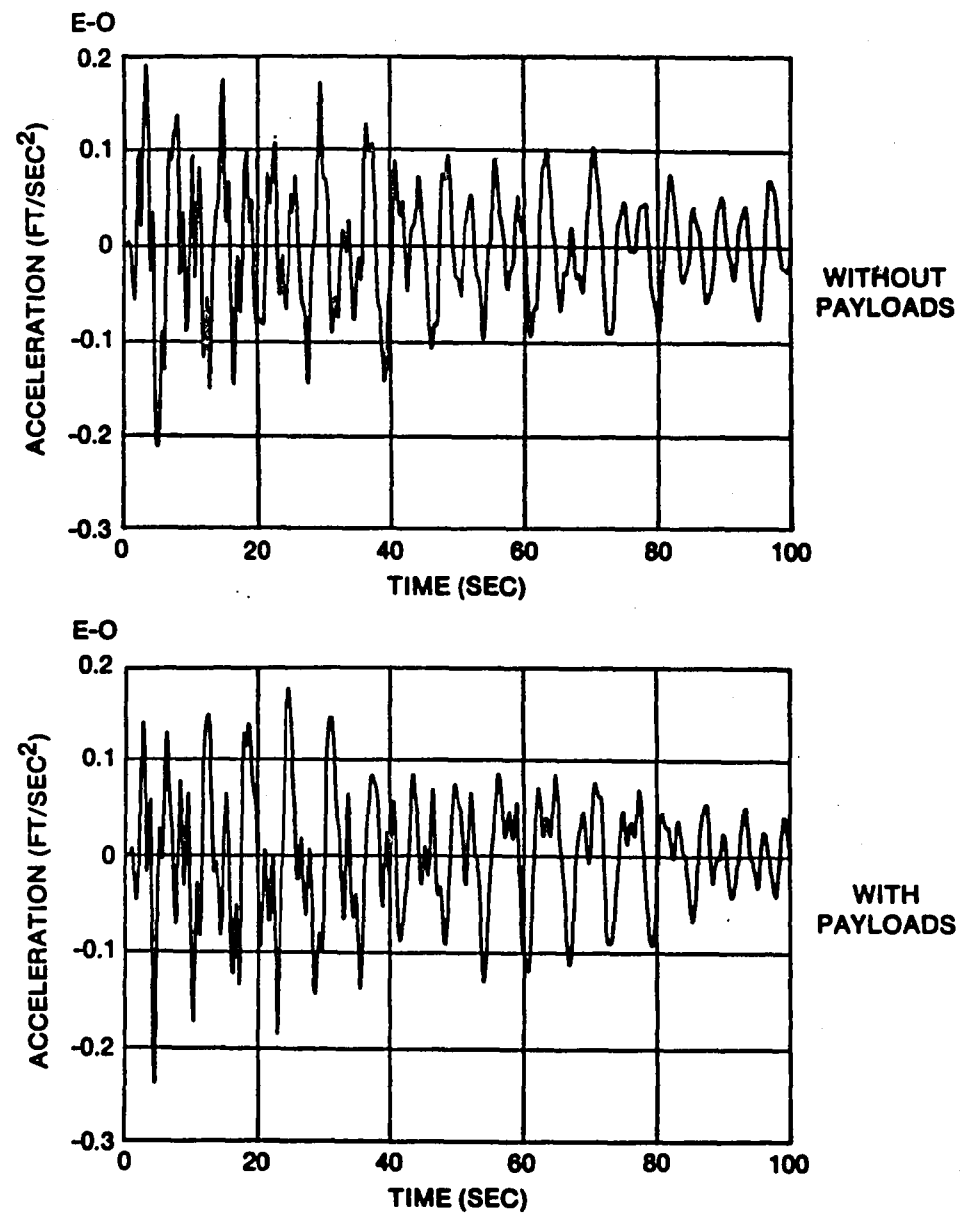


Figure 30. Transient Response at Tip of Array Mast in X Direction
Due to Orbiter Berthing

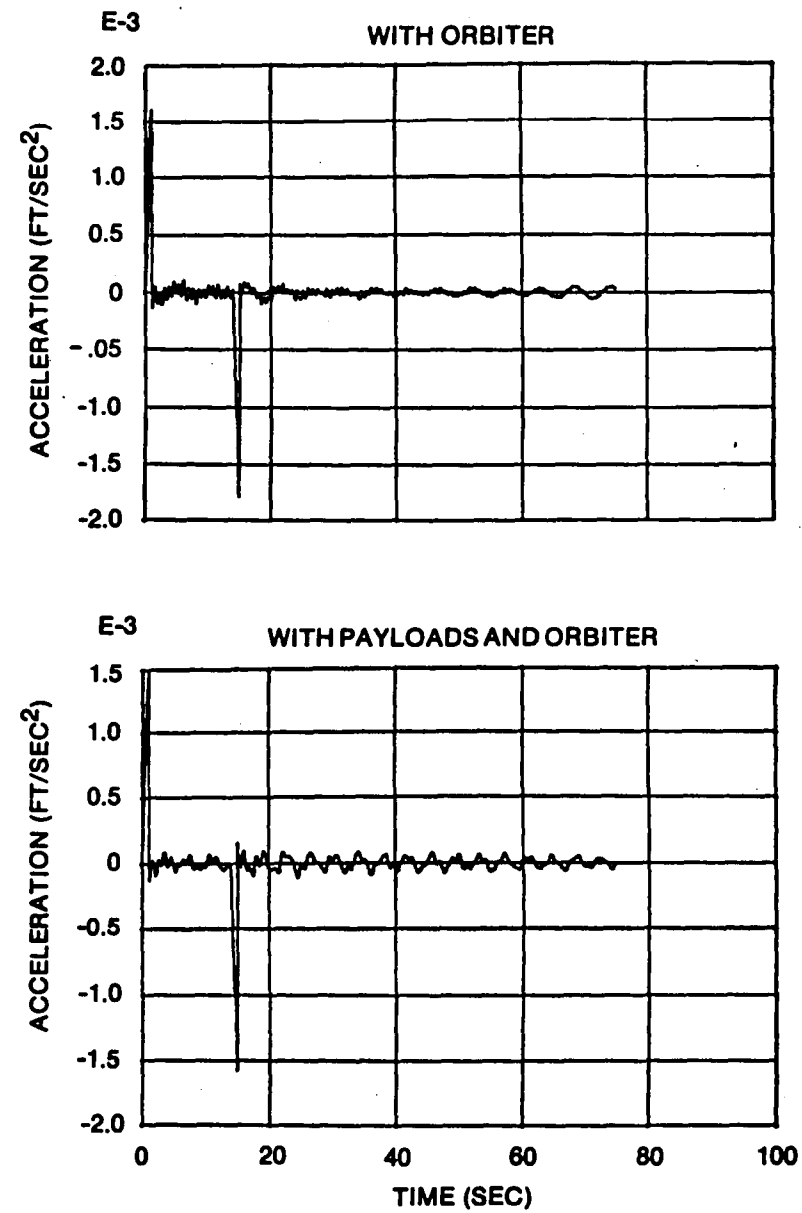
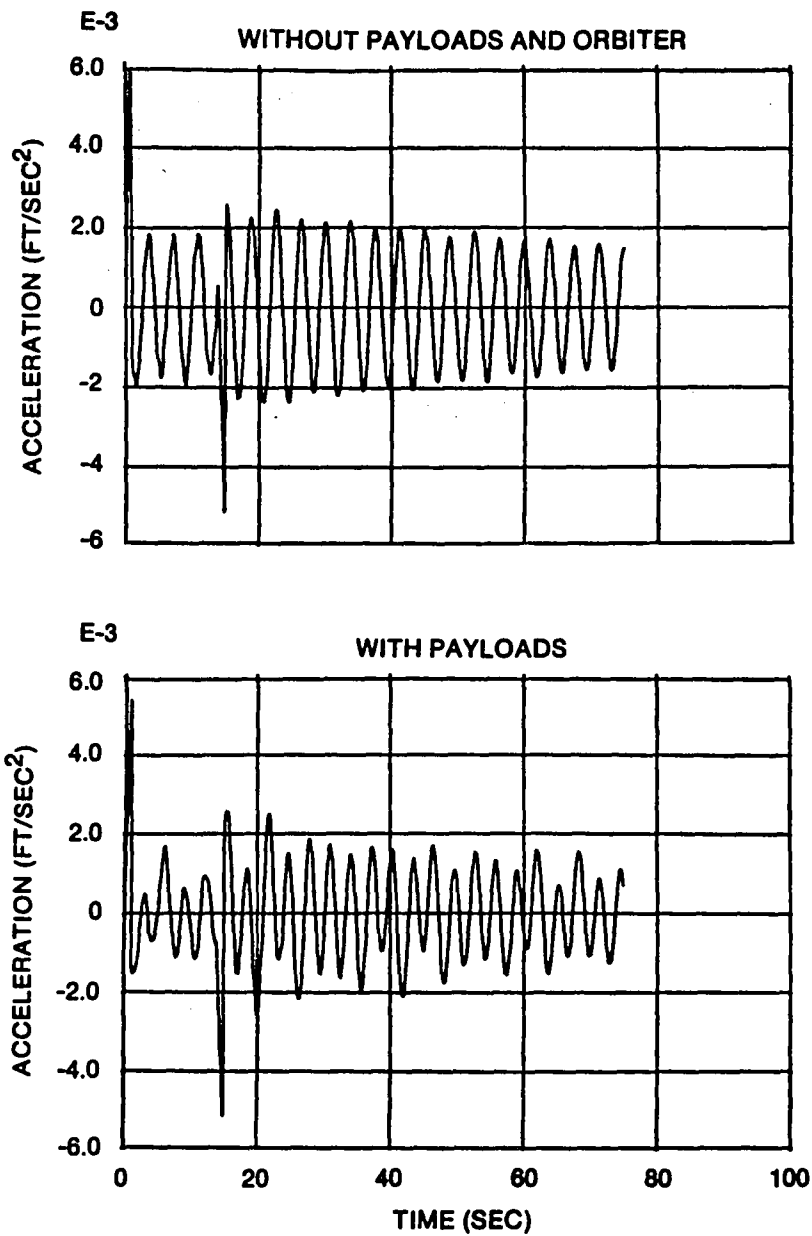


Figure 31. Transient Response at Habitation Module in X Direction
Due to Axial Crew Motion

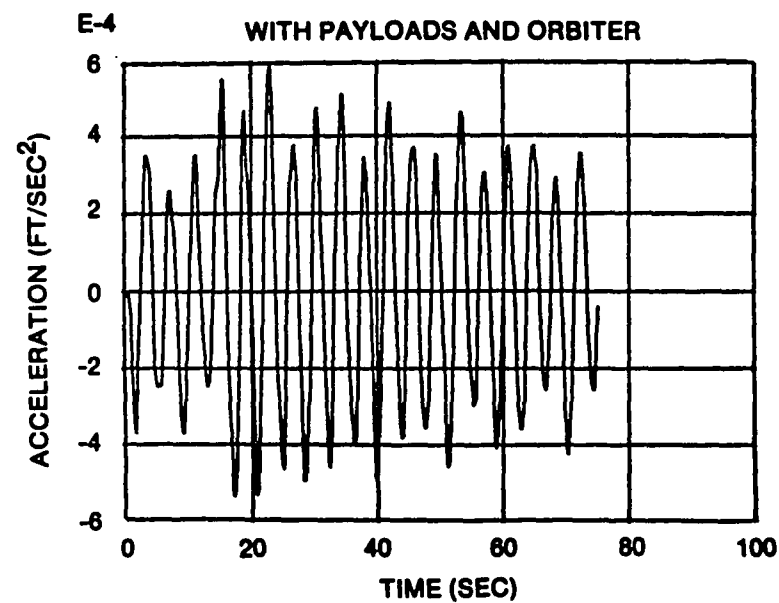
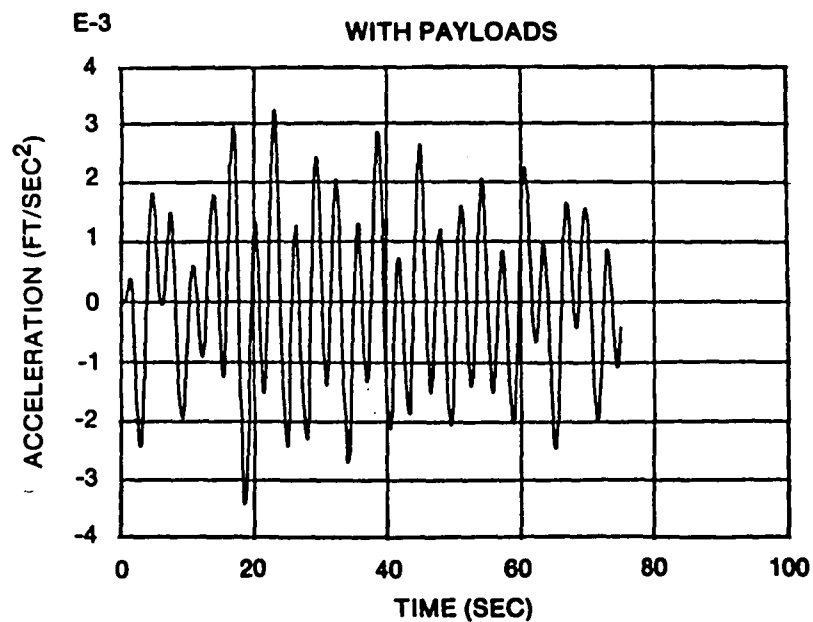
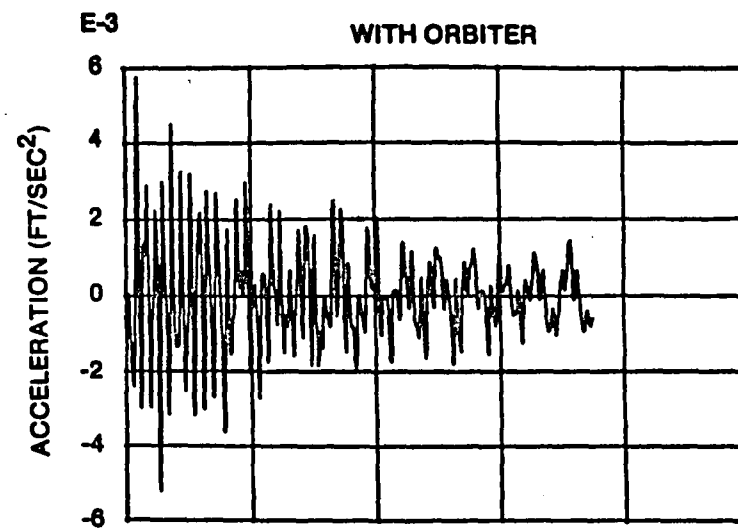
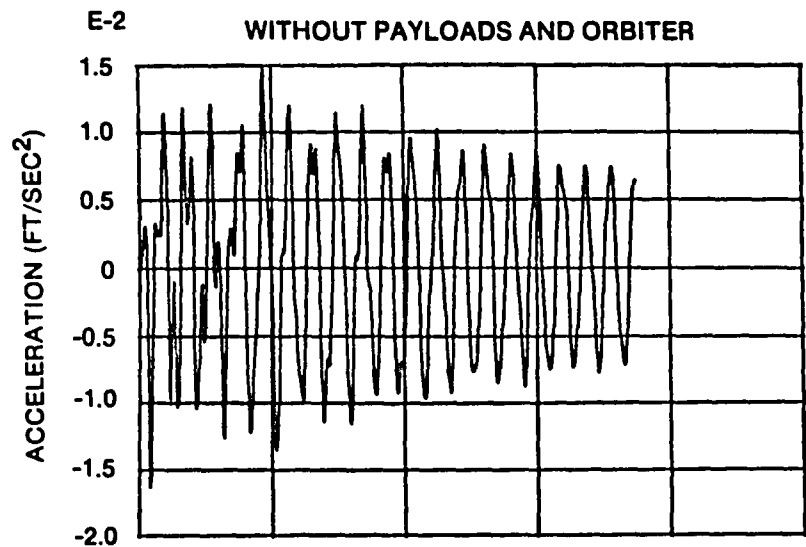


Figure 32. Transient Response at Center of Upper Boom in X Direction
Due to Axial Crew Motion

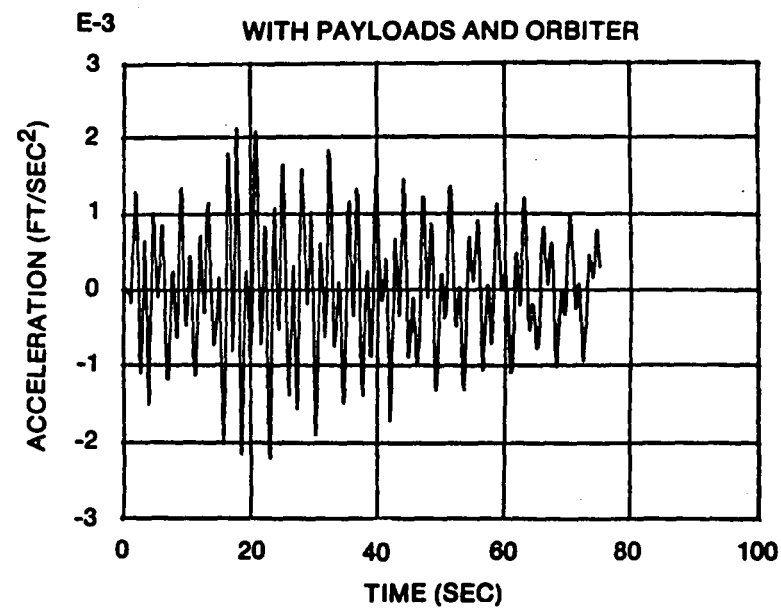
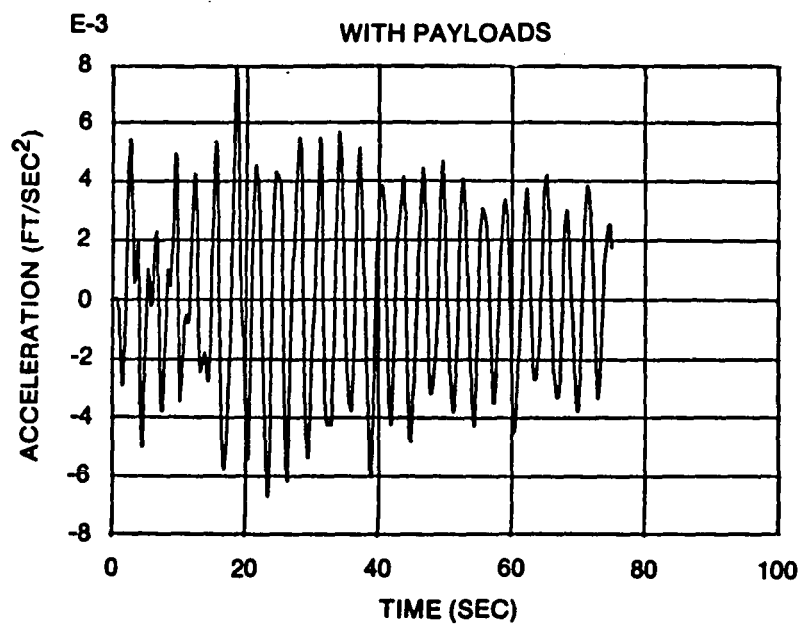
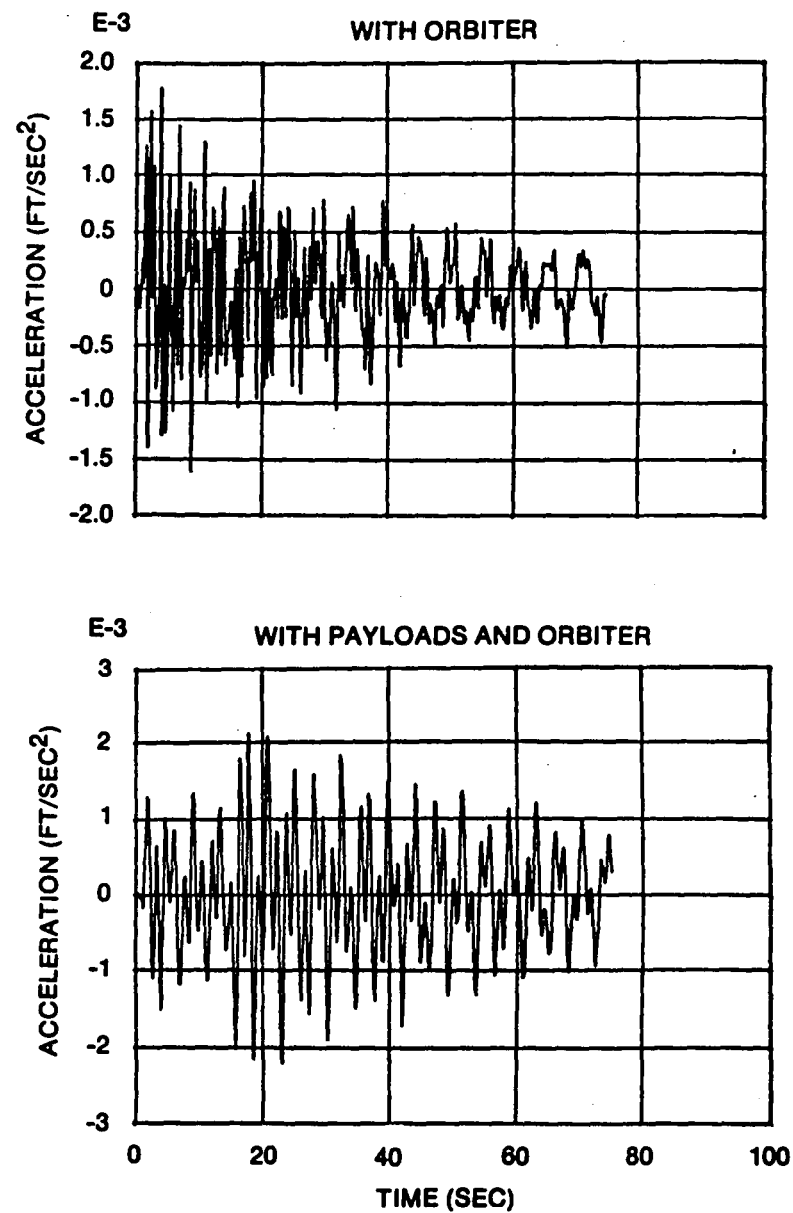
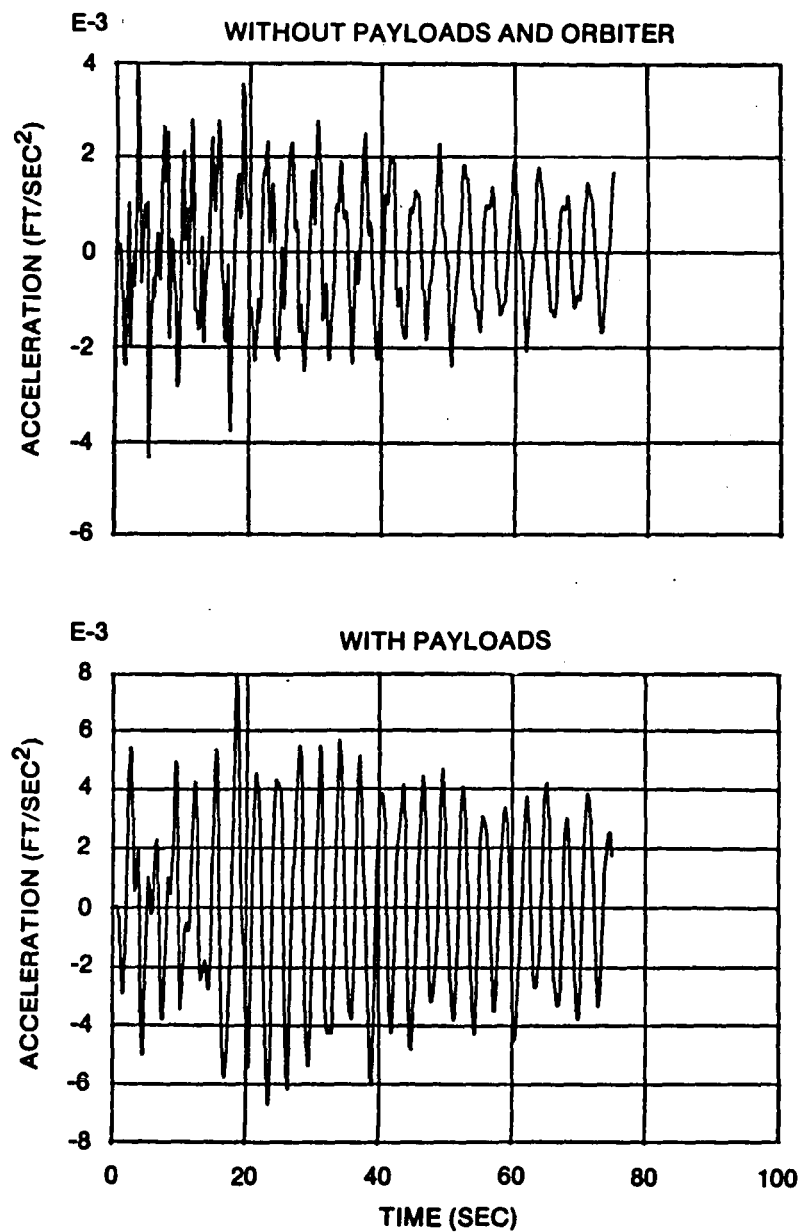


Figure 33. Transient Response at Tip of Transverse Boom in X Direction
Due to Axial Crew Motion

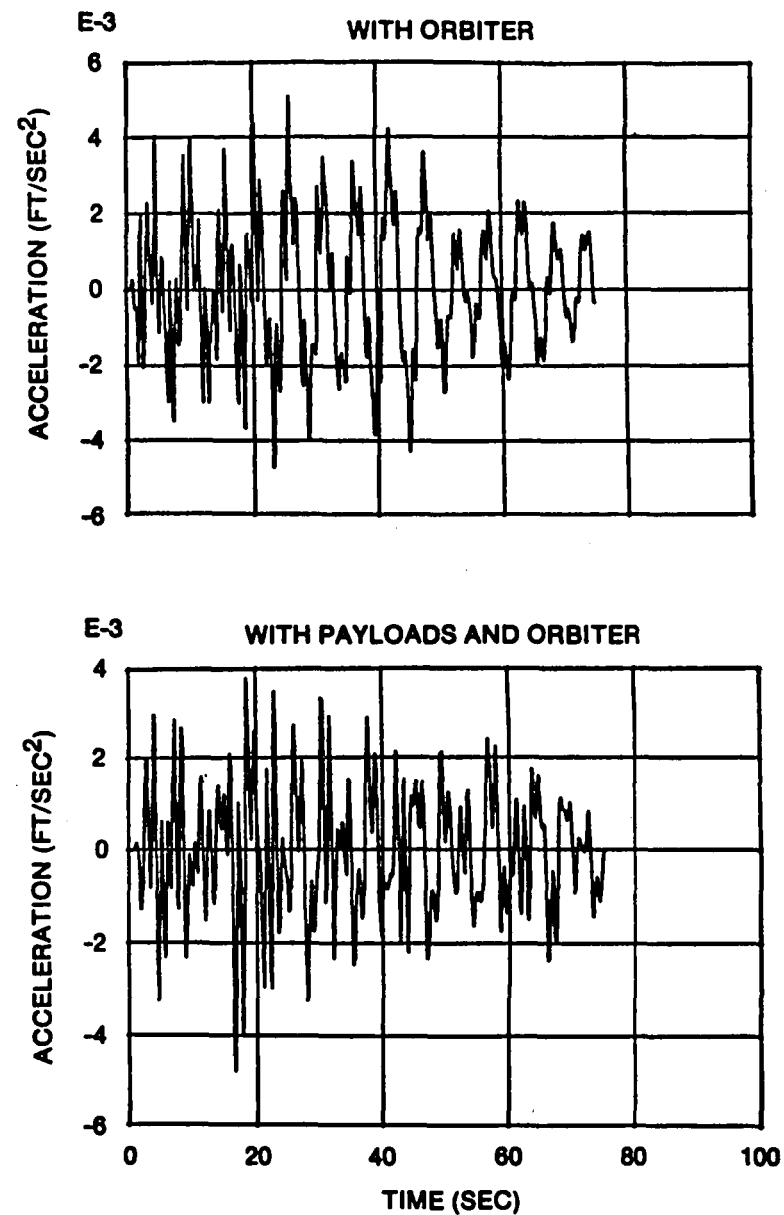
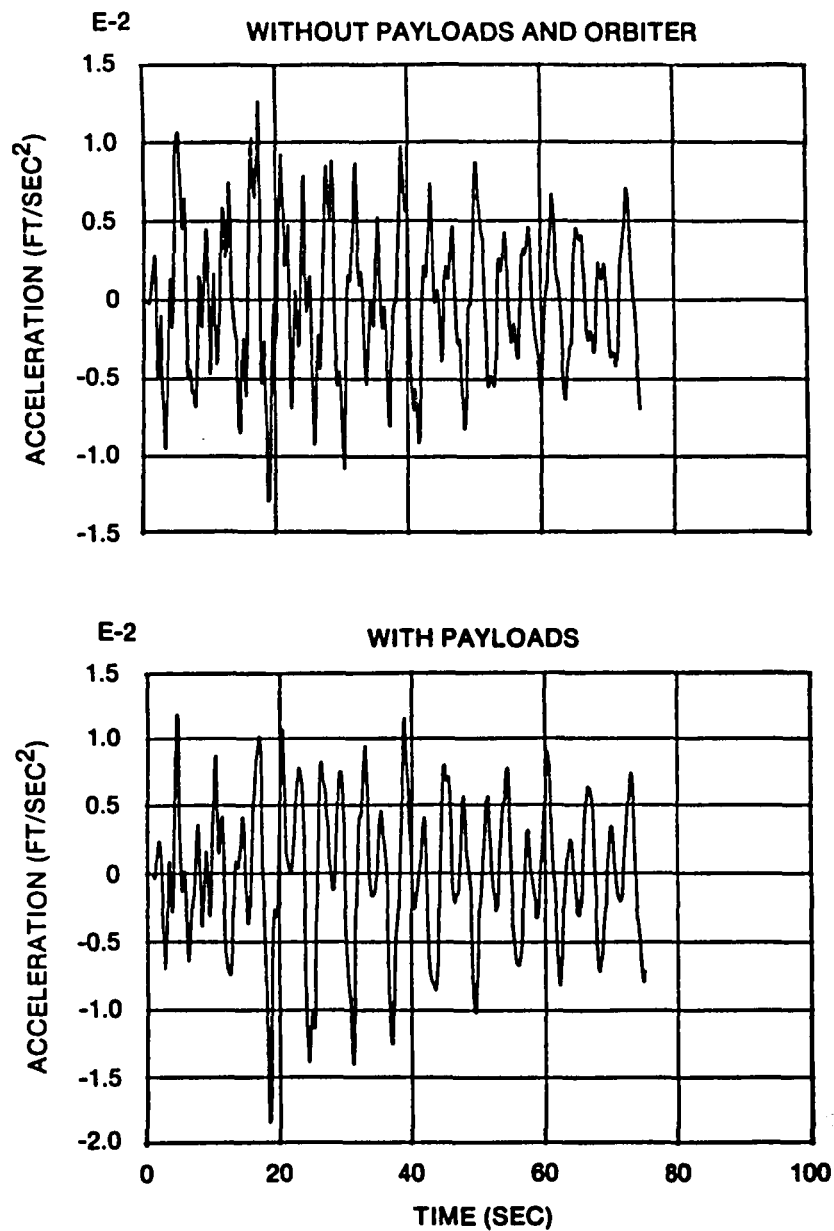


Figure 34. Transient Response at Tip of Array Mast in X Direction
Due to Axial Crew Motion

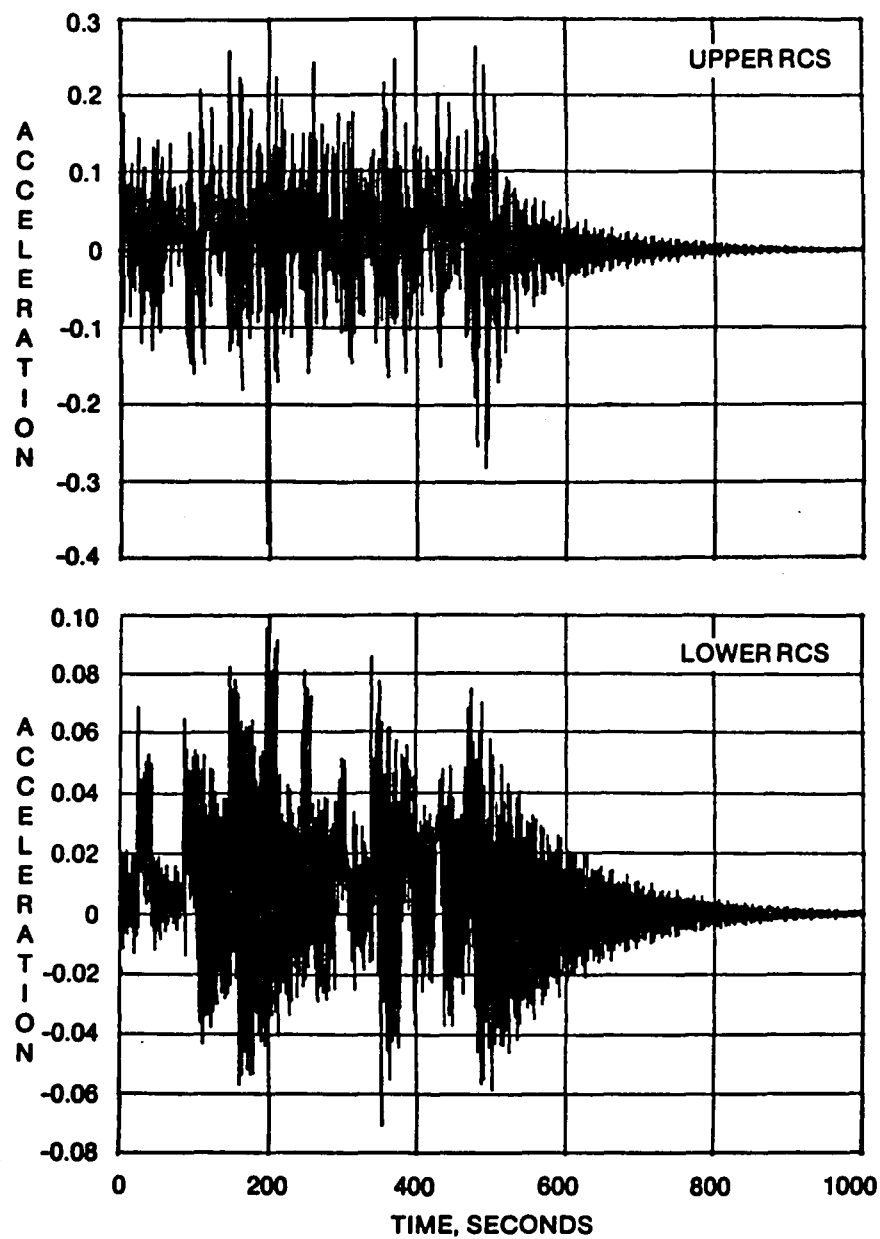


Figure 35. Acceleration Time Histories in Feet/Sec² at Upper and Lower RCS Locations Due to Reboost of IOC Station Without Attachments

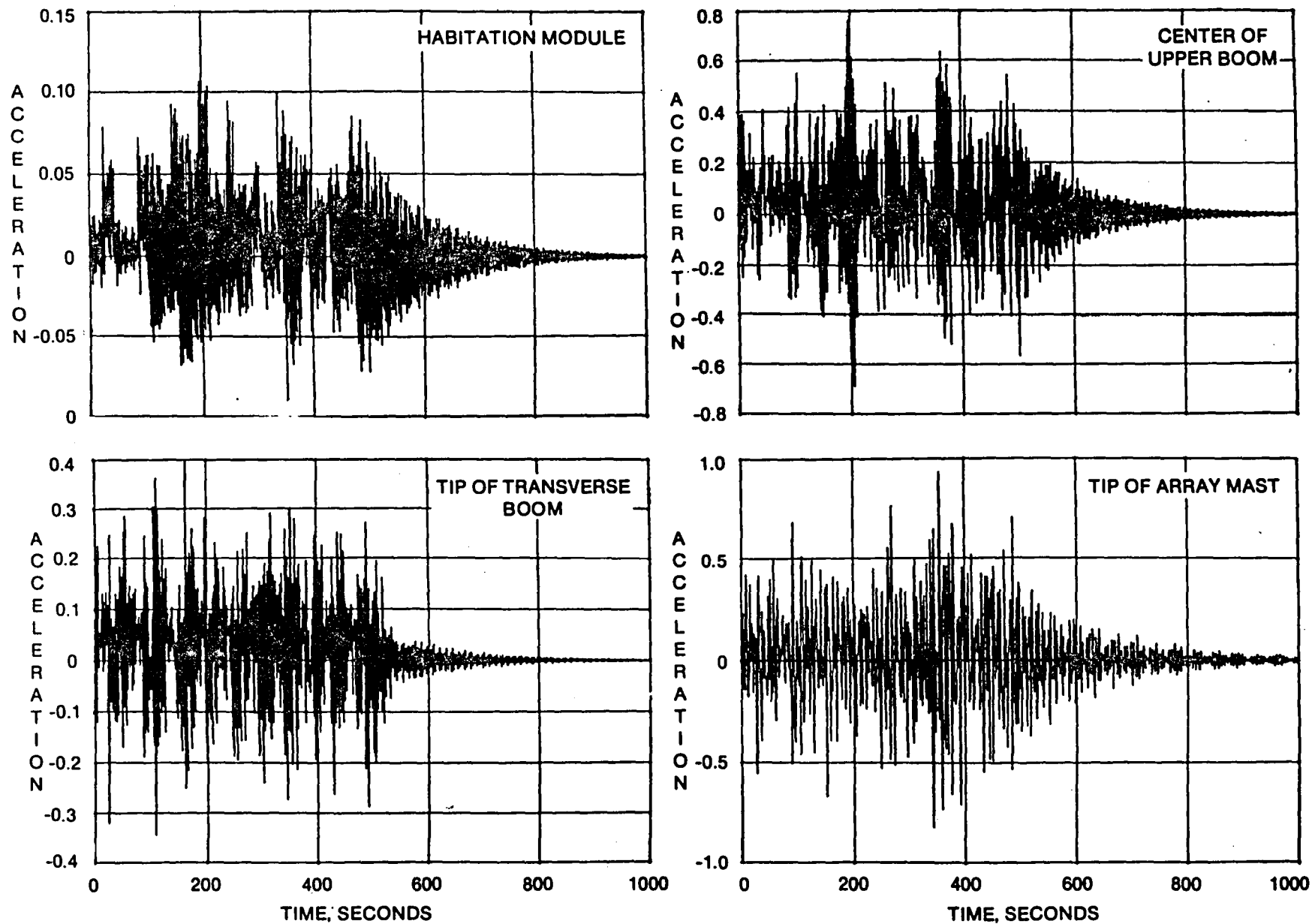


Figure 36. Acceleration Time Histories in Feet/Sec.² at Selected Locations Due To Reboost of IOC Station Without Attachments

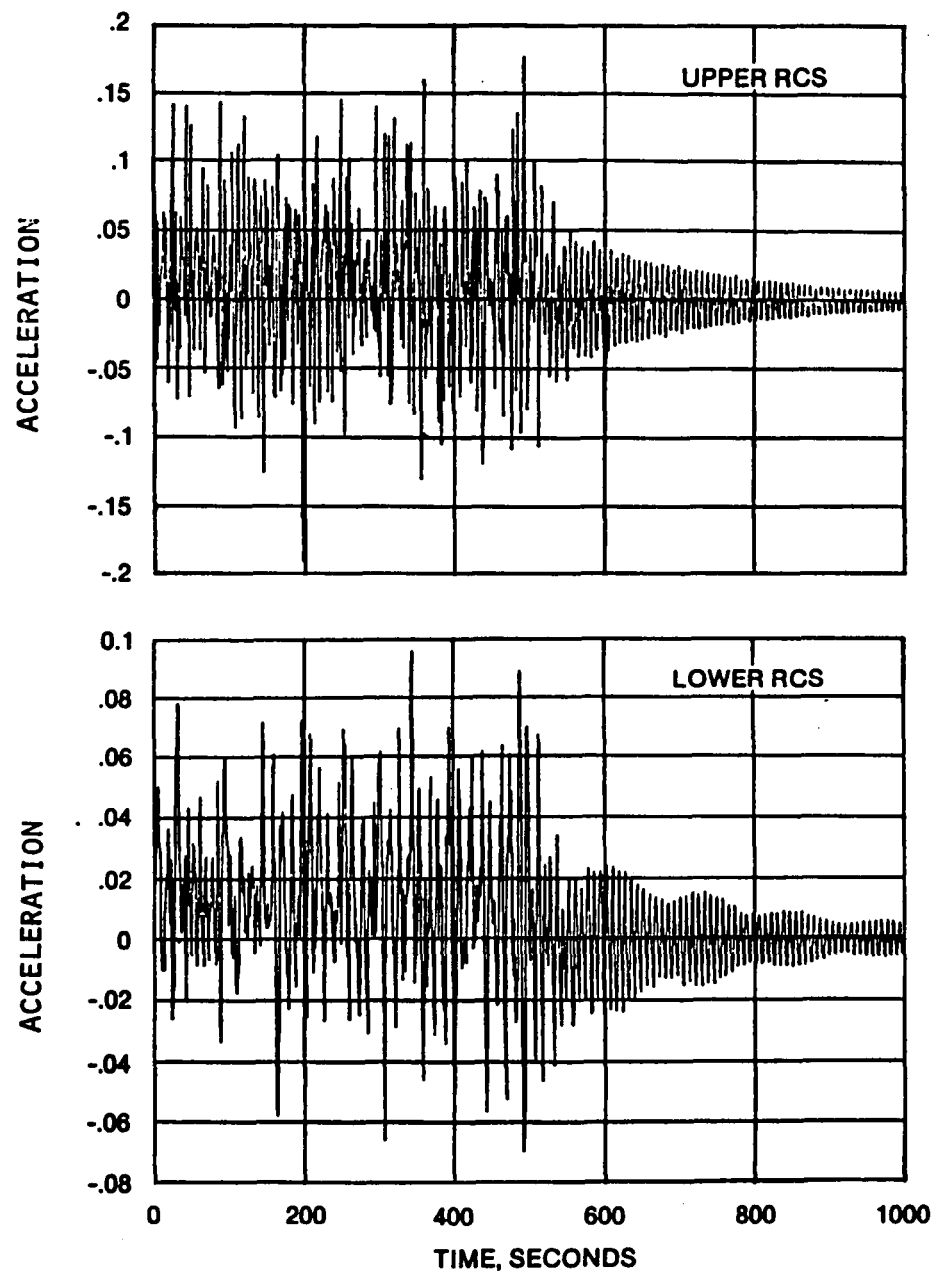


Figure 37. Acceleration Time Histories in Feet /Sec.² at Upper and Lower RCS Locations Due to Reboost of IOC Station With Attached Payloads

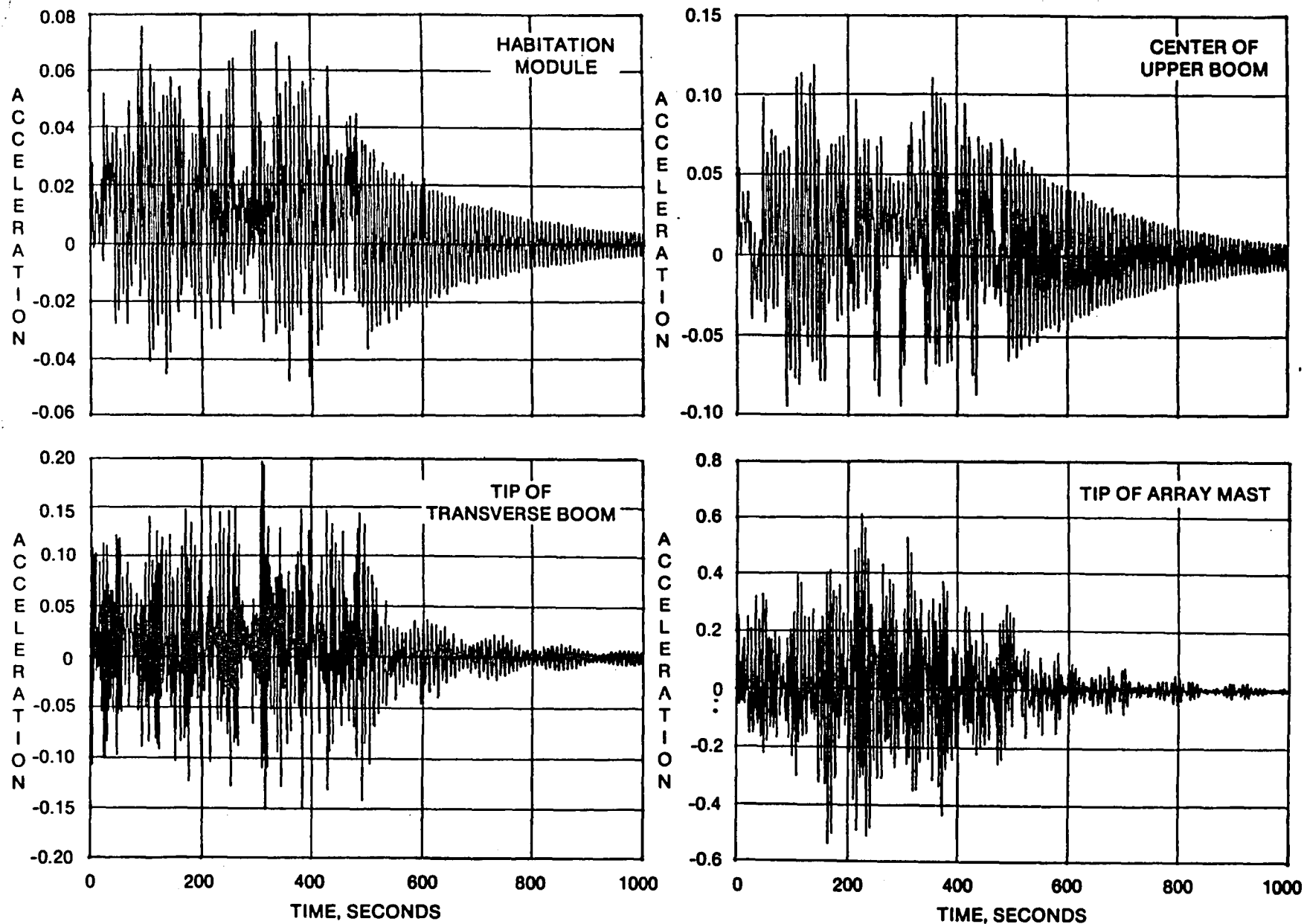


Figure 38. Acceleration Time Histories in Feet/Sec.² at Selected Locations
Due to Reboost of IOC Station With Attached Payloads

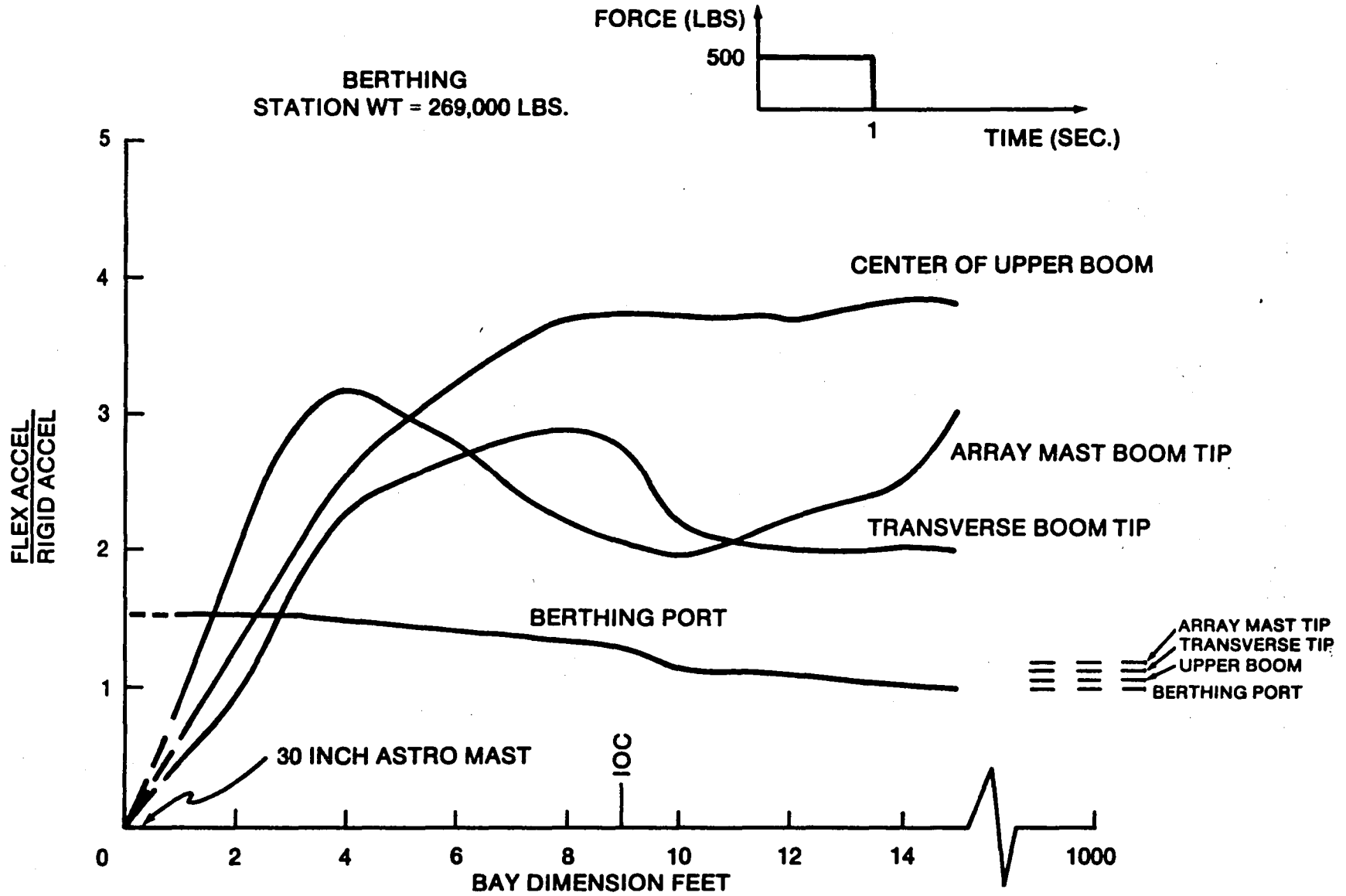


Figure 39. Variation of Peak Response With Bay Dimension
Due to Orbiter Berthing

1. Report No. NASA TM-86386		2. Government Accession No.		3. Recipient's Catalog No.	
4. Title and Subtitle STRUCTURAL DYNAMICS MODEL AND RESPONSE OF THE DEPLOYABLE REFERENCE CONFIGURATION SPACE STATION				5. Report Date MAY 1985	
				6. Performing Organization Code 482-53-53-34	
7. Author(s) Jerrold M. Housner				8. Performing Organization Report No.	
9. Performing Organization Name and Address NASA Langley Research Center Hampton, VA 23665				10. Work Unit No.	
				11. Contract or Grant No.	
12. Sponsoring Agency Name and Address National Aeronautics and Space Administration Washington, DC 20546				13. Type of Report and Period Covered Technical Memorandum	
				14. Sponsoring Agency Code	
15. Supplementary Notes					
16. Abstract <p>The analytical models and results of a structural dynamics investigation of the reference initial operation and evolutionary configurations of the nine foot bay space station are presented. This investigation was carried out between April and August 1984 as part of a team effort to define a reference configuration for the first U.S. manned Space Station. The results presented herein serve as a guide, a point of departure and a standard for future NASA and contractor studies leading to the design of the Space Station. The reference initial operation configuration of the nine foot bay station was found to be very flexible, with its lowest mode between 0.096 and 0.138 Hertz depending on station attachments. However, for the transient load cases which were then available, internal member loads had positive margins of safety and preliminary results indicate that laboratory experiments which require quiescent conditions can be satisfied down to the order of 10^{-5} g's.</p>					
17. Key Words (Suggested by Author(s)) Space Station Truss Structures Deployable Structures			18. Distribution Statement Unclassified - Unlimited Subject Category 39		
19. Security Classif. (of this report) Unclassified	20. Security Classif. (of this page) Unclassified	21. No. of Pages 93	22. Price* A05		

End of Document